Title: DNA Methylation-based prognosis and epidrivers in hepatocellular carcinoma

Authors: Augusto Villanueva (1,2,3)*, Anna Portela (4)*, Sergi Sayols (4,5), Carlo Battiston (6), Yujin Hoshida (1), Jesús Méndez-González (4), Sandrine Imbeaud (7,8), Eric Letouzé (9), Virginia Hernandez-Gea (3), Helena Cornella (3), Roser Pinyol (3), Manel Solé (3), Josep Fuster (3), Jessica Zucman-Rossi (7,8), Vincenzo Mazzaferro (6), Manel Esteller (4,10,11)¥, Josep M. Llovet (1,3,11)¥ on behalf of the HEPTROMIC Consortium.

Affiliations:

1. Liver Cancer Research Program, Division of Liver Diseases, Tisch Cancer Institute, Department of Medicine, Icahn School of Medicine at Mount Sinai, New York, US
2. Division of Hematology and Medical Oncology, Department of Medicine, Icahn School of Medicine at Mount Sinai, New York, US
3. Barcelona-Clínic Liver Cancer Group (Liver Cancer Translational Research Laboratory, Liver Unit, Pathology Department, Surgery Department), Institut d'Investigacions Biomèdiques August Pi i Sunyer (IDIBAPS), CIBEREHD, Hospital Clínic de Barcelona, Universitat de Barcelona (UB), Catalonia, Spain.
4. Cancer Epigenetics and Biology Programme, Bellvitge Biomedical Research Institute (IDIBELL), Barcelona, Catalonia, Spain.
5. Institute of Molecular Biology, Mainz, Germany.
6. Gastrointestinal Surgery and Liver Transplantation Unit, National Cancer Institute, Milan, Italy
7. Inserm, UMR-1162, Génomique fonctionnelle des tumeurs solides, IUH, Paris, F-75010 France.
8. Université Paris Descartes ; Université Paris Diderot, Université Paris 13, Labex Immuno-oncology, Sorbonne Paris Cité, Faculté de Médecine, Paris, France.
9. Programme Cartes d'Identité des Tumeurs, Ligue Nationale Contre le Cancer, F-75013 Paris, France.
10. Department of Physiological Sciences II, School of Medicine, University of Barcelona, Barcelona, Catalonia, Spain
11. Institució Catalana de Recerca i Estudis Avançats, Barcelona, Catalonia, Spain

* These authors equally contributed to this study
¥ Shared senior authorship

Grant support: The study is supported by the European Commission Framework Programme 7 (Heptromic, proposal number 259744). JML is supported by grants from the European Commission Framework Programme 7 (Heptromic, proposal number 259744), The Samuel Waxman Cancer Research Foundation, the Spanish National Health Institute (J.M.L: SAF-2013-41027) and the Asociación Española para el Estudio del Cáncer (AECC). ME is funded by Cellex Foundation, Botin Foundation, Health and Science Departments of the Catalan Government (Generalitat de Catalunya). YH is supported by National Institute of Diabetes and Digestive and Kidney Diseases (R01-DK099558). This work was supported by the INCa within the ICGC project, the Ligue Nationale Contre le Cancer ("Carte d'identité des tumeurs" program), the Réseau national CRB Foie. JB is supported by a grant of the Instituto de Salud Carlos III (PI11/01830). CIBERehd is funded by Instituto de Salud Carlos III.

Abbreviations: AFP: alpha-feto-protein; HCC: hepatocellular carcinoma; HCV: hepatitis C virus; HBV: hepatitis B virus; MI: mortality index; RSF: random survival forests; VIMP: variable importance

This article has been accepted for publication and undergone full peer review but has not been through the copyediting, typesetting, pagination and proofreading process which may lead to differences between this version and the Version of Record. Please cite this article as an 'Accepted Article', doi: 10.1002/hep.27732

Data repository: Submitted microarray and methylation data to a publicly available database, accession numbers GSE56588 and GSE63898.

Acknowledgements: We thank Loreto Boix and Jordi Bruix for their input and critical analysis of the manuscript. Also, we thank Paulette Bioulac-Sage, Charles Balabaud, Jean Saric and Christophe Laurent (CHU Bordeaux) and Jeanne Tran Van Nhieu, Daniel Cherqui, Daniel Azoulay (CHU Henri Mondor, Créteil) and the tumor bank of CHU Bordeaux and CHU Henri Mondor for contributing to the French tissue collection.

Conflict of interests: None relevant to this manuscript

Author's contributions:

- Study concept and design: AV, AP, SS, JMG, YH, JZR, VM, ME, JML
- Acquisition of data: AV, AP, SS, YH, CB, VHG, SI, EL, HC, RP, JF, JZR, VM
- Analysis and interpretation of data: AV, AP, SS, YH, JMG, SI, EL, JZR, VM, ME, JML
- Drafting of the manuscript: AV, AP, SS, ME, JML
- Critical revision of the manuscript for important intellectual content: AV, SP, SS, CB, YH, JMG, SI, EL, VHG, HC, RP, MS, JF, JZR, VM, ME, JML
- Obtained funding: AV, AP, ME, VM, JZR, JML

Correspondence should be addressed to:
Josep M. Llovet, MD
Liver Cancer Translational Research Laboratory
BCLC Group, IDIBAPS
Liver Unit, Hospital Clínic
University of Barcelona.
Villarroel 170, 08036 Barcelona
E-mail: jmllovet@clinic.cat

Manel Esteller, MD, PhD
Cancer Epigenetics and Biology Program (PEBC),
Bellvitge Biomedical Research Institute (IDIBELL),
Hospital Duran i Reynals,
Av. Gran Via de L'Hospitalet 199 – 203,
08908 L'Hospitalet de Llobregat, Barcelona, Catalonia, Spain.
E-mail: mesteller@idibell.cat

ABSTRACT

Epigenetic deregulation has emerged as a driver in human malignancies. There is no clear understanding of the epigenetic alterations in hepatocellular carcinoma and of the potential role of DNA methylation markers as prognostic biomarkers. The analysis of tumor tissue from 304 patients with hepatocellular carcinoma treated with surgical resection allowed us to generate a methylation-based prognostic signature using a training-validation scheme. Methylome profiling was done with the Illumina HumanMethylation450 array, which covers 96% of known CpG islands and 485,000 CpG, and transcriptome profiling was performed with Affymetrix Human Genome U219 Plate and miRNA Chip 2.0. Random Survival Forest enabled us to generate a methylation signature based on 36 methylation probes. We computed a risk score of mortality for each individual that accurately discriminated patient's survival both in the training set (221 patients; 47% hepatitis C-related hepatocellular carcinoma) and validation sets (n=83; 47% alcohol-related hepatocellular carcinoma). This signature correlated with known predictors of poor outcome and retained independent prognostic capacity of survival along with multinodularity and platelet count. The subset of patients identified by this signature was enriched in the molecular subclass of proliferation with progenitor cell features. The study confirmed a high prevalence of genes known de-regulated by aberrant methylation in hepatocellular carcinoma (e.g. *RASSF1*, *IGF2*, *APC*) and other solid tumors (e.g. *NOTCH3*), and describe potential candidate epidrivers (e.g. *SEPT9*, *EFNB2*). Conclusions: A validated signature of 36 DNA methylation markers accurately predicts poor survival in patients with hepatocellular carcinoma. Patients with this methylation profile harbor mRNA-based signatures indicating tumors with progenitor cell features.

Keywords: Liver cancer; epigenetics; biomarker.

INTRODUCTION

Liver cancer represents a major health problem being the second cause of cancer death worldwide[1]. The disease burden of this malignancy continues to grow and it is a leading cause of disability[2]. Surgical resection, liver transplantation and local ablation are the recommended treatment options for early hepatocellular carcinoma (HCC), but can only be applied to around 30% of patients in the West. Current clinical practice guidelines recommend resection in patients with single tumors and well-preserved liver function[3,4]. Even in these cases, tumor recurrence occurs in up to 70% of patients at 5 years, and no adjuvant therapy is presently available. Recent studies demonstrate how mRNA-based gene signatures obtained from HCC resection specimens and biopsies improve prognostic performance of conventional clinical and pathological variables[5-7]. Direct translation of these prognostic signatures into clinical decision-making has not yet occurred. Further understanding of tumour biology in HCC is needed to optimize prognostic accuracy and improve trial design and clinical management.

DNA methylation regulates cell differentiation and participates in tumorigenesis[8]. Global loss of DNA methylation is a hallmark of human cancer, also characterized by selective hyper-methylation confined to gene promoters. Solid evidence indicates that epigenetic marks could be used as prognostic and predictive biomarkers in oncology[9]. Analysis of methylomes enabled classification of colorectal carcinoma patients based on their prognosis[10]. In HCC, there is no clear understanding of the methylome and epidrivers, and few studies have comprehensively evaluated methylation biomarkers using high-throughput platforms[11]. Herein, using genome-wide methylation profiling we introduce and validate a 36-probe methylation signature able to accurately predict survival in HCC patients, and describe the landscape of aberrant methylation of key potential tumors suppressors and oncogenes in this cancer.

MATERIALS AND METHODS

Human samples and molecular profiling

Initially, study included samples from 331 surgically resected HCC and 19 non-tumor tissues including 9 cirrhosis and 10 normal livers. Training set (Heptromic dataset, n=248, flow chart in **Suppl. Fig. 1**) were samples obtained from two institutions of the HCC Genomic Consortium: IRCCS Istituto Nazionale Tumori, Milan (n=217) and Hospital Clínic, Barcelona (n=31). All samples included in this study were fresh-frozen. For RNA and DNA extraction we used the Qiagen RNeasy Mini (500 ng of total RNA at a concentration of 100 ng/μL) and Invitrogen ChargeSwitch gDNA Mini Tissue (1 μg of total DNA at a concentration of 100 ng/μL) kits, respectively. The median sample storage time from collection to DNA/RNA extraction was 7 years. RNA profiling was conducted on 228 HCC and 168 non-tumor liver adjacent cirrhotic tissues using the Affymetrix Human Genome U219 Array Plate, which is able to interrogate more than 20,000 mapped genes. After hybridization, only one tumor sample was discarded for transcriptome analysis due to poor quality. Methylome profiling was performed on 248 samples with the Illumina Infinium HumanMethylation450 BeadChip array that interrogates more than 485,000 CpG sites covering 96% of known CpG islands[12]. Out of the 248 HCC samples from the training set, 221 HCC qualified for final analyses after quality filtering (i.e., less than 5% of the probes incorrectly interrogated (p-value < 0.01)). In 205 patients, there was information on both transcriptome and methylation profiling. For the validation of the methylation-based signature, we analyzed data from a cohort of 83 HCC patients treated with resection in two French institutions (Bordeaux and Créteil hospitals), profiled with the same technology as the training set. The Institutional Review Boards of the participating centers approved the study.

Pyrosequencing validation

DNA methylation was evaluated with a pyrosequencing assay in a subset of samples previously analyzed by the Illumina Infinium Human Methylation450 array. A minimum of 500 ng of DNA was converted using the EZ DNA Methylation Gold (Zymo Research) bisulfite conversion kit following the manufacturer's recommendations. Specific sets of primers for PCR amplification and sequencing were designed using specific software (PyroMark assay design version 2.0.01.15). These are summarized in **Suppl. Table 1**. Primer sequences were designed, when possible, to hybridize with CpG-free sites to ensure methylation-independent amplification. PCR was performed under standard conditions with biotinylated primers, and the PyroMark Vacuum Prep Tool (Biotage, Sweden) was used to prepare single-stranded PCR products according to manufacturer's instructions. PCR

products were observed at 2% agarose gels before pyrosequencing. Reactions were performed in a PyroMark Q96 System version 2.0.6 (Qiagen) using appropriate reagents and protocols.

Data analysis

To study differential methylation between HCC and normal liver tissue, probes containing SNPs or located on sex chromosomes were eliminated, leaving 434,728 probes for analysis. Only those with a high signal quality (P<0.01) were considered. Probes hypo-methylated (B<0.33) in at least 90% of the normal liver samples and hyper-methylated (B>0.5) in at least 5% of the tumors (31,052 CpG sites) and probes hyper-methylated (B>0.5) in at least 90% of the normal liver and hypo-methylated (B<0.33) in at least 5% of the tumors were selected (68,086 CpG sites). The beta value (B) is used to estimate the methylation level of the CpG locus using the ratio of intensities between methylated and unmethylated alleles. For prognosis purposes, analyses focused only on CpGs islands located in TSS1500, TSS200, 5'UTR and 1stExon (n=84,448) shown to be differentially methylated in tumors versus normal liver according to predefined criteria (n=11,307)[13]. This enabled us to select for those methylation markers primarily de-regulated in cancer tissues.

In order to discover potential candidate HCC epidrivers, an F score directly proportional to intergroup variability (normal liver *versus* HCC) and inversely proportional to normal sample intragroup variability was calculated for all probes located in promoters and CpG islands. The first 500 ranked probes were grouped per gene. Genes with more than 5 hits were further studied as epidrivers. Previously reported epigenetically deregulated genes were also analyzed, considering the mean of all probes located in the TSS200 region, which shows the best correlation with expression. For those samples without TSS200 probes in the array, TSS1500 were used instead, as the closest marker available in the array.

We generate a methylome signature able to predict the risk of death for each individual measured by a mortality index (MI). The prediction signature was generated using the Random Survival Forest method (RSF) developed for variable selection[13]. RSF is a method for prediction and variable selection for right-censored survival and competing risk data by growing survival trees to estimate a cumulative hazard function (CHF), which derives from each tree of the RSF. Input variables were the filtered 11,307 CpG sites. First, probes were randomly split in 6 sets of 2,000 or less probes to fit a model each using the RSF method by growing 1,000 survival trees. Variable importance scores (VIMP) were computed for all the probes used to grow the trees, and the 350 most informative from each model were selected to fit a new model using the same RSF method. Once the model was built, we removed

redundant and "noisy" variables by generating incremental RSF models adding one more variable, ranked by the VIMP calculated in the previous model, at each step, getting an estimate of the error as a measure of how much misclassification increases, or decreases, for a new test case if a given variable was not available for that case. The final set of selected variables (36 probes) was used to build the model having the lowest error rate using only the 2 most significant decimals of the obtained error rate. Thus, the methylation signature was based upon those 36 probes. The predictive accuracy of the 36-signature was examined by bootstrap cross-validation[13]. This allows estimating the prediction error curves of different survival models on 100 bootstrap samples, and comparing the performance of the different models (i.e., Cox and RSF) with a reference (estimation for the whole group without splitting based on the prediction variables, **Suppl. Fig. 2**).

From the last RSF model, we generated a DNA methylation-based mortality risk score (i.e., Mortality Index, range 36-360) for every individual computed as a sum of the CHF for each patient evaluated at a set of distinct time points weighed by the number of individuals at risk at the different time points. High mortality index (MI) correlates with higher risk of death. Using this index, we were able to split our training set in 2 risk groups based on percentiles, selecting the patients with the 20% highest levels [high risk (MI>230) and non-high risk (MI<230)] and test the variables selected as a prediction signature by confronting the high and low risk groups. To test the significance of the MI index, the same MI value used to split the training set was also used for the validation set. In other words, for the validation we didn't used percentiles, and split patients using the actual same value of the MI generated in the training set.

Processing of transcriptome data (i.e., normalization, background correction and filtering) was conducted as previously reported[5]. Prediction of liver cancer mRNA-based signatures in the training set was performed using the Nearest Template Prediction (NTP) method as implemented in the specific module of Gene Pattern software[14]. All mRNA signatures analyzed were already reported, being deposited in the Molecular Signature Database (www.broadinstitute.org/gsea/msigdb). To provide biological insight on samples with high mortality risk score (>230, percentile 80), we used the Gene Set Enrichment Analysis (GSEA) as implemented in Gene Pattern. Gene ontology by PANTHER, INTERPRO and KEGG pathways enrichment analysis was performed using the Database for Annotation, Visualization and Integrated Discovery (DAVID; v6.7).

Outcome analyses were framed within current guidelines from the Progress Partnership for prognostic factor research[15]. Kaplan-Meier plots and Cox regression were used to assess

association with outcome of the methylation signature and clinical variables. Overall survival was defined as the time between surgical resection and death of any cause or last follow-up, whereas cancer-related survival (validation set) was the time between resection to HCC-related death, as previously defined[16]. Time to recurrence is the time between resection and the radiological evidence of first tumor recurrence. Several clinical variables previously reported as outcome predictors in HCC were included in the analysis: gender, age, etiology of liver disease, tumor size, serum albumin, serum bilirubin, platelet count, serum AFP, BCLC stage[17], microvascular invasion, satellites, degree of differentiation . Variables with a p-value less than 0.05 in the univariate analysis (log-rank test) were separately evaluated in a multivariate Cox model aimed to identify independent predictors of survival and recurrence. Missing values were less than 10% for each variable included in the Cox model. Analyses were performed using the GenePattern analytical toolkit (www.broad.mit.edu/cancer/software/genepattern/), and the R statistical package (www.r-project.org).

RESULTS

Methylation signature predicts survival in hepatocellular carcinoma

Random survival forests enabled us to generate a methylation-based signature that accurately discriminated patients based on their survival (Training set, n=221). **Table 1** summarizes the clinical characteristics of this cohort, that mostly included males (172, 78%), with a median of 66 years/old, viral-related HCC (HCV: 101,47%, HBV: 44, 20%), and a median tumor size of 3.5 cm. Patients had predominantly uninodular disease (166, 75%), and no microvascular invasion (142, 65%) or satellites (158, 71%), being the majority at early clinical stages (BCLC O/A: 191, 87%) with a median follow-up of 48.5 months. Using the array data, we generated a methylation-based signature formed by 36 unique probes (**Suppl. Table 2**) that enable us to provide a DNA-methylation-based risk score of mortality (mortality index, ranging from 36-360, **Fig. 1A**). As predicted, these 36 probes were hyper-methylated in tumor compared to non-tumor tissue (**Suppl Fig 3**). To ensure reproducibility of the methylation status of these probes, we performed technical validation and determine methylation levels by pyrosequencing in a subset of 10 probes in 20 HCC. As show in **Suppl. Fig 4** there was a significant and high concordance on the methylation status of these probes using both methods.

The mortality index is a metric based on the weighed hazard of death for an individual across all trees (see methods for details). This DNA methylome-based score of mortality risk significantly correlated with known clinical and pathological predictors of survival, such as satellites (P=0.02), multinodularity (P=0.002), vascular invasion (P<0.001), BCLC staging (P=0.001), AFP (P=0.001), bilirubin (P=0.01), platelet count (P=0.009) and albumin (P=0.03, **Fig. 1B-I**). Concordantly, univariate analysis showed that DNA-methylation mortality index significantly correlated with risk of death (P<0.001, **Fig. 2A**). Median survival was significantly lower for patients with DNA-methylation MI> 230 – which represent 20% of the cohort – than for those with MI<230 (13 vs 79.7 months, respectively P<0.001) (**Fig. 2B**). Multivariate Cox modeling confirmed DNA-methylation-MI as an independent predictor of survival (HR: 13.35, 95% CI 7.94-22.42, P<0.001) along with multinodularity (HR: 1.65, 95% CI 1.03-2.62, P<0.001) and platelet count (HR: 1.58, 95% CI 1.01-2.41, P=0.03, **Table 2**). Similarly, DNA-methylation-MI score predicted tumor recurrence (**Fig. 2C**) and Cox modeling showed that the signature was also an independent predictor of overall recurrence (HR: 5.8, 95% CI 3.1-11, P<0.001) along with multinodularity (HR: 1.8, 95% CI 1.1-3, P=0.007, **Table 2**).

We next sought to validate the prognostic performance of our methylation-based MI in an independent dataset. The validation cohort also included 83 HCC patients treated by surgical resection from different French institutions. Unlike the training set, the main etiology of these patients was related to alcohol intake (47%, 39/83), presented with more aggressive disease (microvascular invasion 54%, satellites 42% and tumors >3cm in 83%) and had shorter median follow-up time (35 months). Patients with a high DNA-methylation-based MI had a significantly lower cancer-related survival (P=0.01, **Fig. 2D**). Even when arbitrary categorizing MI by percentiles, there is a direct relation between MI and poor outcome, both in training and validation sets (**Suppl. Fig. 5**). Overall, these data demonstrates how epigenetic de-regulation correlates with patient outcome in surgically resected HCC and introduces a first-in-class DNA validated methylation-based signature.

Integrated prognostic classification with transcriptome-based predictors

In order to further characterize the subset of patients identified by the DNA-methylation signature, we integrate whole-genome mRNA and methylation data of 205 HCCs. DNA-methylation-based high mortality index was significantly enriched in tumors that harbored mRNA signatures capturing progenitor cell features such as EpCAM[18] (P=0.009) and S2 (a reported molecular class of potential progenitor cell origin)[19] (P=0.006, **Fig. 3**). This was further confirmed when we performed GSEA on the samples with the highest MI (**Suppl. Table 3**). In addition, we found a significant enrichment of Gene Ontologies related to chromosomal dynamics and RNA processing in these samples (FDR<0.05). Conversely, tumors with DNA-methylation-based low MI were enriched in gene sets associated with metabolism and homeostasis (**Suppl. Table 3**).

Non-coding mRNA expression profile and DNA methylation data were tested in 205 samples. Patients with a high DNA-methylation MI had a differential non-coding mRNA expression pattern comprising 5 miRNAs and 1 small nucleolar RNA: miR-3193 (P<0.001), miR-27b-star (P=0.002), miR-422a (P=0.02), miR-378c (P=0.03), miR-938 (P=0.03) and SNORD126 (annotated as miR-1201 in the array) (P=0.03). All 6 non-coding RNAs were significantly down regulated in patients with DNA-methylation high MI score (**Suppl. Fig. 6**).

Aberrant methylation in human HCC

Similarly to other malignancies, there was a remarkable predominance of hypo-methylated probes in HCC compared to normal liver (68%, **Fig. 4A**). Hypo-methylated

probes were mainly located in the intergenic (39.9%) and body regions (34.5%), whereas hyper-methylated probes were predominantly located in promoter areas (50.5%). Regarding CpG island relation, hypo-methylated probes were mainly located in open sea regions (63.55%), while hyper-methylated probes tended to locate in CpG islands (63.9%) and shores (24.8%) (**Fig. 4A**).

To identify potential methylation markers of malignant transformation, we searched for probes that could accurately differentiate normal liver tissue and HCC, among the 11,307 above described probes. Analyses focused on probes with low intra-group variability (tumor and non-tumor) but high inter-group variability as defined by an F score (mean-β differences between groups / mean-β differences within groups). The top-100 ranked probes using this score, were able to accurately differentiate normal liver and HCC tissues (**Fig. 4B, Suppl. Table 4**). These 100 probes were all hyper-methylated in HCC and corresponded to 70 different genes. Gene ontology analyses showed enrichment in entries related to gene expression regulation (such as transcription factors ($P=2.9E^{-6}$)), and different signaling cascades such as IGF ($P=2.1E^{-3}$), PI3K ($P=3E^{-3}$), TGF-B ($p=5.8E^{-3}$) and cadherin ($p=3.5E^{-2}$), among others. When compared to a recently published analysis in 24 HCC[20], we found 43 common probes (**Suppl. Fig 7A, Suppl. Table 5**), and validated their ability to distinguish HCC from non-tumor tissue (**Suppl. Fig 7B**).

We next sought to explore the landscape of known and novel genes candidates as potential epidrivers in HCC. First, we validated other previously reported aberrantly DNA methylated genes in HCC such as hyper-methylation of *RASSF1* (82%), *APC* (78%) or *NEFH* (43%)[21] and hypo-methylation of *IGF2* (51%), among others (**Table 3**). Then, we identified that known drivers in other tumors show aberrant promoter methylation in HCC, such as *NOTCH3*[22], *NSD1*[22] and *ZIC1*. Finally, in order to describe novel candidate potential epidrivers not previously described in HCC, we selected the top 500 F-scored probes that were clustered in their target genes (**Suppl. Table 6)**, and identified genes involved in TGFB, or FGF signaling. Those genes with the highest number of de-regulated hits between HCC and normal liver were highlighted as the most appealing candidates (**Table 3**). Some of these candidates were also validated with pyrosequencing (**Suppl. Fig. 8**). Among them *SEPT9*, a tumor suppressor described in colon and ovarian cancer[23], and ephrin-B2 ligand *EFNB2*, which hyper-methylation was reported in patients with acute leukemia[24]. These new candidate epidrivers were also found significantly de-regulated in the validation cohort of 83 HCCs (**Fig. 5)**.

DISCUSSION

The understanding of molecular pathogenesis of HCC and gene-based prognostic prediction has improved during the last decade. By using next generation sequencing and SNP array analysis the main structural alterations and drivers in HCC have been uncovered. Similarly, transcriptome analysis allowed establishing molecular subclasses of this cancer, although with no direct implications in the management of patients so far[11]. Nonetheless, there still is a clear lack of understanding of the role of epigenetics in HCC and whether parameters related to methylation have clinical and outcome relevance. Few studies have addressed the role of epigenetics in hepatocarcinogenesis[20,25,26], and there is even less information regarding the relevance of DNA-methylation based signatures as prognostic biomarkers of this prevalent and lethal cancer. Herein, by using a genome-wide approach, we present a first in class 36-probe DNA methylation signature able to characterize a molecularly aggressive HCC subtype. In addition, we describe a landscape of aberrantly methylated promoters of genes potentially involved in hepatocarcinogenesis.

To develop the signature, we profiled a total of 304 HCCs (221 in training and 83 in validation sets) using high-density methylation arrays in a training-validation approach. Previous studies have looked at epigenetic prognostic markers in HCC, but using lower density arrays, less samples and without independent validation[20,26,27]. Similarly to other solid tumors[8], our study demonstrates the capability of methylation data to accurately classify HCC patients based on their outcome. Unlike previous prediction methods applied in prognostic studies in HCC[5], the design of the 36-probe signature provides a quantitative death risk score (i.e., mortality index) to each new patient eliminating signal redundancy. Correlation with other prognostic clinical parameters in the training set reinforces its prognostic performance. Of note, despite remarkable etiology differences between the training (mostly hepatitis C) and validation (mainly alcohol related) sets, the signature confirmed its ability for outcome prediction. In addition, the DNA-methylation signature defines high risk of mortality in 20% of patients in the cohort with best outcome (i.e., training set), compared to 50% of patients in the validation cohort, proved to have more aggressive tumors, a feature that suggests the ability of the DNA-methylation signature to identify patients with aggressive tumors across different stages.

Frequently, prognosis research studies lack the high standards required in other fields of medicine such as therapeutic trials and genetic epidemiology[28]. This is paradigmatic in prognostic gene signatures considering the high discrepancy between reported ones and those

that are finally implemented in clinical practice. In fact, currently guidelines in HCC management do not include any of such in the routine care of HCC patients[3,4]. Our study is entirely consonant with the prognostic factor research scheme of the PROGESS Partnership[28], an initiative that builds upon previous recommendations for reporting prognostic biomarkers in oncology (REMARK statement[29]). Nonetheless, in order to confirm the clinical strength of the novel information obtained with the DNA-methylation signature, an external independent validation would be required to conform to recent guidelines in HCC[3]. In terms of its clinical implementation, prospective validation of the signature in cohort studies will provide solid evidence to facilitate its inclusion in clinical practice guidelines. Preliminary studies suggest the feasibility of DNA methylation profiling from biopsy specimens or even plasma (i.e., circulating cell-free DNA)[30].

Integrative analysis with transcriptome data enabled us to obtain additional insight into molecular subclasses in HCC. Considering that DNA methylation provides one of the layers of epigenetic control of tissue specification and differentiation[31], it is remarkable that patients within the high mortality risk group based on the methylation signature (defined by a mortality index higher than 230) were significantly enriched in mRNA proliferation subclasses capturing progenitor cell origin (EpCAM[18] and S2[19]). Interestingly, we found a set of non-coding RNA significantly down-regulated in patients within the high-risk methylation group. Of note, miR-27b has been characterized as a regulatory hub in lipid metabolism in liver[32], being also involved in PPAR signaling[33]. The role of the PPAR receptors in HCC remains controversial[34], but in retrospective studies the use of PPARγ agonists was associated with a decrease in liver cancer[35].

Around 140 genetic drivers have been described in oncogenesis[36], among which epidrivers are the most unknown category. We describe a landscape of DNA-methylation aberrations in 221 HCC patients using a last generation technology. Our findings point to IGF, PI3K, TGF-B and WNT signaling as the pathways clearly deregulated by DNA methylation in HCC. We also explored the role of methylation in WNT signaling in a subset of 47 samples for which we had *CTNNB1* mutation status data. Interestingly, we found significant hyper-methylation of the 4 WNT pathway genes included among the top-500 F-scored probes in *CTNNB1* mutated samples (12/47, 25%) compared to wild type ($P<0.05$, **Suppl Fig 9**). Whether epigenetic changes contribute to further de-regulate WNT signaling in addition to *CTNNB1* mutations deserves additional investigations. We confirm the high prevalence of DNA-methylation aberrations of promoters of described tumor suppressors (*RSSFA1*, *APC*, *NEFH*)[21] or potential oncogenes (*IGF2*) in HCC. On the other hand, we

identified aberrant methylation in HCC of epidrivers described in other neoplasms, such as *NOTCH3* in acute leukemias[37], *NSD1* in glioblastoma[38] and *ZIC1* in colorectal cancer[39]. Finally, we are pointing to novel candidates that despite being involved in carcinogenesis, have not been described as de-regulated by DNA methylation, such as *SEPT9*, a tumor suppressor described in colon and ovarian cancer, and ephrin-B2 ligand *EFNB2*, which hyper-methylation was reported in patients with acute leukemia, and others involved in TGF-B receptor signaling pathway (*HOXA9*, *FOXG1* and *RUNX3*) and FGF-signaling pathway (*FGF8* and *FGF6*). This novel information provides a complementary portrait of epigenetic changes in HCC.

In summary, we describe a novel prognostic biomarker based on promoter DNA methylation changes in HCC that identifies patients at high risk of death and provides complementary epigenetic characterization of this tumor. Early detection of 'poor biology' HCCs could have a major impact in the decision-making and allocation of resources such in the adjuvant setting or complex therapies, such as resection or transplantation. In addition, potential candidate epidrivers have been described in HCC, which would require functional studies for biological confirmation.

FIGURE LEGENDS

Figure 1: Distribution of DNA-methylation-derived mortality index in the training set (Heptromic) as per density plot (**A**). Boxplots (with over-imposed individual values) for different clinical and pathological variables known to be prognostic in HCC and the mortality index (**B-I**)

Figure 2: Predicted hazard ratio for survival based on DNA-methylation-derived mortality index values (**A**). Kaplan-Meier plots for outcome analysis in Heptromic (n=221, training, **B-C**) and French datasets (n=83, validation, **D**)

Figure 3: Boxplots (with over-imposed individual values) of mortality index according to S and EpCAM mRNA-based molecular subclasses (**A**). Patients in the S2 and EpCAM classes (reported initially as identifying tumors with a progenitor cell origin) have significant higher levels of DNA-methylation-derived MI based on predictions from the methylation signatures. (**B**) Bottom panel represents enrichment of the 205 samples with methylation and mRNA data based on the levels of risk from the MI score. Top 20% patients with the highest DNA-methylation-derived MI score are significantly enriched in S2 and EpCAM classes

Figure 4: Genome-wide DNA methylation profiling of HCC patients. Genomic distribution of the differentially methylated probes between normal liver and HCC samples according to: i) functional genomic distribution (promoter, body, 3′UTR and intergenic) and, ii) CpG content and neighborhood context (island, shore, shelf and open sea) (**A**). Unsupervised hierarchical clustering of 10 normal liver (yellow), 9 cirrhotic liver (orange) and 221 HCC samples (blue) using the top 100 differentially methylated probes according to F score (**B**).

Figure 5: (Left panels) Boxplots represent de-methylation status of new candidate epidrivers generated from the training cohort (Heptromic). Right panels show their values on the French cohort (validation). P-values computed comparing HCC *versus* normal liver.

Supplementary figure 1: Flow chart summarizing the HCC samples profiled for this study.

Supplementary figure 2: Predictive accuracy of the 36-probe signature. Estimation of the prediction error based on 100 bootstrap samples and comparing the performance of Cox modeling and RSF *versus* a reference model. The reference is a simplification that estimates a survival curve for the whole set (Heptromic cohort) without splitting using the predictor variables.

Supplementary figure 3: Methylation status of the 36 CpG probes of the DNA prognostic methylation signature in HCC *versus* non-tumor tissue. Analysis was performed in samples from the training set. In brackets, P-values computed from one-way ANOVA of comparing ß-values in the three groups (normal liver, cirrhosis and HCC).

Supplementary figure 4: Technical validation of the DNA methylation signature. A subset of 10 probes from the 36-probe signature was analyzed in 20 HCC fresh-frozen samples from the training set using pyrosequencing. DNA methylation results based on Illumina 450K array data (y-axis) and pyrosequencing (x-axis) are plotted for each of the 10 probes tested. R represents Pearson's coefficient.

Supplementary figure 5: Kaplan-Meier curves of training and validation sets for different categorization values of the MI (tertiales, quartiles, quintiles and sextiles). Since the validation set has more advanced tumors, the proportion of patients in low percentiles is low. For each category, there is a dose-dependent effect between MI level and outcome.

Supplementary figure 6: Boxplots (with over-imposed individual values) for expression levels of miRNAs differentially expressed after characterization in low-mid MI (MI<230) and high MI (MI>230) subgroups (t-test p-values corrected by FDR reported).

Supplementary figure 7: Overlap of significant de-methylation probes in our dataset compared with previous studies. Panel **A** shows a Venn diagram with the 43 common differentially methylated probes in our study compare to the ones found by Song *et al*[20]. These 43 probes are depicted in Suppl. Table 5. Panel **B** shows the resulting heatmap after supervised clustering of the samples in our training set (n=221) using these 43 overlapped probes.

Supplementary figure 8: Technical validation of novel epidrivers. A set of 4 candidate epidrivers was analyzed in 10 HCC and 10 non-tumor fresh-frozen samples from the training set (5 normal liver and 5 cirrhotics) using pyrosequencing. DNA methylation results based on Illumina 450K array data (y-axis) and pyrosequencing (x-axis) are plotted for each of the candidate. Dots are colored based on the sample type (HCC, cirrhosis or normal liver). R represents Pearson's coefficient.

Supplementary figure 9: Methylation status of WNT pathway genes in samples according to their *CTNNB1* mutation status (sub-analysis conducted in 47 samples of the training set).

TABLES

Table 1: Clinical characteristics of HCC patients in the training and validation set.

Variable	Training (n=221)	Validation (n=83)
Median age	66	66
Gender (male)	172 (78%)	68 (81%)
Aetiology		
Hepatitis C	101 (47%)	9 (11%)
Hepatitis B	44 (20%)	17 (20%)
Alcohol	35 (16%)	39 (47%)
Others	37 (17%)	NA
Child-Pugh score:		
A	216 (96%)	74 (92%)
B	4 (2%)	9 (8%)
Tumour size (cm)		
<2	26 (11%)	5 (6%)
2-3	73 (33%)	9 (11%)
>3	122 (55%)	69 (83%)
Multiple nodules		
Absent	166 (75%)	69 (84%)
Present	55 (25%)	16 (16%)
Micro-vascular invasion		
Absent	142 (64%)	38 (46%)
Present	77 (35%)	44 (54%)
Satellites		
Absent	158 (71%)	48 (58%)
Present	63 (29%)	35 (42%)
BCLC early stage (0-A)	191 (87%)	59 (73%)
Degree of tumour differentiation		
Well	34 (18%)	28 (34%)
Moderately	105 (57%)	35 (43%)
Poor	45 (24%)	19 (23%)
Bilirubin (>1 mg/dL)	92 (42%)	10 (19%)†
Albumin (<3.5 g/L)	25 (11%)	NA
Platelet count (<100,000/mm3)	43 (19%)	NA
AFP (>100 mg/dL)	51 (23%)	31 (41%)†
Events		
Recurrence	151 (69%)	NA
Death	139 (62%)	36 (43%)*
Median follow-up (months)	48.5	35

* Cancer-related death in the validation set, as defined in Nault et al. Gastroenterology 2013. † Missing values: bilirubin (n=32), AFP (n=7)

Table 2: Univariate and multivariate survival analyses of HCC patients (n=221)

	Univariate analysis	Multivariate analysis (Cox Regression)		
Variable	**P-value**	**HR**	**CI (95% low - high limits)**	**P-value**
DNA methylation Mortality Index	<0.001	13.35	7.94 - 22.42	<0.001
Tumor size (>35 mm)	<0.001			
Vascular invasion	<0.001			
BCLC stage B or C	<0.001			
Multinodularity	<0.001	1.65	1.03 - 2.62	0.03
Albumin levels (<3.5 gr/L)	0.001			
186-gene signature[6]	0.001			
Gender	0.005			
Platelet count (<100,000/mm3)	0.006	1.56	1.01 - 2.41	0.04
AFP levels (>100 mg/dL)	0.02			
Bilirubin (>1 mg/dL)	0.02			
Satellites	0.03			
Etiology (HCV)	0.04			

Table 3: Candidate tumor suppressors and oncogenes with aberrant methylation of promoters in hepatocellular carcinoma (Heptromic cohort, n=221).

	Gene	Chromosome location	% hyper-methylated		P value
			HCC samples (n=221)	Normal liver (n=10)	
Genes reported aberrantly methylated in HCC	*RASSF1*	3	82	10	<0.001
	IGF2	11	51	100	0.001
	APC	5	78	0	<0.001
	NKX6-2	10	36	0	0.01
	SFRP5	10	7	0	ns
	NEFH	22	43	0	0.006
	RASSF5	1	6	0	ns
Genes reported as drivers in other cancers	*NOTCH3*	19	40	0	0.007
	NSD1	5	80	0	<0.001
	ZIC1	3	58	0	<0.001
Candidate potential novel epidrivers in HCC	*SEPT9*	17	61	0	<0.001
	CDKL2	4	59	0	<0.001
	DRD4	11	57	0	<0.001
	FOXE3	1	57	0	<0.001
	EFNB2	13	53	0	<0.001
	TBX15	1	51	0	0.001
	FAM196A	10	44	0	0.005

REFERENCES

1 Lozano R, Naghavi M, Foreman K, *et al.* Global and regional mortality from 235 causes of death for 20 age groups in 1990 and 2010: a systematic analysis for the Global Burden of Disease Study 2010. *Lancet* 2012; 380: 2095–128.

2 Murray CJL, Vos T, Lozano R, *et al.* Disability-adjusted life years (DALYs) for 291 diseases and injuries in 21 regions, 1990-2010: a systematic analysis for the Global Burden of Disease Study 2010. *Lancet* 2013; 380: 2197–223.

3 European Association For The Study Of The Liver, European Organisation For Research And Treatment Of Cancer. EASL-EORTC Clinical Practice Guidelines: Management of hepatocellular carcinoma. *J Hepatol* 2012; 56: 908–43.

4 Bruix J, Sherman M, American Association for the Study of Liver Diseases. Management of hepatocellular carcinoma: an update. *Hepatology* 2011; 53: 1020–2.

5 Villanueva A, Hoshida Y, Battiston C, *et al.* Combining Clinical, Pathology, and Gene Expression Data to Predict Recurrence of Hepatocellular Carcinoma. *Gastroenterology* 2011; 140: 1501–2.

6 Hoshida Y, Villanueva A, Kobayashi M, *et al.* Gene expression in fixed tissues and outcome in hepatocellular carcinoma. *N Engl J Med* 2008; 359: 1995–2004.

7 Hoshida Y, Villanueva A, Sangiovanni A et cl. Prognostic Gene Expression Signature for Patients With Hepatitis C-Related Early-Stage Cirrhosis. *Gastroenterology* 2013;144:1024-1030.

8 Portela A, Esteller M. Epigenetic modifications and human disease. *Nature Biotechnology* 2010; 28: 1057–68.

9 Heyn H, Esteller M. DNA methylation profiling in the clinic: applications and challenges. *Nat Rev Genet* 2012; 13: 679–92.

10 Hinoue T, Weisenberger DJ, Lange CPE, *et al.* Genome-scale analysis of aberrant DNA methylation in colorectal cancer. *Genome Research* 2012; 22: 271–82.

11 Villanueva A, Hoshida Y, Toffanin S, *et al.* New strategies in hepatocellular carcinoma: genomic prognostic markers. *Clin Cancer Res* 2010; 16: 4688–94.

12 Sandoval J, Heyn HA, Moran S, *et al.* Validation of a DNA methylation microarray for 450,000 CpG sites in the human genome. *Epigenetics* 2011; 6: 692–702.

13 Ishwaran H, Kogalur UB. Consistency of Random Survival Forests. *Statistics and Probability Letters* 2010; 80: 1056–64.

14 Hoshida Y. Nearest template prediction: a single-sample-based flexible class prediction with confidence assessment. *PLoS ONE* 2010; 5: e15543.

15 Riley RD, Hayden JA, Steyerberg EW, *et al.* Prognosis Research Strategy (PROGRESS) 2: Prognostic Factor Research. *PLoS Med* 2013; 10: e1001380.

16 **Nault JC, de Reyniès A**, Villanueva A, *et al.* A Hepatocellular Carcinoma 5-Gene Score Associated with Survival of Patients Following Liver Resection. *Gastroenterology* 2013; : 1–32.

17 Forner A, Llovet JM, Bruix J. Hepatocellular carcinoma. *Lancet* 2012. doi:10.1016/S0140-6736(11)61347-0.

18 Yamashita T, Ji J, Budhu A, *et al.* EpCAM-Positive Hepatocellular Carcinoma Cells Are Tumor-Initiating Cells With Stem/Progenitor Cell Features. *Gastroenterology* 2008; : 17.

19 Hoshida Y, Nijman SMB, Kobayashi M, *et al.* Integrative transcriptome analysis reveals common molecular subclasses of human hepatocellular carcinoma. *Cancer Res* 2009; 69: 7385–92.

20 Song M-A, Tiirikainen M, Kwee S, Okimoto G, Yu H, Wong LL. Elucidating the landscape of aberrant DNA methylation in hepatocellular carcinoma. *PLoS ONE* 2013; 8: e55761.

21 Revill K, Wang T, Lachenmayer A, *et al.* Genome-wide methylation analysis and epigenetic unmasking identify tumor suppressor genes in hepatocellular carcinoma. *Gastroenterology* 2013; 145: 1424–5.

22 Garraway LA, Lander ES. Lessons from the Cancer Genome. *Cell* 2013; 153: 17–37.

23 Gyparaki M-T, Basdra EK, Papavassiliou AG. DNA methylation biomarkers as diagnostic and prognostic tools in colorectal cancer. *J Mol Med* 2013; 91: 1249–56.

24 Kuang S-Q, Bai H, Fang Z-H, *et al.* Aberrant DNA methylation and epigenetic inactivation of Eph receptor tyrosine kinases and ephrin ligands in acute lymphoblastic leukemia. *Blood* 2010; 115: 2412–9.

25 Toffanin S, Hoshida Y, Lachenmayer A, *et al.* MicroRNA-Based Classification of Hepatocellular Carcinoma and Oncogenic Role of miR-517a. *Gastroenterology* 2011; 140: 1618–1628.e16.

26 Mah W-C, Thurnherr T, Chow PKH, *et al.* Methylation profiles reveal distinct subgroup of hepatocellular carcinoma patients with poor prognosis. *PLoS ONE* 2014; 9: e104158.

27 **Shen J, Wang S**, Zhang Y-J, *et al.* Exploring genome-wide DNA methylation profiles altered in hepatocellular carcinoma using Infinium HumanMethylation 450 BeadChips. *Epigenetics* 2013; 8. doi:10.4161/epi.23062.

28 Hemingway H, Croft P, Perel P, *et al.* Prognosis research strategy (PROGRESS) 1: A framework for researching clinical outcomes. *BMJ* 2013; 346: e5595–5.

29 McShane LM, Altman DG, Sauerbrei W, *et al.* Reporting recommendations for tumor marker prognostic studies (REMARK). Journal of the National Cancer Institute. 2005; 97: 1180–4.

30 **Li X, Zhou F**, Jiang C, *et al.* Identification of a DNA Methylome Profile of Esophageal Squamous Cell Carcinoma and Potential Plasma Epigenetic Biomarkers for Early Diagnosis. *PLoS ONE* 2014; 9: e103162.

31 Esteller M. Cancer epigenomics: DNA methylomes and histone-modification maps. *Nat Rev Genet* 2007; 8: 286–98.

32 Vickers KC, Shoucri BM, Levin MG, *et al.* MicroRNA-27b is a regulatory hub in lipid metabolism and is altered in dyslipidemia. *Hepatology* 2013; 57: 533–42.

33 Lee J-J, Drakaki A, Iliopoulos D, Struhl K. MiR-27b targets PPARγ to inhibit growth, tumor progression and the inflammatory response in neuroblastoma cells. *Oncogene* 2012; 31: 3818–

25.

34 Tanaka N, Moriya K, Kiyosawa K, Koike K, Gonzalez FJ, Aoyama T. PPARalpha activation is essential for HCV core protein-induced hepatic steatosis and hepatocellular carcinoma in mice. *J Clin Invest* 2008; 118: 683–94.

35 **Chang C-H, Lin J-W**, Wu L-C, Lai M-S, Chuang L-M, Chan KA. Association of thiazolidinediones with liver cancer and colorectal cancer in type 2 diabetes mellitus. *Hepatology* 2012; 55: 1462–72.

36 Vogelstein B, Papadopoulos N, Velculescu VE, Zhou S, Diaz LA, Kinzler KW. Cancer Genome Landscapes. *Science* 2013; 339: 1546–58.

37 Cui H, Kong Y, Xu M, Zhang H. Notch3 Functions as a Tumor Suppressor by Controlling Cellular Senescence. *Cancer Res* 2013; 73: 3451–9.

38 Berdasco M, Ropero S, Setien F, *et al.* Epigenetic inactivation of the Sotos overgrowth syndrome gene histone methyltransferase NSD1 in human neuroblastoma and glioma. *Proc Natl Acad Sci USA* 2009; 106: 21830–5.

39 **Gan L, Chen S**, Zhong J, *et al.* ZIC1 Is Downregulated through Promoter Hypermethylation, and Functions as a Tumor Suppressor Gene in Colorectal Cancer. *PLoS ONE* 2011; 6: e16916.

Figure 1

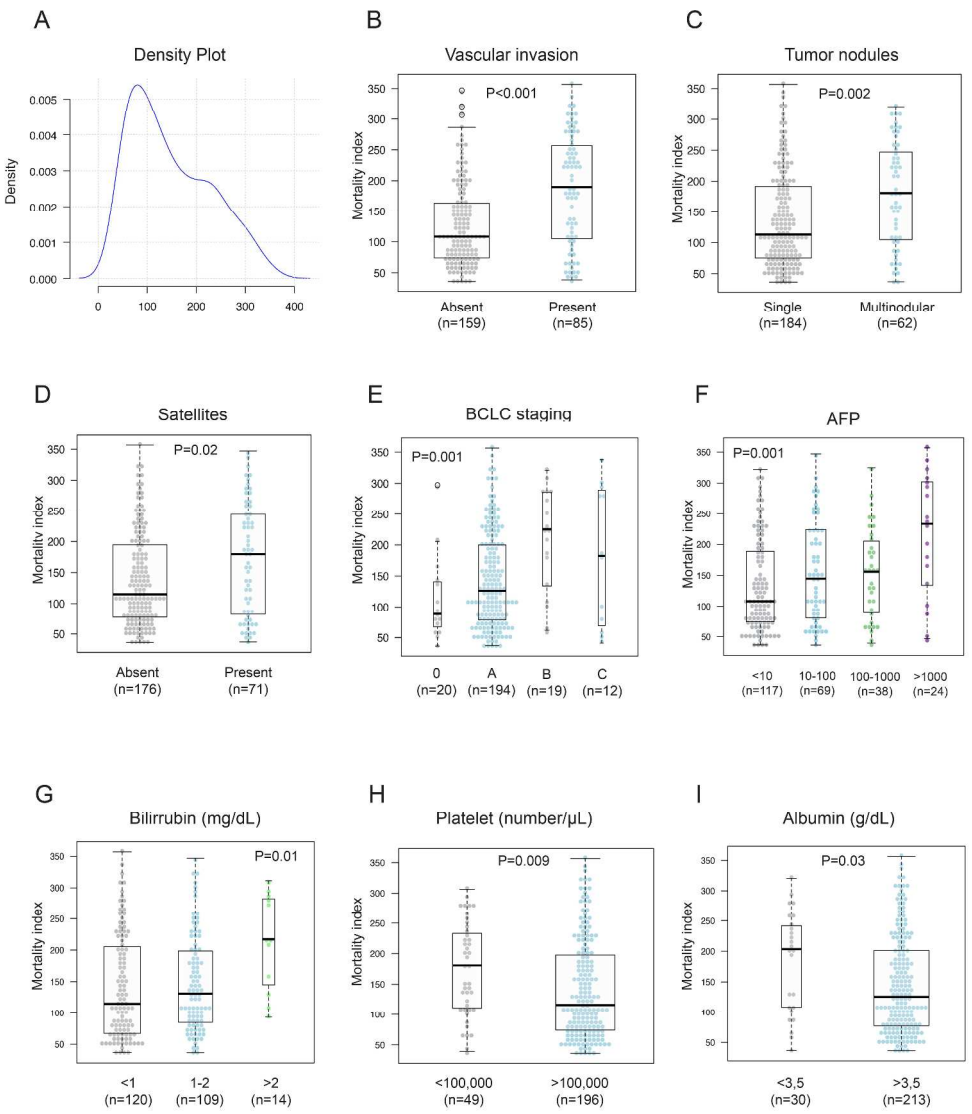

Figure 1
403x492mm (300 x 300 DPI)

Figure 2

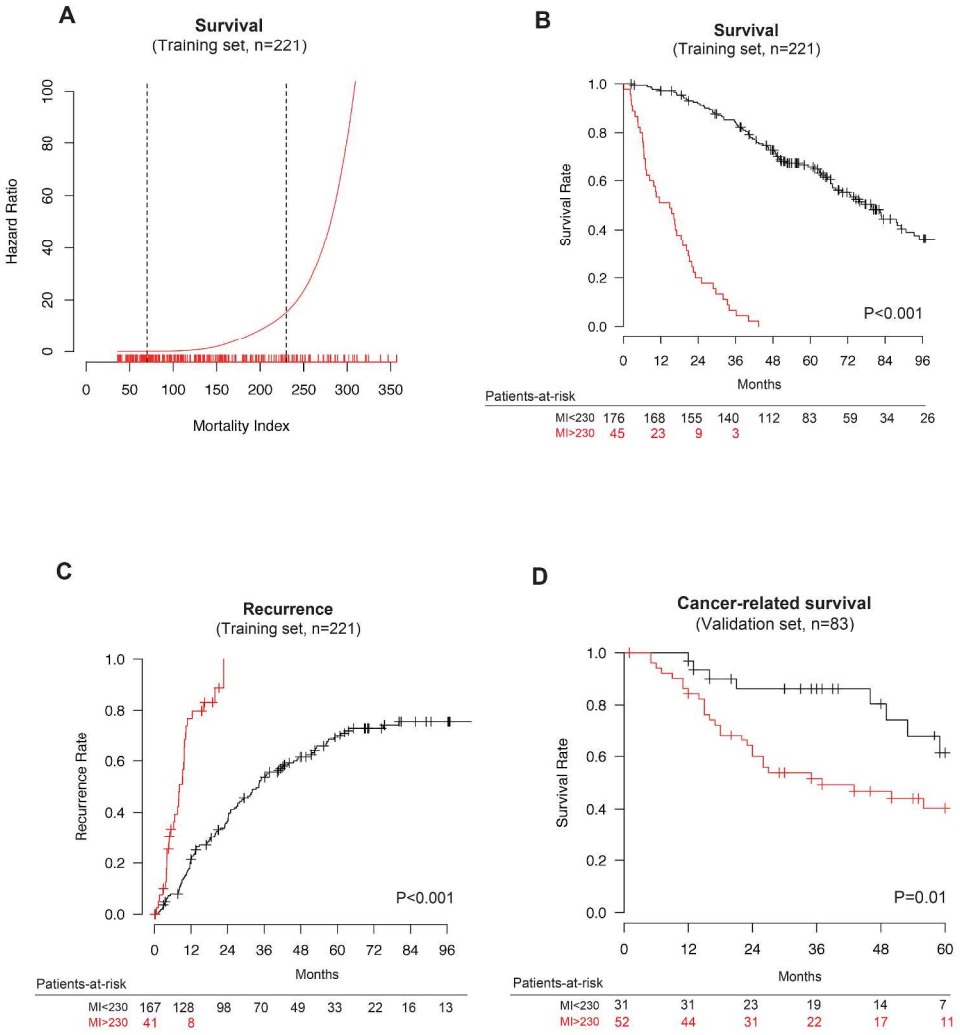

Figure 2
422x461mm (300 x 300 DPI)

Figure 3

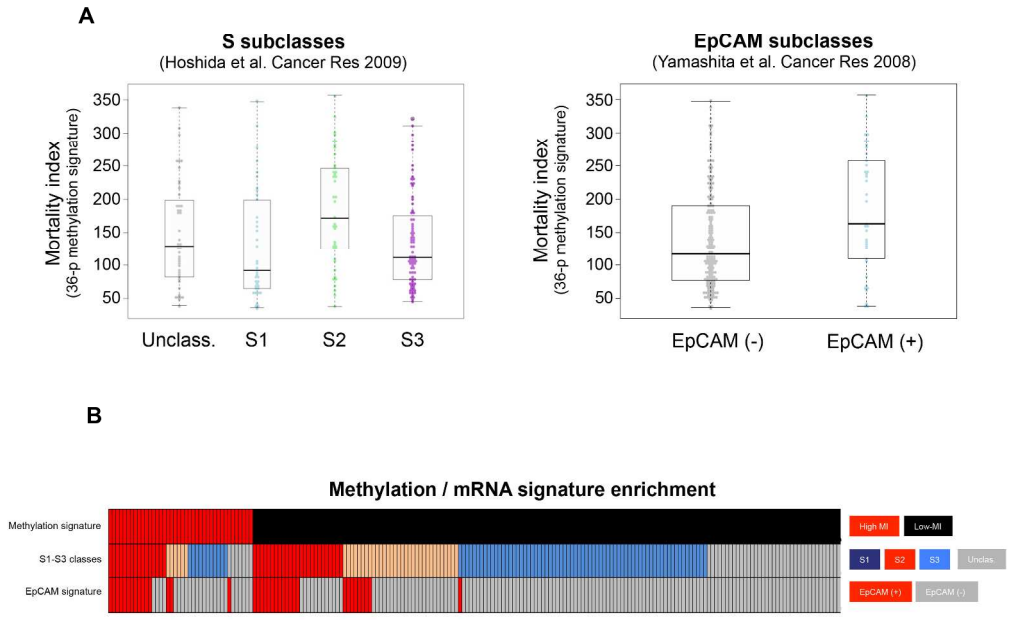

Figure 3
254x190mm (300 x 300 DPI)

Figure 4

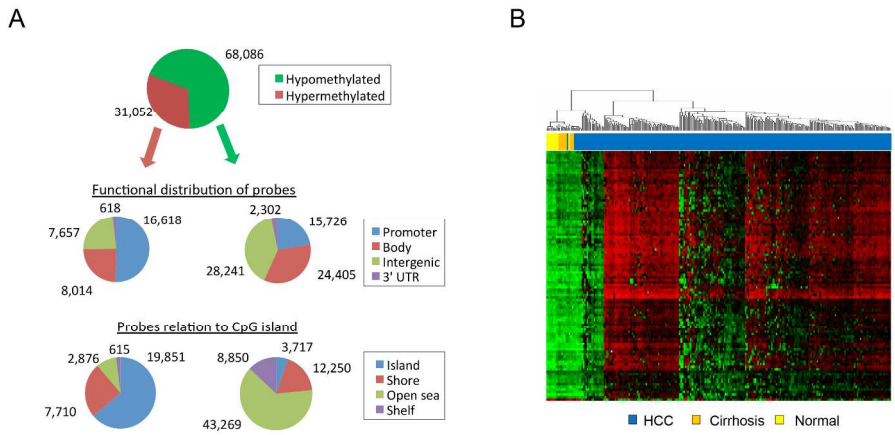

Figure 4
254x190mm (300 x 300 DPI)

Figure 5

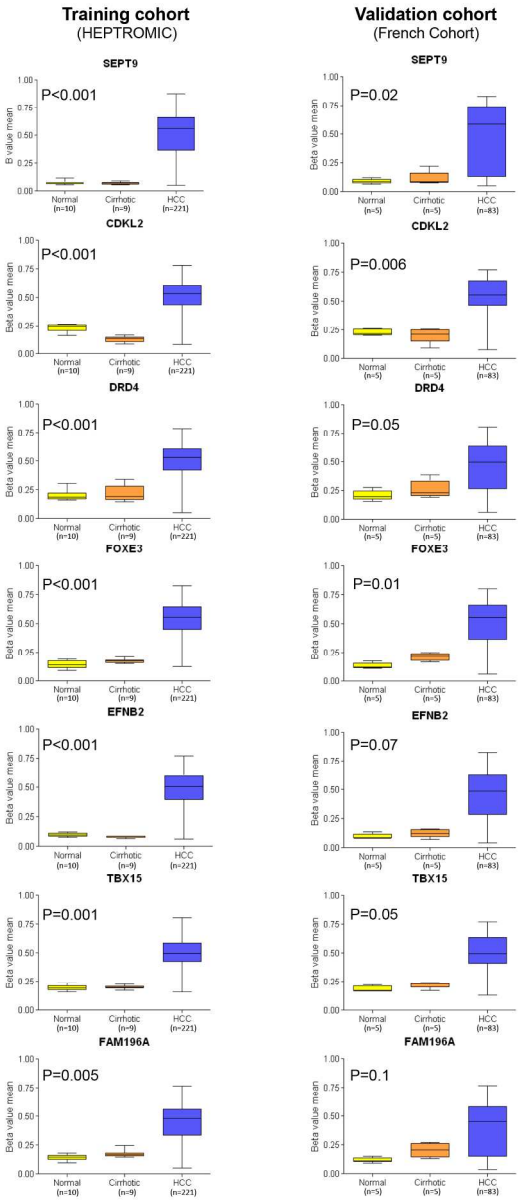

Figure 5
190x254mm (300 x 300 DPI)

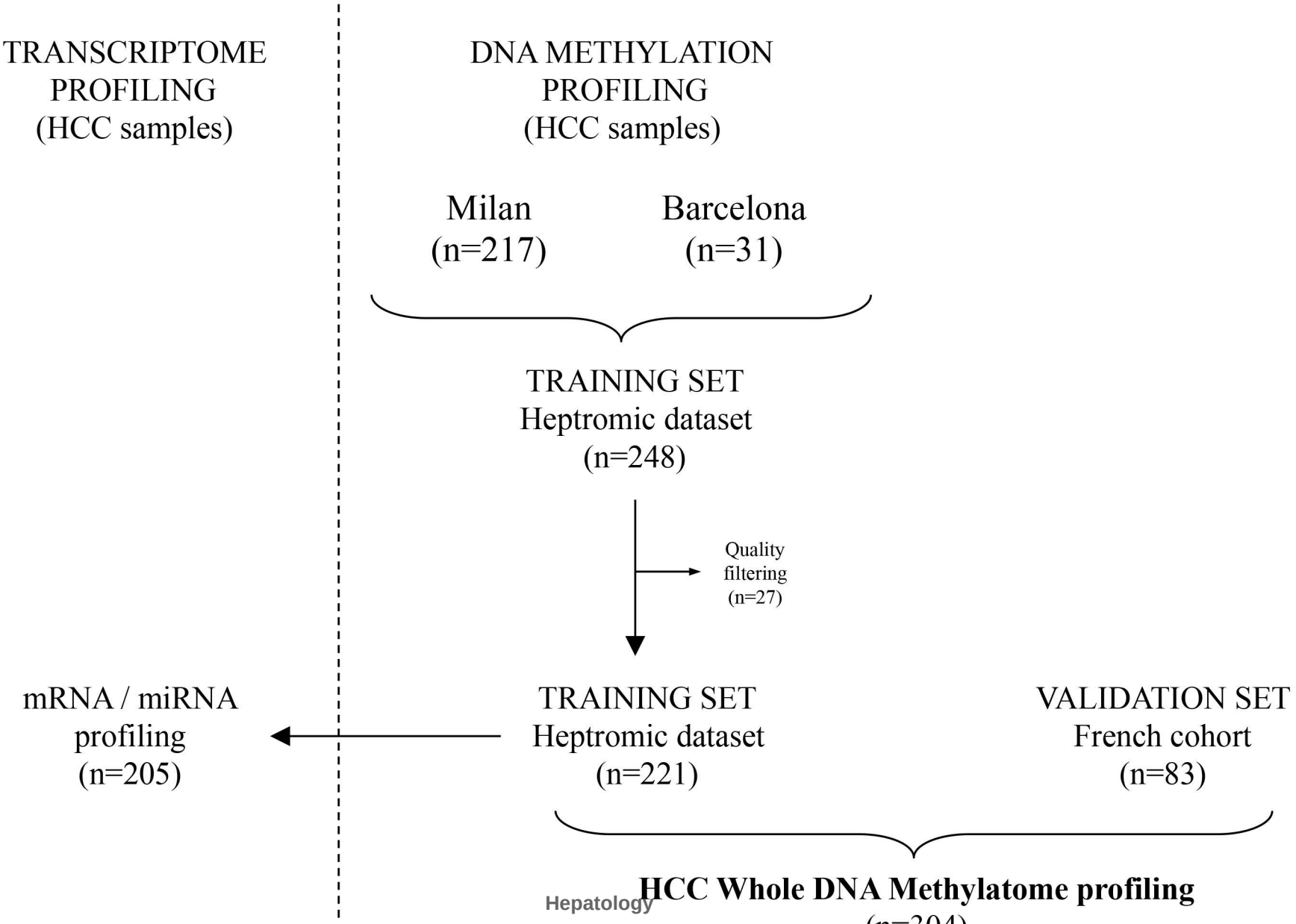

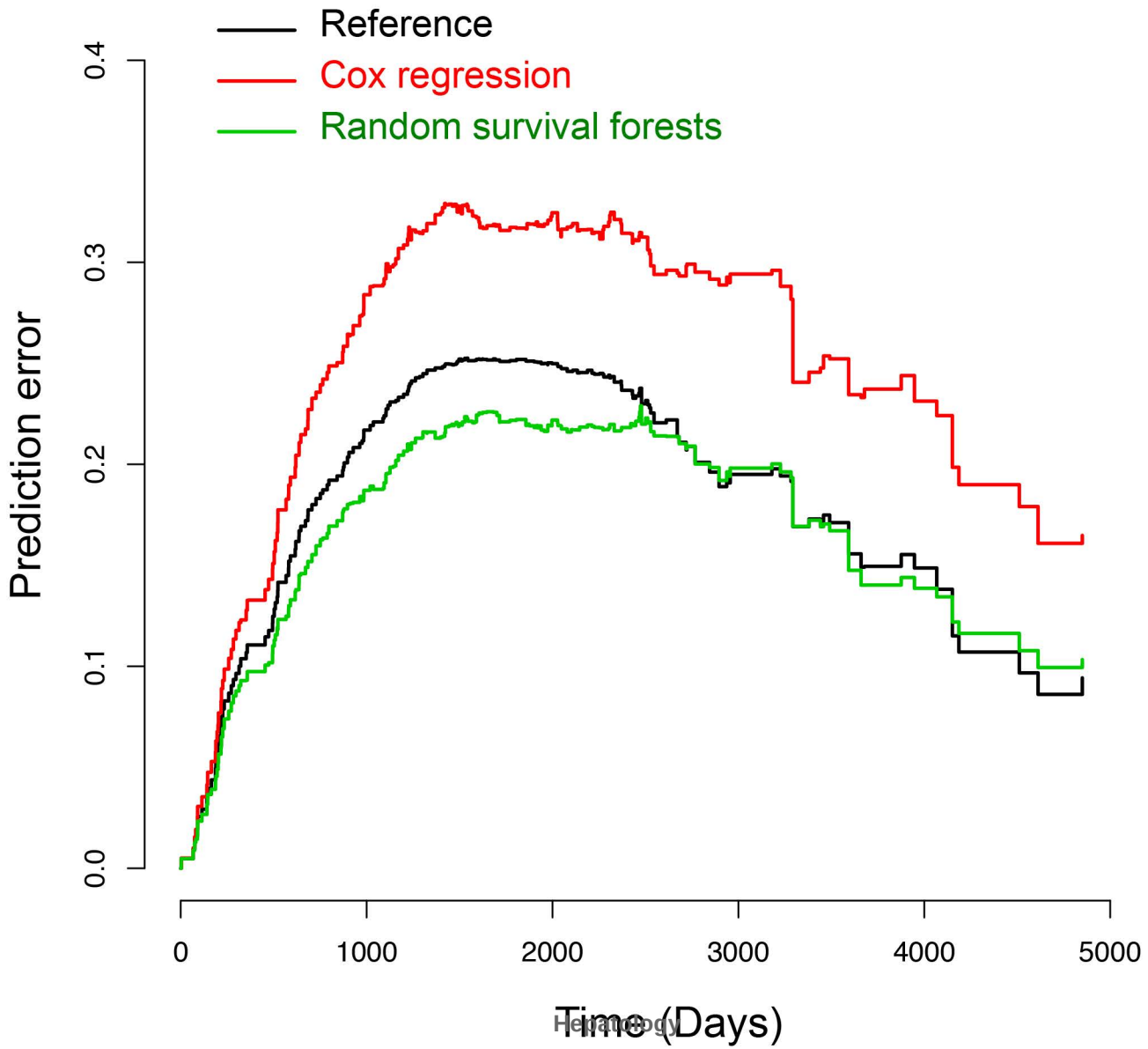

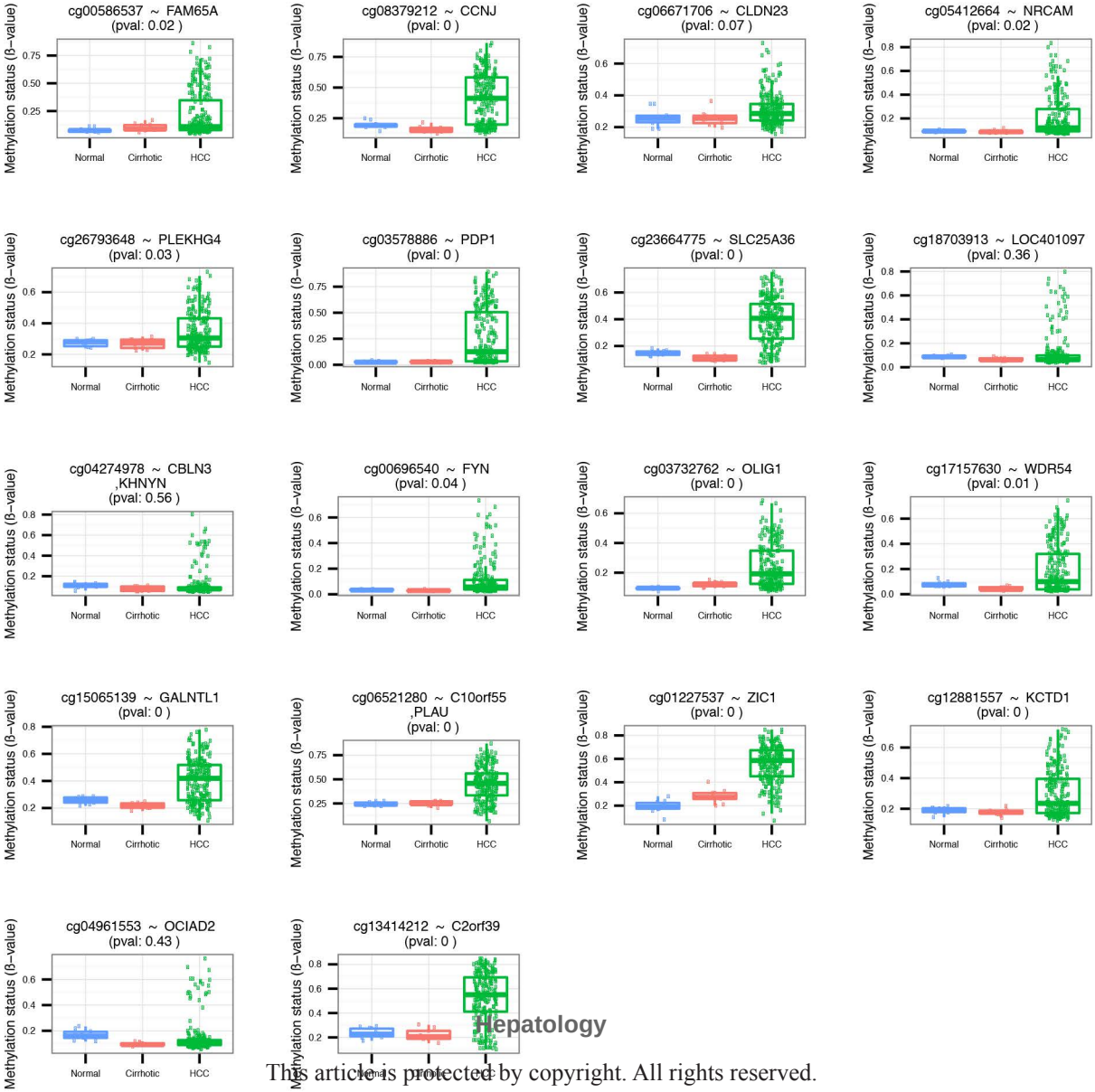

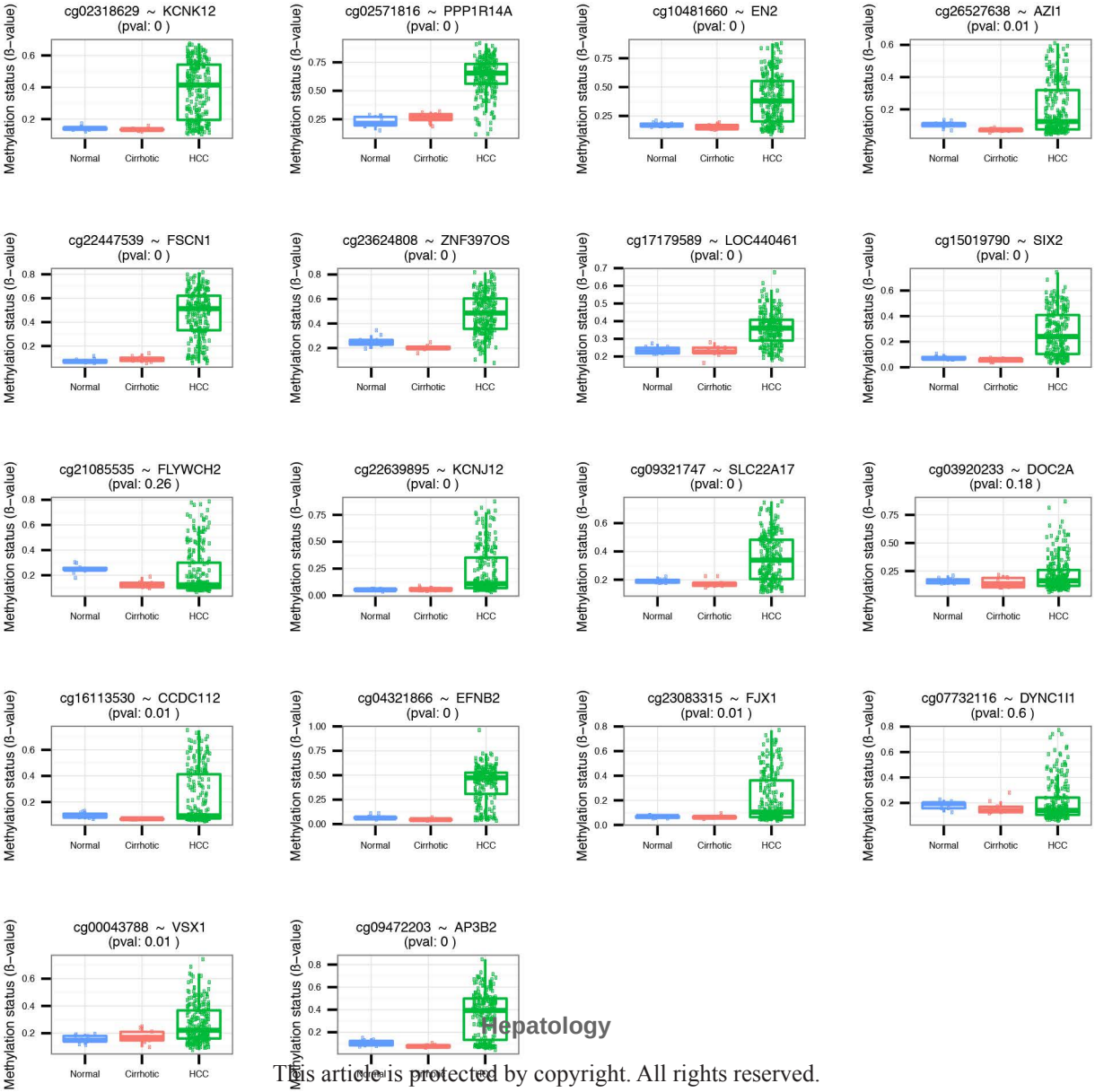

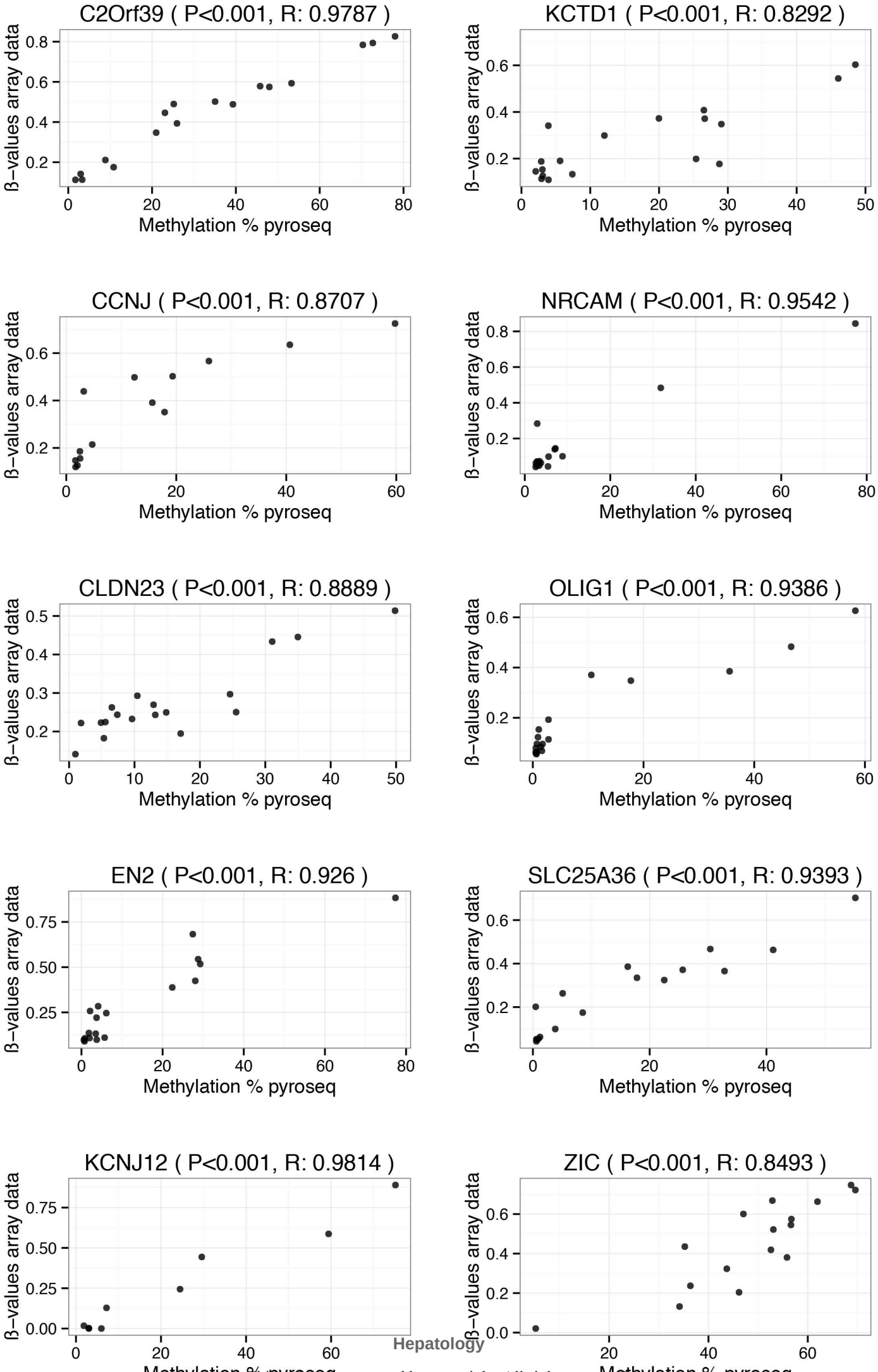

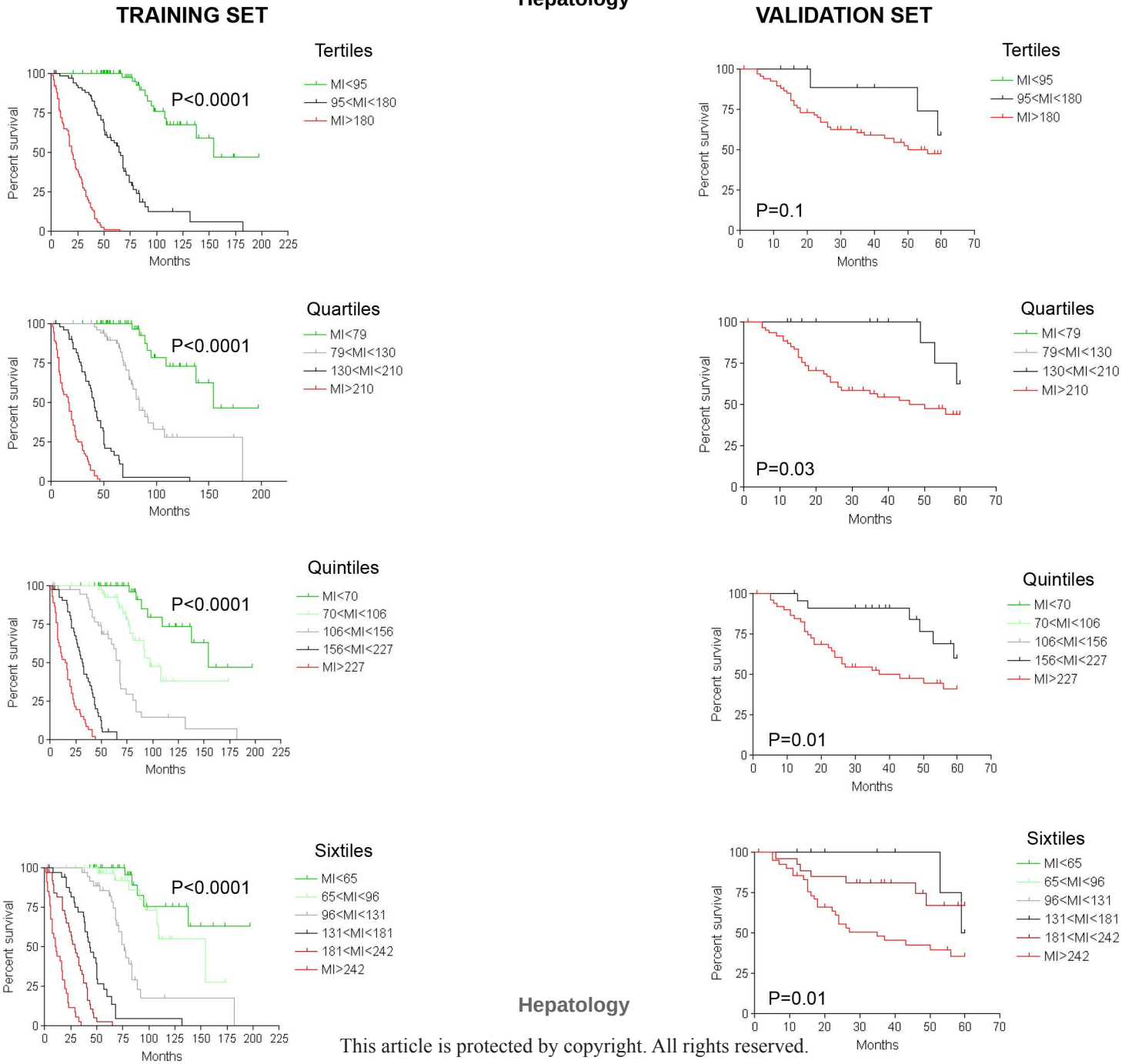

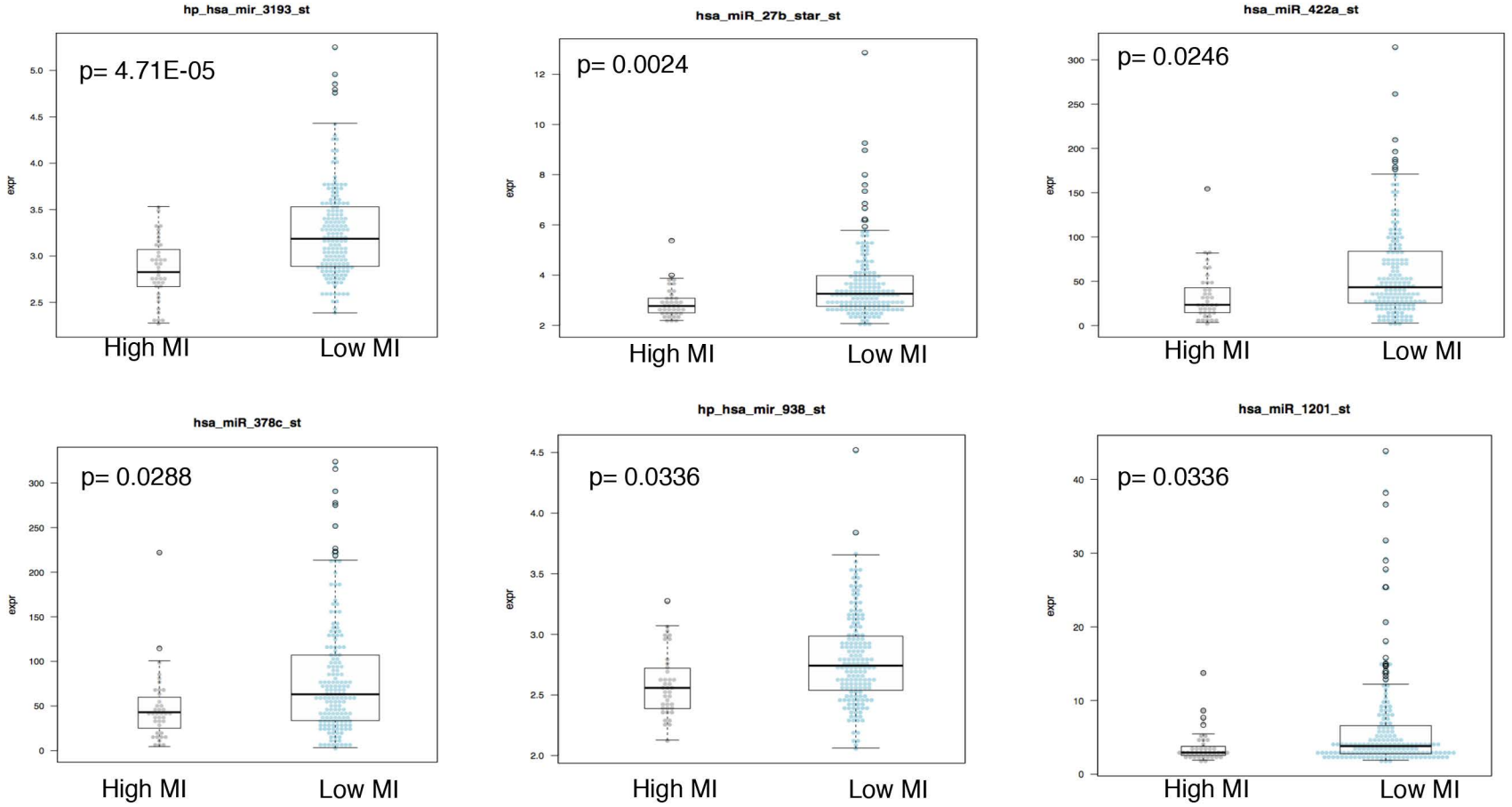

A

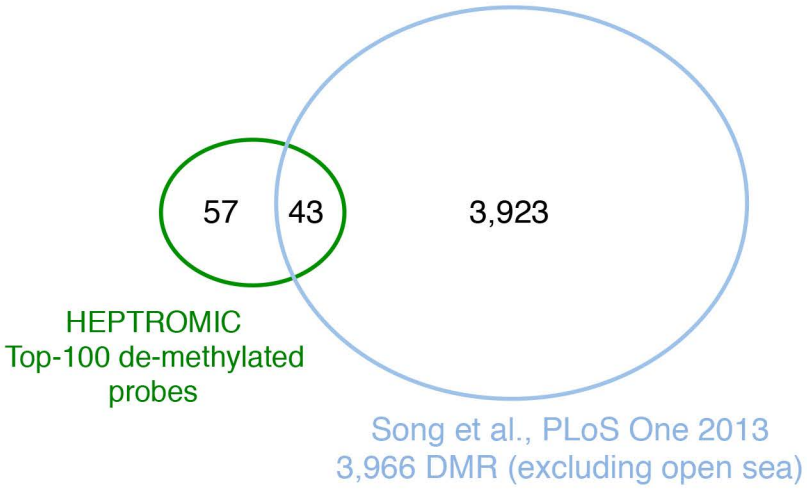

B

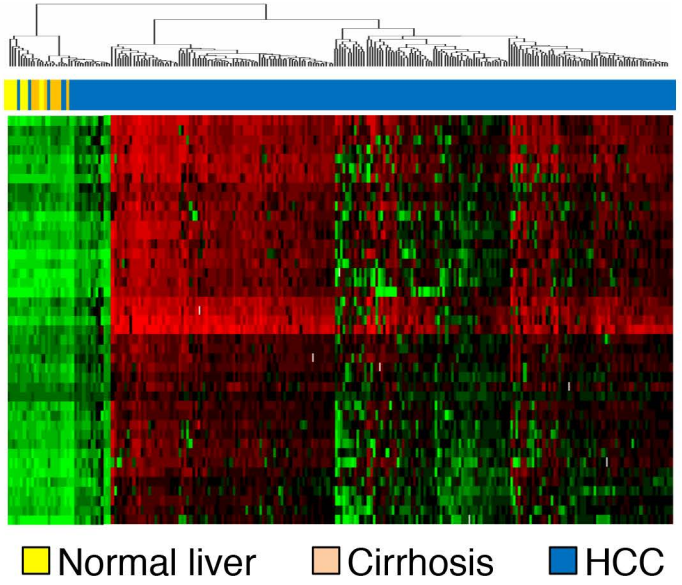

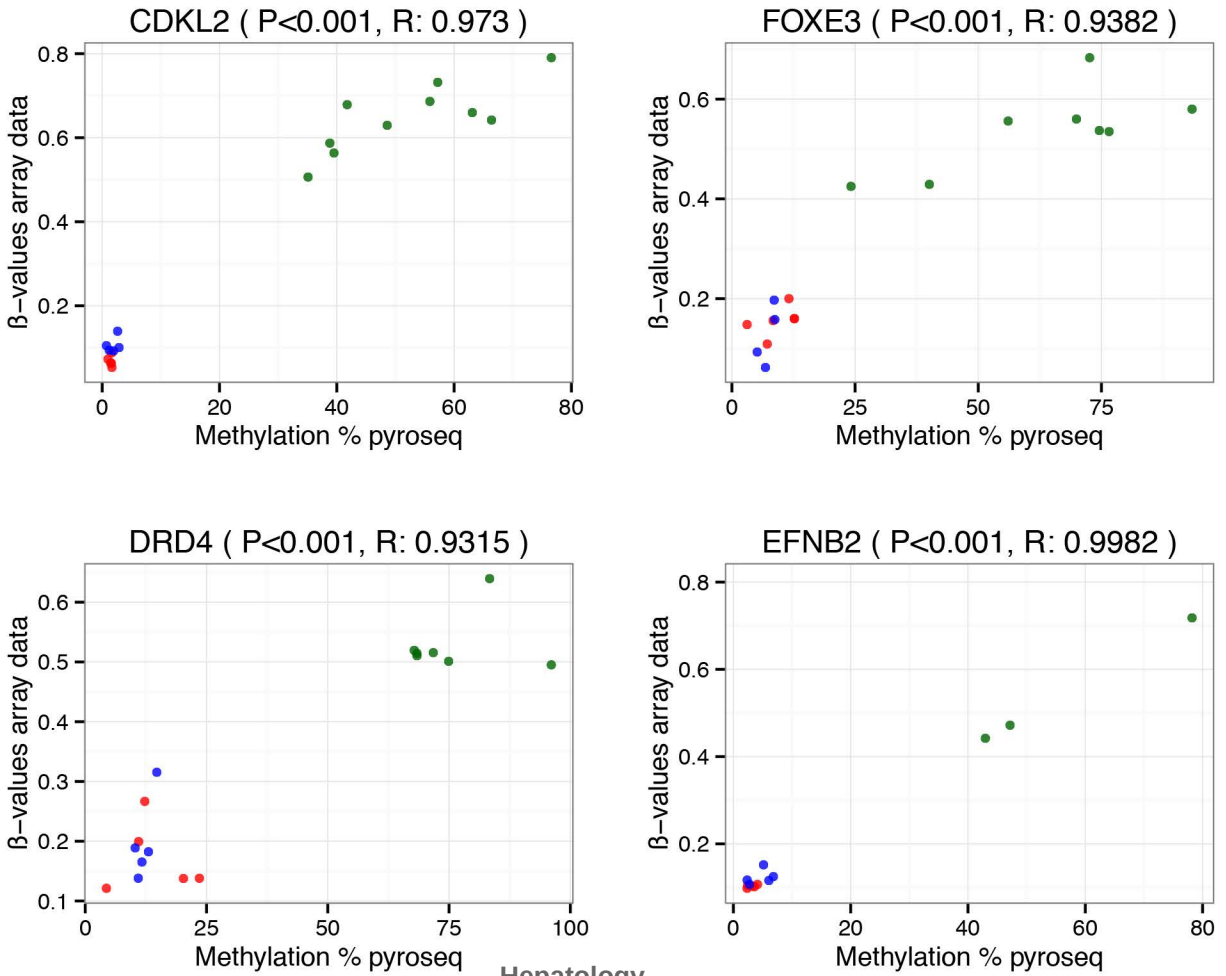

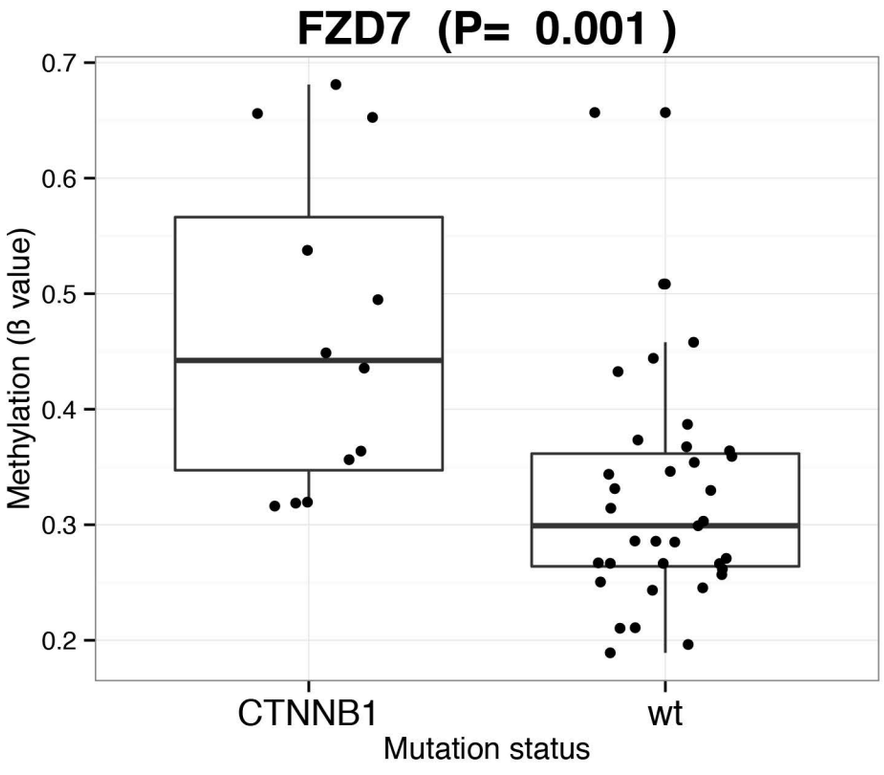

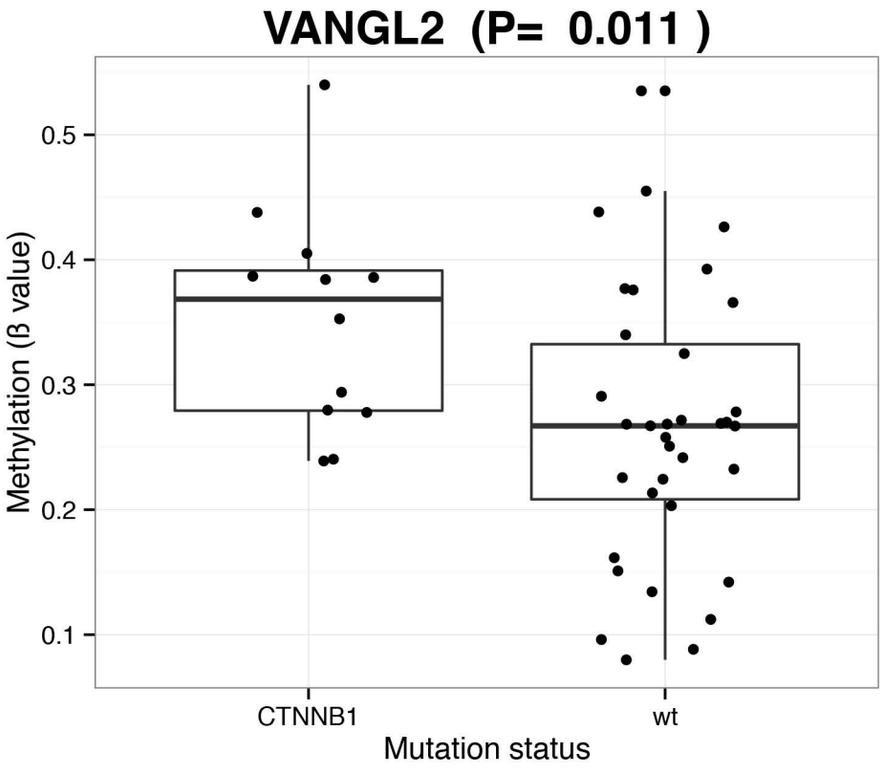

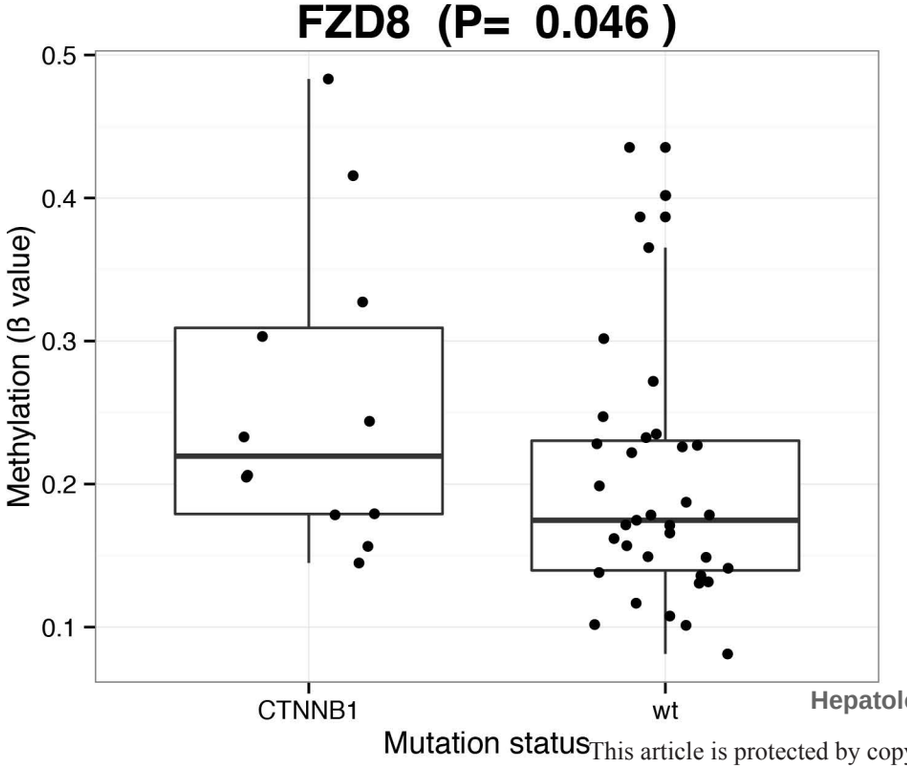

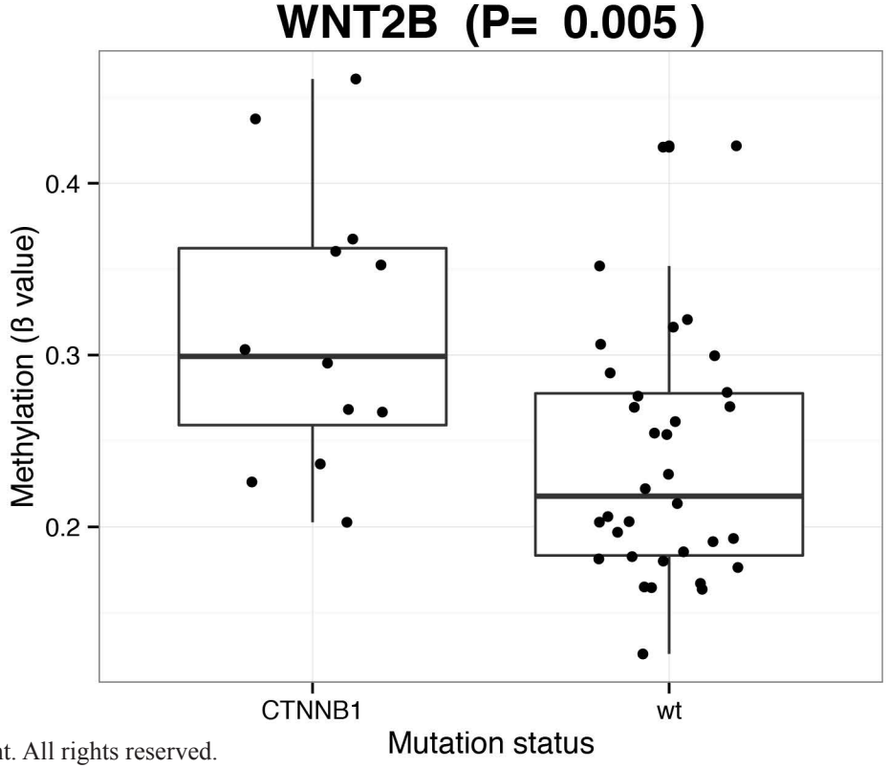

Supplementary Table 1: Primers for pyrosequencing

Gene	Sequence
CDKL2_FW_pyro	GGTTTTTGYGTGTTAGGGAGTAGAAT
CDKL2_RV_pyro	[Btn]CCAAACCTCCCTTCTTCTAAT
CDKL2_S	GTGTTAGGGAGTAGAATT
DRD4_FW_pyro	[Btn]AGGTTTTGTTAGATATTAGGTGGATTA
DRD4_RV_pyro	AACCCAATATTTACTCATCTTAAAA
DRD4_S	AACAAACCAACATC
FOXE3_FW_pyro	ATAGTTTGGTGAATTTGTAGT
FOXE3_RV_pyro	[Btn]AAACCCRACTACCTCAAATAAACCT
FOXE3_S	AGTTTGGTGAATTTGT
EFNB2_FW_pyro	GGGTGTTTTGATGGTTTTATGTAGAA
EFNB3_RV_pyro	[Btn]AAAAATTCCAATAAATAAACTCTAAAACTA
EFNB4_S	TGTTTTGATGGTTTTATGTAGA
C2Orf39_FW_pyro	GTTGGYGGTAGGTTGGGTTTAG
C2Orf39_RV_pyro	[Btn]CATAACAAAAATCCCTAATCCC
C2Orf39_S	GTTTGTTTTTAGTAATTAGTTTGAG
CCNJ_FW_pyro	TTAATTGGATTGGTTATTGTAGTGATTTAT
CCNJ_RV_pyro	[Btn]ACTCCRCATACAAAACCAAC
CCNJ_S	GATTTATTTTATAATTTT
KCNJ12_FW_pyro	AGGGGTTYGGGGTTAGGT
KCNJ12_RV_pyro	[Btn]AACTCAACTCRACAACTCCTCTAACTC
KCNJ12_S	GTGGTAGGTTGGTGTA
SLC25A36_FW_pyro	GATAGATATTAAGGGAATTGTTGGGTTATA
SLC25A36_RV_pyro	[Btn]CCCRACATAAACAAAAACTCCCATT
SLC25A36_S	GTTTATTTAGGTTAGGG
CLDN23_FW_pyro	[Btn]AAGGAAGGTAGGTTGTAGG
CLDN23_RV_pyro	ACTAACTAATTCAAAAAACCCTTCAC
CLDN23_S	CAAAAAACCCTTCACC
NRCAM_FW_pyro	[Btn]TGGAGTAGTTAGAGGGGATAG
NRCAM_RV_pyro	CCCCCRAACAAAACCCAATATCAC
NRCAM_S	ACTACCCAAAACCCTAA
EN2_FW_pyro	AAGTGTTTGTAGGAGGAGTGT
EN2_RV_pyro	[Btn]AAAAAAAAATAATATCACTCCCATTTAACT
EN2_S	GTTTAAGATAGGAAGT
KCTD1_FW_pyro	TGGGGGTTTTAGTGTGTAAT
KCTD1_RV_pyro	[Btn]ACAAATTAAAACAAATCCCTACCT
KCTD1_S	GTAGTGTATTGTGAAT
ZIC1_FW_pyro	TGGTTTGTTAAAAGGGGATGTT
ZIC1_RV_pyro	[Btn]ACCRTCCCCCCCTTAATAAATAAAAACA
ZIC1_S	ATAATATTTGGGATTGATGAG
OLIG1_FW_pyro	ATGTAGGATTTGAATTTGGTTATGG
OLIG1_RV_pyro	[Btn]CCTACAACRAACTACCCAACAATAAAATAT
OLIG1_S	GTAAGTTTTTTAAGATAGT

Supplementary Table 2: Methylation gene signature markers

	TargetID	UCSC_REFGENE_NAME
1	cg00043788	VSX1
2	cg00586537	FAM65A
3	cg00696540	FYN
4	cg01227537	ZIC1
5	cg02318629	KCNK12
6	cg02571816	PPP1R14A
7	cg03578886	PDP1
8	cg03732762	OLIG1
9	cg03920233	DOC2A
10	cg04274978	CBLN3; KHNYN
11	cg04321866	EFNB2
12	cg04961553	OCIAD2
13	cg05412664	NRCAM
14	cg06521280	C10orf55; PLAU
15	cg06671706	CLDN23
16	cg07732116	DYNC1I1
17	cg08379212	CCNJ
18	cg09321747	SLC22A17
19	cg09472203	AP3B2
20	cg10481660	EN2
21	cg12881557	KCTD1
22	cg13414212	C2orf39
23	cg15019790	SIX2
24	cg15065139	GALNTL1
25	cg16113530	CCDC112
26	cg17157630	WDR54
27	cg17179589	LOC440461
28	cg18703913	LOC401097
29	cg21085535	FLYWCH2
30	cg22447539	FSCN1
31	cg22639895	KCNJ12
32	cg23083315	FJX1
33	cg23624808	ZNF397OS
34	cg23664775	SLC25A36
35	cg26527638	AZI1
36	cg26793648	PLEKHG4

Supplementary table 3: Gene sets enrichment analysis

Gene sets enriched (FDR<0.25) in patients with high mortality index (>230)

Gene Set (ordered based on FDR value)	#genes	Normalized Enrichment Score	p-value	FDR(<0.25)	Database (http://www.broadinstitute.org/gsea/msigdb/)
WNT_SIGNALING	89	1,52	0,010	0,010	SuperArray
MOTOR_ACTIVITY	28	2,04	0,000	0,020	Gomf
YAMASHITA_LIVER_CANCER_EPCAM	46	1,90	0,002	0,036	HCCsignatures
ATP_DEPENDENT_RNA_HELICASE_ACTIVITY	16	1,90	0,004	0,040	Gomf
ATP_DEPENDENT_HELICASE_ACTIVITY	26	1,96	0,000	0,043	Gomf
HOSHIDA_S2	109	1,83	0,011	0,047	HCCsignatures
TUBULIN_BINDING	47	1,91	0,002	0,047	Gomf
DNA_POLYMERASE_ACTIVITY	18	1,87	0,000	0,048	Gomf
HELICASE_ACTIVITY	49	1,85	0,000	0,048	Gomf
CHROMATIN_BINDING	31	1,86	0,005	0,050	Gomf
BOYAULT_LIVER_CANCER_SUBCLASS_G12	30	1,79	0,011	0,051	HCCsignatures
RNA_DEPENDENT_ATPASE_ACTIVITY	17	1,81	0,015	0,051	Gomf
SPINDLE	39	1,93	0,008	0,054	GOcc
PROTEIN_C_TERMINUS_BINDING	71	1,83	0,000	0,054	Gomf
MICROTUBULE_MOTOR_ACTIVITY	16	1,92	0,002	0,056	Gomf
MICROTUBULE_ASSOCIATED_COMPLEX	47	1,88	0,002	0,056	GOcc
RNA_HELICASE_ACTIVITY	23	1,81	0,004	0,056	Gomf
CHIANG_LIVER_CANCER_SUBCLASS_PROLIFERATION	133	1,71	0,035	0,056	HCCsignatures
SPINDLE_POLE	18	1,89	0,004	0,059	GOcc
SPLICEOSOME	50	1,85	0,004	0,060	GOcc
CHROMATIN	35	1,83	0,005	0,061	GOcc
NUCLEAR_PORE	31	1,70	0,004	0,063	GOcc

CHROMOSOMAL_PART	96	1,78	0,014	0,065	GOcc
NUCLEOLUS	124	1,77	0,009	0,065	GOcc
CENTROSOME	55	1,69	0,018	0,065	GOcc
ORGANELLE_LUMEN	452	1,70	0,000	0,066	GOcc
CK19SIGNATURE_FDR010	149	1,66	0,049	0,066	HCCsignatures
MICROTUBULE	32	1,80	0,004	0,067	GOcc
BOYAULT_LIVER_CANCER_SUBCLASS_G3	132	1,71	0,030	0,067	HCCsignatures
TRANSCRIPTION_FACTOR_COMPLEX	89	1,76	0,002	0,069	GOcc
MEMBRANE_ENCLOSED_LUMEN	452	1,70	0,000	0,069	GOcc
NUCLEAR_LUMEN	382	1,79	0,005	0,071	GOcc
NUCLEAR_ENVELOPE	71	1,68	0,027	0,073	GOcc
NUCLEOPLASM	275	1,70	0,009	0,073	GOcc
CYTOSKELETAL_PART	228	1,67	0,007	0,074	GOcc
MICROTUBULE_CYTOSKELETON	148	1,96	0,000	0,074	GOcc
NUCLEOPLASM_PART	208	1,74	0,007	0,074	GOcc
SPINDLE_MICROTUBULE	16	1,70	0,015	0,077	GOcc
CHROMOSOME	123	1,72	0,029	0,080	GOcc
RNA_BINDING	253	1,76	0,013	0,081	Gomf
GOLGI_ASSOCIATED_VESICLE	29	1,70	0,013	0,081	GOcc
LEE_LIVER_CANCER_POOR_SURVIVAL	122	1,62	0,043	0,082	HCCsignatures
CCAGGTT,MIR-490	64	1,77	0,002	0,082	MIR
MICROTUBULE_ORGANIZING_CENTER	64	1,72	0,002	0,082	GOcc
PORE_COMPLEX	36	1,64	0,016	0,083	GOcc
SMALL_NUCLEAR_RIBONUCLEOPROTEIN_COMPLEX	22	1,65	0,020	0,083	GOcc
RIBONUCLEOPROTEIN_COMPLEX	142	1,71	0,011	0,084	GOcc
MICROTUBULE_BINDING	33	1,74	0,009	0,085	Gomf
NUCLEAR_MEMBRANE_PART	42	1,64	0,015	0,086	GOcc
GTTAAAG,MIR-302B	68	1,73	0,005	0,093	MIR

SIG_INSULIN_RECEPTOR_PATHWAY_IN_CARDIAC_MYOCYTES	51	1,54	0,019	0,094	SignalGateway
REACTOME_MITOTIC_G2_G2_M_PHASES	74	1,76	0,011	0,099	Reactome
REACTOME_ACTIVATION_OF_CHAPERONE_GENES_BY_XBP1S	43	1,68	0,017	0,101	Reactome
REACTOME_GLOBAL_GENOMIC_NER_GG_NER	31	1,74	0,007	0,101	Reactome
REACTOME_ACTIVATION_OF_THE_PRE_REPLICATIVE_COMPLEX	30	1,74	0,027	0,101	Reactome
REACTOME_SHC_MEDIATED_CASCADE	28	1,72	0,005	0,102	Reactome
REACTOME_DEPOSITION_OF_NEW_CENPA_CONTAINING_NUCLEOSOMES_AT_THE_CENTROMERE	55	1,68	0,030	0,102	Reactome
REACTOME_INFLUENZA_VIRAL_RNA_TRANSCRIPTION_AND_REPLICATION	100	1,75	0,019	0,103	Reactome
REACTOME_CELL_CYCLE_MITOTIC	303	1,74	0,020	0,103	Reactome
REACTOME_RNA_POL_II_PRE_TRANSCRIPTION_EVENTS	57	1,69	0,017	0,103	Reactome
REACTOME_ARMS_MEDIATED_ACTIVATION	17	1,68	0,022	0,103	Reactome
REACTOME_DNA_STRAND_ELONGATION	30	1,72	0,030	0,103	Reactome
REACTOME_E2F_MEDIATED_REGULATION_OF_DNA_REPLICATION	33	1,76	0,013	0,103	Reactome
REACTOME_SIGNALLING_TO_P38_VIA_RIT_AND_RIN	15	1,69	0,022	0,103	Reactome
REACTOME_HIV_LIFE_CYCLE	112	1,76	0,004	0,104	Reactome
REACTOME_DEADENYLATION_OF_MRNA	19	1,69	0,009	0,104	Reactome
REACTOME_NONSENSE_MEDIATED_DECAY_ENHANCED_BY_THE_EXON_JUNCTION_COMPLEX	103	1,73	0,027	0,104	Reactome
REACTOME_SIGNAL_TRANSDUCTION_BY_L1	34	1,68	0,007	0,105	Reactome
MYC_UP.V1_UP	174	1,53	0,044	0,105	C6
REACTOME_SIGNALLING_TO_RAS	26	1,69	0,014	0,105	Reactome
PRC2_EDD_UP.V1_UP	191	1,55	0,018	0,105	C6
REACTOME_SIGNALLING_TO_ERKS	35	1,73	0,007	0,106	Reactome
REACTOME_DEADENYLATION_DEPENDENT_MRNA_DECAY	44	1,70	0,004	0,106	Reactome
REACTOME_PROTEIN_FOLDING	49	1,70	0,000	0,106	Reactome
REACTOME_TRANSLATION	143	1,70	0,021	0,107	Reactome
REACTOME_FRS2_MEDIATED_CASCADE	36	1,75	0,008	0,107	Reactome
REACTOME_DIABETES_PATHWAYS	124	1,71	0,005	0,107	Reactome
REACTOME_LAGGING_STRAND_SYNTHESIS	19	1,76	0,007	0,108	Reactome

REACTOME_RNA_POL_II_TRANSCRIPTION_PRE_INITIATION_AND_PROMOTER_OPENING	38	1,67	0,018	0,108	Reactome
REACTOME_PROLONGED_ERK_ACTIVATION_EVENTS	19	1,67	0,018	0,109	Reactome
REACTOME_METABOLISM_OF_NON_CODING_RNA	47	1,70	0,020	0,109	Reactome
REACTOME_PEPTIDE_CHAIN_ELONGATION	84	1,71	0,030	0,109	Reactome
ATPASE_ACTIVITY	110	1,71	0,009	0,109	Gomf
REACTOME_NUCLEOTIDE_EXCISION_REPAIR	46	1,71	0,009	0,109	Reactome
WANG_LIVER_CANCER_RECURRENCE	16	1,55	0,046	0,109	HCCsignatures
REACTOME_TRANSCRIPTION	192	1,66	0,015	0,110	Reactome
REACTOME_INFLUENZA_LIFE_CYCLE	134	1,77	0,013	0,110	Reactome
REACTOME_3_UTR_MEDIATED_TRANSLATIONAL_REGULATION	103	1,66	0,041	0,110	Reactome
REACTOME_TRANSPORT_OF_RIBONUCLEOPROTEINS_INTO_THE_HOST_NUCLEUS	27	1,66	0,026	0,112	Reactome
REACTOME_NGF_SIGNALLING_VIA_TRKA_FROM_THE_PLASMA_MEMBRANE	132	1,65	0,005	0,112	Reactome
DNA_HELICASE_ACTIVITY	24	1,69	0,011	0,113	Gomf
PHOSPHATASE_REGULATOR_ACTIVITY	26	1,69	0,007	0,114	Gomf
REACTOME_MITOTIC_M_M_G1_PHASES	168	1,77	0,015	0,115	Reactome
CHROMATIN_REMODELING_COMPLEX	17	1,59	0,046	0,115	GOcc
REACTOME_INSULIN_RECEPTOR_SIGNALLING_CASCADE	82	1,78	0,000	0,115	Reactome
REACTOME_MRNA_SPLICING	107	1,64	0,048	0,116	Reactome
REACTOME_SYNTHESIS_OF_DNA	90	1,64	0,027	0,116	Reactome
REACTOME_SRP_DEPENDENT_COTRANSLATIONAL_PROTEIN_TARGETING_TO_MEMBRANE	107	1,77	0,012	0,116	Reactome
TCTAGAG,MIR-517	46	1,80	0,000	0,116	MIR
STRUCTURAL_CONSTITUENT_OF_RIBOSOME	79	1,68	0,022	0,117	Gomf
REACTOME_TRANSCRIPTION_COUPLED_NER_TC_NER	41	1,64	0,031	0,117	Reactome
REACTOME_PREFOLDIN_MEDIATED_TRANSFER_OF_SUBSTRATE_TO_CCT_TRIC	25	1,64	0,018	0,117	Reactome
NUCLEAR_BODY	32	1,58	0,040	0,118	GOcc
REACTOME_RECRUITMENT_OF_MITOTIC_CENTROSOME_PROTEINS_AND_COMPLEXES	59	1,62	0,028	0,118	Reactome
REACTOME_S_PHASE	106	1,63	0,029	0,119	Reactome
REACTOME_RNA_POL_II_TRANSCRIPTION	100	1,61	0,020	0,119	Reactome

REACTOME_MRNA_PROCESSING	154	1,61	0,045	0,119	Reactome
REACTOME_M_G1_TRANSITION	78	1,62	0,029	0,119	Reactome
REACTOME_RESOLUTION_OF_AP_SITES_VIA_THE_MULTIPLE_NUCLEOTIDE_PATCH_REPLACEMENT_PATHWAY	17	1,63	0,042	0,119	Reactome
REACTOME_LOSS_OF_NLP_FROM_MITOTIC_CENTROSOMES	52	1,61	0,027	0,119	Reactome
REACTOME_MRNA_SPLICING_MINOR_PATHWAY	42	1,62	0,028	0,119	Reactome
REACTOME_APC_CDC20_MEDIATED_DEGRADATION_OF_NEK2A	21	1,63	0,030	0,119	Reactome
INTERPHASE_OF_MITOTIC_CELL_CYCLE	61	1,72	0,017	0,119	Gobp
REACTOME_L1CAM_INTERACTIONS	83	1,62	0,012	0,120	Reactome
REACTOME_SIGNALING_BY_FGFR	108	1,61	0,008	0,120	Reactome
REACTOME_BASE_EXCISION_REPAIR	19	1,61	0,045	0,120	Reactome
RIBONUCLEOPROTEIN_COMPLEX_BIOGENESIS_AND_ASSEMBLY	82	1,74	0,015	0,121	Gobp
REACTOME_NEP_NS2_INTERACTS_WITH_THE_CELLULAR_EXPORT_MACHINERY	27	1,63	0,033	0,121	Reactome
GACAGGG,MIR-339	66	1,67	0,002	0,121	MIR
REACTOME_METABOLISM_OF_PROTEINS	415	1,78	0,004	0,122	Reactome
WELCSH_BRCA1_TARGETS_DN	137	1,99	0,000	0,123	CGP
CELL_CYCLE_PHASE	167	1,71	0,035	0,123	Gobp
M_PHASE_OF_MITOTIC_CELL_CYCLE	85	1,73	0,022	0,123	Gobp
MITOSIS	82	1,72	0,022	0,124	Gobp
REACTOME_SHC_RELATED_EVENTS	15	1,88	0,002	0,124	Reactome
REACTOME_DNA_REPLICATION	188	1,78	0,017	0,125	Reactome
ESTABLISHMENT_AND_OR_MAINTENANCE_OF_CHROMATIN_ARCHITECTURE	74	1,70	0,014	0,126	Gobp
MRNA_PROCESSING_GO_0006397	70	1,74	0,015	0,127	Gobp
ST_G_ALPHA_I_PATHWAY	35	1,60	0,011	0,127	SignalTransductionKE
DNA_DEPENDENT_DNA_REPLICATION	54	1,69	0,032	0,127	Gobp
TRANSCRIPTION_INITIATION_FROM_RNA_POLYMERASE_II_PROMOTER	29	1,70	0,015	0,129	Gobp
MITOCHONDRIAL_OUTER_MEMBRANE	18	1,56	0,049	0,129	GOcc
PROTEIN_N_TERMINUS_BINDING	36	1,66	0,008	0,130	Gomf
NUCLEAR_MEMBRANE	50	1,56	0,031	0,130	GOcc

RNA_SPLICING	87	1,68	0,015	0,130	Gobp
COATED_VESICLE	47	1,55	0,018	0,130	GOcc
REACTOME_METABOLISM_OF_RNA	250	1,82	0,004	0,130	Reactome
MICROTUBULE_BASED_PROCESS	80	1,68	0,007	0,131	Gobp
REACTOME_POST_CHAPERONIN_TUBULIN_FOLDING_PATHWAY	16	1,59	0,035	0,131	Reactome
BIOCARTA_INSULIN_PATHWAY	21	1,65	0,009	0,131	BIOCARTA
NUCLEOBASENUCLEOSIDENUCLEOTIDE_AND_NUCLEIC_ACID_TRANSPORT	30	1,74	0,005	0,132	Gobp
REACTOME_MITOTIC_PROMETAPHASE	86	1,78	0,019	0,132	Reactome
REACTOME_SHC1_EVENTS_IN_EGFR_SIGNALING	15	1,59	0,032	0,132	Reactome
REACTOME_METABOLISM_OF_MRNA	206	1,79	0,002	0,132	Reactome
REACTOME_G1_S_TRANSITION	106	1,59	0,043	0,132	Reactome
REACTOME_PROCESSING_OF_CAPPED_INTRON_CONTAINING_PRE_MRNA	136	1,59	0,065	0,133	Reactome
RPS14_DN.V1_DN	183	1,56	0,041	0,133	C6
COATED_VESICLE_MEMBRANE	17	1,54	0,043	0,133	GOcc
REACTOME_CYCLIN_A_B1_ASSOCIATED_EVENTS_DURING_G2_M_TRANSITION	15	1,58	0,068	0,134	Reactome
CONDENSED_CHROMOSOME	33	1,52	0,064	0,134	GOcc
REACTOME_EXTENSION_OF_TELOMERES	27	1,89	0,002	0,135	Reactome
MEMBRANE_COAT	17	1,52	0,058	0,135	GOcc
PROTEASOME_COMPLEX	23	1,50	0,066	0,135	GOcc
DNA_DIRECTED_RNA_POLYMERASEII_HOLOENZYME	66	1,50	0,025	0,135	GOcc
RNA_EXPORT_FROM_NUCLEUS	19	1,67	0,018	0,136	Gobp
PROTEIN_DNA_COMPLEX_ASSEMBLY	48	1,75	0,004	0,136	Gobp
TRANSCRIPTION_INITIATION	35	1,75	0,011	0,136	Gobp
RRNA_PROCESSING	15	1,66	0,022	0,137	Gobp
INTERPHASE	67	1,66	0,026	0,137	Gobp
ENDOMEMBRANE_SYSTEM	218	1,51	0,030	0,137	GOcc
CSR_LATE_UP.V1_UP	168	1,67	0,010	0,137	C6
REACTOME_LATE_PHASE_OF_HIV_LIFE_CYCLE	99	1,83	0,000	0,138	Reactome

MICROTUBULE_ORGANIZING_CENTER_PART	19	1,50	0,048	0,138	GOcc
SIG_IL4RECEPTOR_IN_B_LYPHOCYTES	27	1,26	0,164	0,139	SignalGateway
COATED_MEMBRANE	17	1,52	0,058	0,139	GOcc
PERINUCLEAR_REGION_OF_CYTOPLASM	54	1,51	0,023	0,139	GOcc
BIOCARTA_ERK_PATHWAY	28	1,86	0	0,140	BIOCARTA
CELL_CYCLE_PROCESS	189	1,76	0,018	0,140	Gobp
ORGANELLE_OUTER_MEMBRANE	24	1,49	0,058	0,140	GOcc
REACTOME_NEGATIVE_REGULATION_OF_FGFR_SIGNALING	36	1,79	0,005	0,140	Reactome
CHROMOSOMEPERICENTRIC_REGION	31	1,53	0,085	0,141	GOcc
KINETOCHORE	25	1,52	0,069	0,141	GOcc
M_PHASE	111	1,65	0,046	0,141	Gobp
TCTGATA,MIR-361	87	1,64	0,005	0,141	MIR
ER_GOLGI_INTERMEDIATE_COMPARTMENT	23	1,48	0,092	0,141	GOcc
NUCLEAR_CHROMOSOME	54	1,48	0,059	0,142	GOcc
REACTOME_CELL_CYCLE	387	1,80	0,013	0,142	Reactome
CHROMATIN_REMODELING	25	1,64	0,031	0,143	Gobp
REACTOME_SIGNALING_BY_FGFR_IN_DISEASE	121	1,57	0,013	0,143	Reactome
DNA_REPLICATION	98	1,78	0,002	0,143	Gobp
REACTOME_UNFOLDED_PROTEIN_RESPONSE	75	1,81	0,009	0,143	Reactome
PROTEIN_RNA_COMPLEX_ASSEMBLY	63	1,63	0,040	0,143	Gobp
BIOCARTA_MCM_PATHWAY	18	1,66	0,028	0,144	BIOCARTA
REACTOME_DARPP_32_EVENTS	24	1,57	0,017	0,145	Reactome
REACTOME_ACTIVATION_OF_THE_MRNA_UPON_BINDING_OF_THE_CAP_BINDING_COMPLEX_AND_EIFS_AND_SUBSEQUENT_BINDING_TO_43S	54	1,56	0,078	0,145	Reactome
RAS_GTPASE_BINDING	25	1,60	0,022	0,146	Gomf
BIOCARTA_WNT_PATHWAY	26	1,70	0,000	0,146	BIOCARTA
RRNA_METABOLIC_PROCESS	16	1,64	0,033	0,147	Gobp
REACTOME_ELONGATION_ARREST_AND_RECOVERY	31	1,56	0,045	0,147	Reactome
REGULATION_OF_TRANSCRIPTION_FROM_RNA_POLYMERASE_II_PROMOTER	287	1,64	0,005	0,148	Gobp

CHROMATIN_MODIFICATION	52	1,62	0,021	0,149	Gobp
TCCAGAG,MIR-518C	143	1,58	0,008	0,149	MIR
TRANSCRIPTION_COREPRESSOR_ACTIVITY	91	1,60	0,000	0,150	Gomf
CELL_CYCLE_GO_0007049	311	1,76	0,007	0,150	Gobp
REACTOME_REGULATION_OF_MITOTIC_CELL_CYCLE	76	1,54	0,071	0,151	Reactome
REACTOME_CELL_CYCLE_CHECKPOINTS	111	1,53	0,076	0,151	Reactome
ATPASE_ACTIVITY_COUPLED	91	1,62	0,007	0,151	Gomf
REACTOME_GOLGI_ASSOCIATED_VESICLE_BIOGENESIS	51	1,54	0,051	0,152	Reactome
REACTOME_FORMATION_OF_THE_TERNARY_COMPLEX_AND_SUBSEQUENTLY_THE_43S_COMPLEX	46	1,54	0,089	0,152	Reactome
REACTOME_HIV_INFECTION	191	1,54	0,045	0,152	Reactome
REACTOME_SIGNALING_BY_EGFR_IN_CANCER	105	1,54	0,016	0,153	Reactome
REACTOME_PROCESSIVE_SYNTHESIS_ON_THE_LAGGING_STRAND	15	1,85	0,000	0,154	Reactome
ORGANELLE_ENVELOPE	164	1,46	0,085	0,154	GOcc
REACTOME_FORMATION_OF_RNA_POL_II_ELONGATION_COMPLEX_	41	1,55	0,039	0,154	Reactome
DNA_DEPENDENT_ATPASE_ACTIVITY	21	1,62	0,035	0,154	Gomf
REACTOME_ACTIVATION_OF_ATR_IN_RESPONSE_TO_REPLICATION_STRESS	35	1,54	0,097	0,154	Reactome
DNA_PACKAGING	34	1,88	0,002	0,154	Gobp
GTAGGCA,MIR-189	27	1,61	0,015	0,155	MIR
RNA_POLYMERASE_II_TRANSCRIPTION_FACTOR_ACTIVITY	180	1,61	0,010	0,155	Gomf
REACTOME_APC_C_CDC20_MEDIATED_DEGRADATION_OF_CYCLIN_B	19	1,54	0,054	0,155	Reactome
EARLY_ENDOSOME	18	1,45	0,084	0,155	GOcc
REACTOME_DNA_REPAIR	102	1,55	0,029	0,155	Reactome
REACTOME_FANCONI_ANEMIA_PATHWAY	21	1,83	0,000	0,155	Reactome
UNFOLDED_PROTEIN_BINDING	42	1,60	0,035	0,155	Gomf
REACTOME_PI3K_CASCADE	67	1,53	0,007	0,155	Reactome
CHROMOSOME_ORGANIZATION_AND_BIOGENESIS	121	1,61	0,026	0,155	Gobp
TRANSLATION_FACTOR_ACTIVITY_NUCLEIC_ACID_BINDING	35	1,63	0,028	0,155	Gomf
REACTOME_G1_S_SPECIFIC_TRANSCRIPTION	17	1,52	0,096	0,156	Reactome

NUCLEAR_TRANSPORT	85	1,60	0,009	0,156	Gobp
TRANSLATION	175	1,61	0,041	0,156	Gobp
CHROMATIN_ASSEMBLY	16	1,78	0,002	0,156	Gobp
REACTOME_ORC1_REMOVAL_FROM_CHROMATIN	65	1,52	0,077	0,156	Reactome
REACTOME_ASSEMBLY_OF_THE_PRE_REPLICATIVE_COMPLEX	63	1,52	0,077	0,156	Reactome
REACTOME_G2_M_CHECKPOINTS	41	1,55	0,082	0,156	Reactome
REACTOME_SIGNALING_BY_INSULIN_RECEPTOR	103	1,53	0,014	0,156	Reactome
REACTOME_FORMATION_OF_THE_HIV1_EARLY_ELONGATION_COMPLEX	31	1,52	0,062	0,157	Reactome
REACTOME_EGFR_DOWNREGULATION	24	1,52	0,047	0,157	Reactome
ENVELOPE	164	1,46	0,085	0,157	GOcc
ST_G_ALPHA_S_PATHWAY	16	1,41	0,073	0,158	SignalTransductionKE
BIOCARTA_G1_PATHWAY	28	1,67	0,019	0,159	BIOCARTA
VESICLE_COAT	16	1,45	0,101	0,159	GOcc
CTACCTC,LET-7A,LET-7B,LET-7C,LET-7D,LET-7E,LET-7F,MIR-98,LET-7G,LET-7I	384	1,59	0,003	0,160	MIR
NUCLEOCYTOPLASMIC_TRANSPORT	84	1,59	0,012	0,161	Gobp
TANG_SENESCENCE_TP53_TARGETS_DN	56	1,76	0,018	0,161	CGP
BIOCARTA_PITX2_PATHWAY	15	1,71	0,014	0,162	BIOCARTA
NUCLEOTIDYLTRANSFERASE_ACTIVITY	47	1,57	0,039	0,162	Gomf
REACTOME_FORMATION_OF_TUBULIN_FOLDING_INTERMEDIATES_BY_CCT_TRIC	19	1,51	0,074	0,163	Reactome
MAYBURD_RESPONSE_TO_L663536_UP	26	1,75	0,004	0,164	CGP
CROONQUIST_IL6_DEPRIVATION_DN	96	1,75	0,027	0,164	CGP
HOFMANN_MYELODYSPLASTIC_SYNDROM_LOW_RISK_DN	28	1,72	0,012	0,165	CGP
FOURNIER_ACINAR_DEVELOPMENT_LATE_2	273	1,72	0,020	0,165	CGP
SOTIRIOU_BREAST_CANCER_GRADE_1_VS_3_UP	146	1,76	0,030	0,165	CGP
WHITFIELD_CELL_CYCLE_G2	171	1,63	0,030	0,165	CGP
KOBAYASHI_EGFR_SIGNALING_24HR_DN	246	1,72	0,030	0,166	CGP
REACTOME_SIGNALING_BY_CONSTITUTIVELY_ACTIVE_EGFR	17	1,50	0,045	0,166	Reactome
SIG_PIP3_SIGNALING_IN_CARDIAC_MYOCTES	67	1,28	0,094	0,166	SignalGateway

WHITFIELD_CELL_CYCLE_M_G1	136	1,62	0,005	0,166	CGP
LEONARD_HYPOXIA	46	1,61	0,044	0,166	CGP
BENPORATH_PROLIFERATION	143	1,63	0,060	0,166	CGP
TRANSCRIPTION_FACTOR_BINDING	300	1,52	0,010	0,167	Gomf
SHEDDEN_LUNG_CANCER_POOR_SURVIVAL_A6	447	1,75	0,024	0,167	CGP
NIKOLSKY_BREAST_CANCER_20Q11_AMPLICON	31	1,63	0,028	0,167	CGP
HORIUCHI_WTAP_TARGETS_DN	302	1,75	0,023	0,167	CGP
WU_APOPTOSIS_BY_CDKN1A_VIA_TP53	53	1,62	0,091	0,167	CGP
HOLLEMAN_ASPARAGINASE_RESISTANCE_B_ALL_UP	26	1,61	0,046	0,167	CGP
FUJII_YBX1_TARGETS_DN	199	1,73	0,023	0,167	CGP
KORKOLA_CORRELATED_WITH_POU5F1	31	1,63	0,024	0,167	CGP
AMIT_SERUM_RESPONSE_480_MCF10A	37	1,64	0,009	0,168	CGP
NAGY_TFTC_COMPONENTS_HUMAN	19	1,63	0,015	0,168	CGP
ACTIN_FILAMENT_BINDING	25	1,57	0,027	0,168	Gomf
THYROID_HORMONE_RECEPTOR_BINDING	17	1,56	0,039	0,168	Gomf
AMUNDSON_GAMMA_RADIATION_RESPONSE	39	1,76	0,024	0,168	CGP
FARMER_BREAST_CANCER_CLUSTER_2	32	1,62	0,041	0,168	CGP
REACTOME_MITOTIC_G1_G1_S_PHASES	130	1,50	0,078	0,168	Reactome
REACTOME_MEMBRANE_TRAFFICKING	125	1,50	0,041	0,168	Reactome
CHAUHAN_RESPONSE_TO_METHOXYESTRADIOL_UP	47	1,63	0,014	0,169	CGP
LY_AGING_OLD_DN	55	1,63	0,033	0,169	CGP
ROY_WOUND_BLOOD_VESSEL_DN	22	1,64	0,028	0,169	CGP
WINNEPENNINCKX_MELANOMA_METASTASIS_UP	157	1,63	0,052	0,169	CGP
WINTER_HYPOXIA_UP	86	1,62	0,021	0,169	CGP
WEST_ADRENOCORTICAL_TUMOR_MARKERS_UP	21	1,62	0,043	0,170	CGP
BROWNE_HCMV_INFECTION_2HR_DN	48	1,73	0,010	0,170	CGP
LI_AMPLIFIED_IN_LUNG_CANCER	175	1,64	0,031	0,170	CGP
TIEN_INTESTINE_PROBIOTICS_6HR_UP	55	1,63	0,043	0,170	CGP

SCHLOSSER_SERUM_RESPONSE_AUGMENTED_BY_MYC	107	1,62	0,024	0,170	CGP
CACGTTT,MIR-302A	30	1,55	0,025	0,171	MIR
RIBOSOME	39	1,43	0,121	0,171	GOcc
REACTOME_DOWNSTREAM_SIGNALING_OF_ACTIVATED_FGFR	97	1,49	0,023	0,171	Reactome
REACTOME_CHROMOSOME_MAINTENANCE	111	1,93	0,002	0,171	Reactome
TRANSLATION_INITIATION_FACTOR_ACTIVITY	23	1,52	0,063	0,171	Gomf
VESICLE_MEMBRANE	30	1,42	0,086	0,171	GOcc
STRUCTURAL_MOLECULE_ACTIVITY	237	1,54	0,067	0,171	Gomf
LIN_MELANOMA_COPY_NUMBER_UP	69	1,62	0,018	0,171	CGP
NUCLEAR_CHROMOSOME_PART	34	1,42	0,084	0,171	GOcc
LY_AGING_MIDDLE_DN	16	1,64	0,026	0,171	CGP
G1_PHASE	15	1,78	0,009	0,171	Gobp
LEE_LIVER_CANCER_SURVIVAL_DN	169	1,73	0,020	0,172	CGP
KUUSELO_PANCREATIC_CANCER_19Q13_AMPLIFICATION	31	1,62	0,030	0,172	CGP
REACTOME_KINESINS	23	1,90	0,002	0,172	Reactome
NAGY_STAGA_COMPONENTS_HUMAN	15	1,61	0,026	0,172	CGP
VECCHI_GASTRIC_CANCER_EARLY_UP	406	1,76	0,019	0,172	CGP
REACTOME_SHC1_EVENTS_IN_ERBB4_SIGNALING	20	1,49	0,053	0,172	Reactome
BIOCARTA_CARM_ER_PATHWAY	34	1,57	0,024	0,172	BIOCARTA
CYTOSKELETON_DEPENDENT_INTRACELLULAR_TRANSPORT	26	1,58	0,020	0,172	Gobp
MISSIAGLIA_REGULATED_BY_METHYLATION_DN	117	1,73	0,038	0,173	CGP
CAMPS_COLON_CANCER_COPY_NUMBER_UP	86	1,64	0,007	0,173	CGP
NUCLEAR_HORMONE_RECEPTOR_BINDING	28	1,55	0,040	0,173	Gomf
BIOCARTA_UCALPAIN_PATHWAY	18	1,60	0,038	0,173	BIOCARTA
OXFORD_RALA_OR_RALB_TARGETS_UP	48	1,64	0,046	0,173	CGP
JAZAERI_BREAST_CANCER_BRCA1_VS_BRCA2_UP	49	1,61	0,018	0,173	CGP
SONG_TARGETS_OF_IE86_CMV_PROTEIN	59	1,60	0,065	0,173	CGP
REACTOME_INTERACTIONS_OF_VPR_WITH_HOST_CELLULAR_PROTEINS	32	1,49	0,053	0,174	Reactome

PROTEIN_SERINE_THREONINE_PHOSPHATASE_ACTIVITY	24	1,52	0,058	0,174	Gomf
IIZUKA_LIVER_CANCER_PROGRESSION_G1_G2_DN	25	1,64	0,028	0,174	CGP
BIOCARTA_IGF1R_PATHWAY	23	1,53	0,038	0,174	BIOCARTA
ZHAN_MULTIPLE_MYELOMA_PR_UP	42	1,73	0,017	0,174	CGP
KAUFFMANN_MELANOMA_RELAPSE_UP	58	1,64	0,048	0,175	CGP
BLUM_RESPONSE_TO_SALIRASIB_DN	332	1,65	0,048	0,175	CGP
FERREIRA_EWINGS_SARCOMA_UNSTABLE_VS_STABLE_UP	162	1,60	0,050	0,175	CGP
BIOCARTA_IGF1_PATHWAY	21	1,59	0,019	0,175	BIOCARTA
SCHLOSSER_MYC_AND_SERUM_RESPONSE_SYNERGY	32	1,65	0,027	0,175	CGP
FOURNIER_ACINAR_DEVELOPMENT_LATE_DN	21	1,65	0,016	0,175	CGP
REACTOME_INHIBITION_OF_THE_PROTEOLYTIC_ACTIVITY_OF_APC_C_REQUIRED_FOR_THE_ONSET_OF_ANAPHASE_BY_MITOTIC_SPINDLE_CHECKPOINT_COMPONENTS	18	1,48	0,083	0,175	Reactome
SCIBETTA_KDM5B_TARGETS_DN	78	1,60	0,031	0,175	CGP
HEIDENBLAD_AMPLICON_8Q24_UP	37	2,00	0,000	0,175	CGP
LASTOWSKA_NEUROBLASTOMA_COPY_NUMBER_UP	169	1,64	0,025	0,176	CGP
EGUCHI_CELL_CYCLE_RB1_TARGETS	23	1,64	0,037	0,176	CGP
TRANSLATION_REGULATOR_ACTIVITY	37	1,54	0,048	0,176	Gomf
NUCLEOSIDE_TRIPHOSPHATASE_ACTIVITY	204	1,53	0,009	0,176	Gomf
PURBEY_TARGETS_OF_CTBP1_AND_SATB1_DN	175	1,60	0,003	0,176	CGP
PYROPHOSPHATASE_ACTIVITY	218	1,51	0,016	0,176	Gomf
HORMONE_RECEPTOR_BINDING	29	1,53	0,049	0,176	Gomf
MUELLER_PLURINET	288	1,64	0,021	0,176	CGP
RIBOSOME_BIOGENESIS_AND_ASSEMBLY	18	1,57	0,063	0,176	Gobp
CHENG_IMPRINTED_BY_ESTRADIOL	102	1,60	0,005	0,176	CGP
NUTT_GBM_VS_AO_GLIOMA_DN	45	1,64	0,021	0,176	CGP
KYNG_RESPONSE_TO_H2O2_VIA_ERCC6_UP	39	1,60	0,007	0,176	CGP
DANG_MYC_TARGETS_UP	138	1,71	0,014	0,176	CGP
SCIAN_CELL_CYCLE_TARGETS_OF_TP53_AND_TP73_DN	22	1,73	0,015	0,176	CGP
BENPORATH_ES_2	39	1,74	0,008	0,176	CGP

REPLICATION_FORK	18	1,41	0,109	0,177	GOcc
BACOLOD_RESISTANCE_TO_ALKYLATING_AGENTS_DN	60	1,60	0,010	0,177	CGP
PENG_RAPAMYCIN_RESPONSE_DN	241	1,65	0,017	0,177	CGP
BOYAULT_LIVER_CANCER_SUBCLASS_G3_UP	185	1,76	0,024	0,177	CGP
AATGGAG,MIR-136	76	1,50	0,025	0,178	MIR
ROSTY_CERVICAL_CANCER_PROLIFERATION_CLUSTER	138	1,71	0,041	0,178	CGP
WHITEFORD_PEDIATRIC_CANCER_MARKERS	112	1,65	0,044	0,179	CGP
VANTVEER_BREAST_CANCER_METASTASIS_DN	117	1,59	0,045	0,179	CGP
DAIRKEE_CANCER_PRONE_RESPONSE_BPA	51	1,59	0,017	0,179	CGP
ODONNELL_TFRC_TARGETS_DN	130	1,59	0,091	0,179	CGP
MOHANKUMAR_TLX1_TARGETS_UP	400	1,59	0,012	0,180	CGP
CHANG_CYCLING_GENES	143	1,77	0,029	0,180	CGP
TIEN_INTESTINE_PROBIOTICS_24HR_DN	207	1,76	0,005	0,180	CGP
GRAHAM_NORMAL_QUIESCENT_VS_NORMAL_DIVIDING_DN	87	1,59	0,073	0,180	CGP
MOLENAAR_TARGETS_OF_CCND1_AND_CDK4_DN	57	1,73	0,029	0,180	CGP
CHEN_HOXA5_TARGETS_9HR_DN	40	1,65	0,030	0,181	CGP
WONG_EMBRYONIC_STEM_CELL_CORE	330	1,65	0,037	0,181	CGP
REACTOME_TRANS_GOLGI_NETWORK_VESICLE_BUDDING	58	1,48	0,069	0,181	Reactome
DELPUECH_FOXO3_TARGETS_DN	39	1,69	0,019	0,181	CGP
KAUFFMANN_DNA_REPLICATION_GENES	142	1,66	0,043	0,181	CGP
DAZARD_UV_RESPONSE_CLUSTER_G4	18	1,58	0,023	0,181	CGP
NUCLEOLAR_PART	18	1,40	0,125	0,181	GOcc
LEE_EARLY_T_LYMPHOCYTE_UP	100	1,66	0,064	0,181	CGP
BIOCARTA_HER2_PATHWAY	22	1,54	0,026	0,181	BIOCARTA
GRADE_COLON_AND_RECTAL_CANCER_UP	280	1,70	0,011	0,181	CGP
FLOTHO_PEDIATRIC_ALL_THERAPY_RESPONSE_UP	53	1,58	0,057	0,182	CGP
HONRADO_BREAST_CANCER_BRCA1_VS_BRCA2	18	1,58	0,057	0,182	CGP
PUJANA_BRCA2_PCC_NETWORK	414	1,58	0,041	0,182	CGP

MARIADASON_RESPONSE_TO_CURCUMIN_SULINDAC_7	18	1,69	0,014	0,182	CGP
REACTOME_APC_C_CDH1_MEDIATED_DEGRADATION_OF_CDC20_AND_OTHER_APC_C_CDH1_TARGETED_PROTEINS_IN_LATE_MITOSIS_EARLY_G1	63	1,48	0,097	0,182	Reactome
MENSSEN_MYC_TARGETS	52	1,58	0,043	0,182	CGP
SCHLOSSER_MYC_TARGETS_AND_SERUM_RESPONSE_DN	47	1,66	0,025	0,182	CGP
POMEROY_MEDULLOBLASTOMA_DESMOPLASIC_VS_CLASSIC_UP	59	1,58	0,005	0,182	CGP
AIYAR_COBRA1_TARGETS_DN	29	1,58	0,024	0,182	CGP
GRAHAM_CML_DIVIDING_VS_NORMAL_QUIESCENT_UP	177	1,65	0,052	0,183	CGP
WHITFIELD_CELL_CYCLE_G2_M	213	1,58	0,025	0,183	CGP
REACTOME_CYTOSOLIC_TRNA_AMINOACYLATION	24	1,48	0,076	0,183	Reactome
REN_BOUND_BY_E2F	59	1,58	0,071	0,183	CGP
HEDENFALK_BREAST_CANCER_BRACX_UP	20	1,57	0,048	0,184	CGP
LOPEZ_MESOTHELIOMA_SURVIVAL_OVERALL_DN	15	1,67	0,005	0,184	CGP
SPIELMAN_LYMPHOBLAST_EUROPEAN_VS_ASIAN_UP	468	1,57	0,011	0,184	CGP
REACTOME_SYNTHESIS_OF_GLYCOSYLPHOSPHATIDYLINOSITOL_GPI	17	1,47	0,088	0,184	Reactome
BOYAULT_LIVER_CANCER_SUBCLASS_G12_UP	37	1,70	0,036	0,185	CGP
PUJANA_BRCA_CENTERED_NETWORK	116	1,66	0,041	0,185	CGP
HYDROLASE_ACTIVITY_ACTING_ON_ACID_ANHYDRIDES	220	1,50	0,018	0,185	Gomf
THILLAINADESAN_ZNF217_TARGETS_UP	42	1,69	0,018	0,185	CGP
BASAKI_YBX1_TARGETS_UP	277	1,67	0,027	0,185	CGP
GAJATE_RESPONSE_TO_TRABECTEDIN_DN	18	1,77	0,002	0,185	CGP
CHNG_MULTIPLE_MYELOMA_HYPERPLOID_UP	51	1,66	0,050	0,186	CGP
MACLACHLAN_BRCA1_TARGETS_UP	21	1,68	0,007	0,186	CGP
WANG_METASTASIS_OF_BREAST_CANCER_ESR1_UP	21	1,70	0,014	0,186	CGP
ATAGGAA,MIR-202	100	1,44	0,063	0,186	MIR
FLECHNER_PBL_KIDNEY_TRANSPLANT_REJECTED_VS_OK_DN	51	1,66	0,007	0,186	CGP
CTGTTAC,MIR-194	105	1,43	0,060	0,187	MIR
CTCTGGA,MIR-520A,MIR-525	153	1,48	0,026	0,187	MIR
PENG_LEUCINE_DEPRIVATION_DN	183	1,70	0,009	0,187	CGP

KANG_DOXORUBICIN_RESISTANCE_UP	53	1,67	0,037	0,187	CGP
RAMASWAMY_METASTASIS_UP	64	1,80	0,002	0,188	CGP
REACTOME_REGULATION_OF_GLUCOKINASE_BY_GLUCOKINASE_REGULATORY_PROTEIN	27	1,46	0,073	0,188	Reactome
BIOCARTA_CK1_PATHWAY	17	1,57	0,037	0,188	BIOCARTA
WEST_ADRENOCORTICAL_TUMOR_UP	286	1,66	0,021	0,188	CGP
DAIRKEE_CANCER_PRONE_RESPONSE_BPA_E2	116	1,66	0,009	0,188	CGP
SARRIO_EPITHELIAL_MESENCHYMAL_TRANSITION_UP	172	1,68	0,030	0,188	CGP
LI_WILMS_TUMOR_VS_FETAL_KIDNEY_2_UP	29	1,68	0,021	0,189	CGP
REACTOME_ABORTIVE_ELONGATION_OF_HIV1_TRANSCRIPT_IN_THE_ABSENCE_OF_TAT	23	1,46	0,085	0,189	Reactome
RHODES_CANCER_META_SIGNATURE	62	1,56	0,045	0,189	CGP
APPIERTO_RESPONSE_TO_FENRETINIDE_UP	38	1,57	0,024	0,189	CGP
SILIGAN_TARGETS_OF_EWS_FLI1_FUSION_DN	18	1,67	0,016	0,189	CGP
TCATCTC,MIR-143	145	1,44	0,010	0,190	MIR
CHEMNITZ_RESPONSE_TO_PROSTAGLANDIN_E2_UP	142	1,80	0,014	0,190	CGP
HOSHIDA_LIVER_CANCER_SUBCLASS_S2	113	1,80	0,015	0,190	CGP
BORCZUK_MALIGNANT_MESOTHELIOMA_UP	296	1,57	0,052	0,190	CGP
DUTERTRE_ESTRADIOL_RESPONSE_24HR_UP	315	1,77	0,037	0,190	CGP
SMID_BREAST_CANCER_LUMINAL_A_DN	17	1,56	0,074	0,190	CGP
REACTOME_ENDOSOMAL_SORTING_COMPLEX_REQUIRED_FOR_TRANSPORT_ESCRT	25	1,46	0,076	0,190	Reactome
REACTOME_BASIGIN_INTERACTIONS	24	1,45	0,059	0,190	Reactome
SHIPP_DLBCL_CURED_VS_FATAL_DN	45	1,56	0,029	0,190	CGP
BENPORATH_MYC_TARGETS_WITH_EBOX	219	1,56	0,012	0,191	CGP
REACTOME_DESTABILIZATION_OF_MRNA_BY_TRISTETRAPROLIN_TTP	17	1,46	0,067	0,191	Reactome
ABRAMSON_INTERACT_WITH_AIRE	45	1,84	0,009	0,191	CGP
AGTCTAG,MIR-151	24	1,50	0,039	0,191	MIR
REACTOME_ACTIVATION_OF_GENES_BY_ATF4	24	1,45	0,075	0,192	Reactome
CHIANG_LIVER_CANCER_SUBCLASS_PROLIFERATION_UP	172	1,67	0,044	0,192	CGP
REACTOME_SIGNALLING_BY_NGF	210	1,46	0,022	0,192	Reactome

TCCCCAC,MIR-491	56	1,48	0,053	0,193	MIR
HOXA9_DN.V1_DN	185	1,56	0,008	0,193	C6
MRNA_METABOLIC_PROCESS	81	1,78	0,013	0,193	Gobp
CONDENSED_NUCLEAR_CHROMOSOME	18	1,38	0,122	0,193	GOcc
CAATGCA,MIR-33	91	1,44	0,025	0,193	MIR
BROWNE_HCMV_INFECTION_18HR_UP	172	1,67	0,000	0,193	CGP
BIOCARTA_SPRY_PATHWAY	18	1,54	0,043	0,195	BIOCARTA
NIKOLSKY_BREAST_CANCER_17Q21_Q25_AMPLICON	319	1,55	0,080	0,196	CGP
LEE_METASTASIS_AND_RNA_PROCESSING_UP	17	1,55	0,048	0,196	CGP
FURUKAWA_DUSP6_TARGETS_PCI35_DN	71	1,67	0,032	0,196	CGP
PUJANA_BREAST_CANCER_LIT_INT_NETWORK	100	1,67	0,019	0,196	CGP
NEGATIVE_REGULATION_OF_DNA_METABOLIC_PROCESS	18	1,56	0,037	0,196	Gobp
RNA_POLYMERASE_ACTIVITY	16	1,48	0,095	0,196	Gomf
MITSIADES_RESPONSE_TO_APLIDIN_DN	244	1,77	0,016	0,196	CGP
CROONQUIST_NRAS_VS_STROMAL_STIMULATION_DN	97	1,55	0,050	0,197	CGP
MARIADASON_RESPONSE_TO_BUTYRATE_SULINDAC_6	48	1,55	0,015	0,197	CGP
ACTGCAG,MIR-17-3P	109	1,45	0,037	0,197	MIR
MANALO_HYPOXIA_DN	282	1,77	0,020	0,197	CGP
GAZDA_DIAMOND_BLACKFAN_ANEMIA_PROGENITOR_DN	64	1,55	0,033	0,198	CGP
SCHLOSSER_MYC_TARGETS_AND_SERUM_RESPONSE_UP	46	1,79	0,000	0,198	CGP
NADERI_BREAST_CANCER_PROGNOSIS_UP	48	1,67	0,038	0,198	CGP
DANG_REGULATED_BY_MYC_UP	70	1,55	0,038	0,199	CGP
BHATTACHARYA_EMBRYONIC_STEM_CELL	85	1,80	0,010	0,199	CGP
KYNG_NORMAL_AGING_UP	17	1,55	0,040	0,199	CGP
ST_WNT_BETA_CATENIN_PATHWAY	33	1,44	0,050	0,199	SignalTransductionKE
NEGATIVE_REGULATION_OF_RNA_METABOLIC_PROCESS	131	1,55	0,013	0,200	Gobp
UBIQUITIN_LIGASE_COMPLEX	26	1,37	0,104	0,200	GOcc
LI_WILMS_TUMOR_ANAPLASTIC_UP	18	1,67	0,032	0,200	CGP

NEGATIVE_REGULATION_OF_NUCLEOBASENUCLEOSIDENUCLEOTIDE_AND_NUCLEIC_ACID_METABOLIC_PROCESS	206	1,54	0,008	0,200	Gobp
ZHANG_RESPONSE_TO_CANTHARIDIN_DN	67	1,55	0,064	0,201	CGP
REACTOME_MEIOTIC_SYNAPSIS	66	1,44	0,102	0,201	Reactome
CYTOSKELETON	358	1,37	0,034	0,201	GOcc
TRANSCRIPTION_FROM_RNA_POLYMERASE_II_PROMOTER	453	1,55	0,005	0,201	Gobp
MITOTIC_CELL_CYCLE	152	1,81	0,012	0,202	Gobp
REGULATION_OF_TRANSCRIPTIONDNA_DEPENDENT	457	1,53	0,011	0,202	Gobp
GARCIA_TARGETS_OF_FLI1_AND_DAX1_DN	169	1,85	0,002	0,202	CGP
MACROMOLECULE_BIOSYNTHETIC_PROCESS	316	1,53	0,027	0,202	Gobp
SMALL_GTPASE_BINDING	33	1,47	0,038	0,203	Gomf
LINSLEY_MIR16_TARGETS	202	1,78	0,000	0,203	CGP
TRANSCRIPTION_COFACTOR_ACTIVITY	224	1,47	0,016	0,203	Gomf
CHANDRAN_METASTASIS_UP	204	1,54	0,005	0,203	CGP
GAGACTG,MIR-452	92	1,44	0,028	0,203	MIR
HEDENFALK_BREAST_CANCER_HEREDITARY_VS_SPORADIC	49	1,54	0,028	0,203	CGP
ORGANELLE_MEMBRANE	297	1,36	0,101	0,203	GOcc
CYTOPLASMIC_VESICLE_PART	28	1,36	0,125	0,203	GOcc
TIEN_INTESTINE_PROBIOTICS_2HR_UP	27	1,54	0,049	0,203	CGP
REACTOME_PI3K_AKT_ACTIVATION	36	1,44	0,061	0,203	Reactome
KEGG_NUCLEOTIDE_EXCISION_REPAIR	42	1,75	0,000	0,203	KEGG
TOYOTA_TARGETS_OF_MIR34B_AND_MIR34C	429	1,78	0,007	0,204	CGP
NEGATIVE_REGULATION_OF_TRANSCRIPTION_DNA_DEPENDENT	129	1,54	0,013	0,204	Gobp
REGULATION_OF_MITOTIC_CELL_CYCLE	23	1,52	0,049	0,205	Gobp
HOFMANN_MYELODYSPLASTIC_SYNDROM_RISK_UP	22	1,77	0,005	0,205	CGP
GAGCTGG,MIR-337	156	1,50	0,032	0,205	MIR
REACTOME_POST_TRANSLATIONAL_MODIFICATION_SYNTHESIS_OF_GPI_ANCHORED_PROTEINS	26	1,43	0,101	0,205	Reactome
REGULATION_OF_RNA_METABOLIC_PROCESS	466	1,53	0,011	0,205	Gobp
ZHOU_CELL_CYCLE_GENES_IN_IR_RESPONSE_6HR	85	1,82	0,021	0,206	CGP

ZHOU_CELL_CYCLE_GENES_IN_IR_RESPONSE_24HR	125	1,85	0,018	0,206	CGP
CYTOPLASMIC_VESICLE_MEMBRANE	28	1,36	0,125	0,207	GOcc
REACTOME_FACTORS_INVOLVED_IN_MEGAKARYOCYTE_DEVELOPMENT_AND_PLATELET_PRODUCTION	120	1,43	0,039	0,208	Reactome
MICROTUBULE_BASED_MOVEMENT	16	1,52	0,045	0,208	Gobp
CAGCCTC,MIR-485-5P	139	1,45	0,032	0,208	MIR
VEGF_A_UP.V1_DN	191	1,39	0,059	0,208	C6
REACTOME_PIP3_ACTIVATES_AKT_SIGNALING	27	1,43	0,082	0,208	Reactome
RHODES_UNDIFFERENTIATED_CANCER	66	1,54	0,084	0,208	CGP
POMEROY_MEDULLOBLASTOMA_PROGNOSIS_DN	43	1,81	0,011	0,208	CGP
BROWNE_HCMV_INFECTION_24HR_UP	146	1,54	0,003	0,209	CGP
OZEN_MIR125B1_TARGETS	25	1,53	0,017	0,209	CGP
BENPORATH_ES_1	369	1,53	0,031	0,209	CGP
BONOME_OVARIAN_CANCER_POOR_SURVIVAL_DN	22	1,83	0,002	0,209	CGP
GLYCOLIPID_METABOLIC_PROCESS	16	1,52	0,043	0,209	Gobp
ORGANELLE_ORGANIZATION_AND_BIOGENESIS	464	1,50	0,008	0,209	Gobp
MATTIOLI_MGUS_VS_MULTIPLE_MYELOMA	16	1,80	0,002	0,210	CGP
REACTOME_MEIOSIS	102	1,43	0,115	0,210	Reactome
MICROTUBULE_ORGANIZING_CENTER_ORGANIZATION_AND_BIOGENESIS	15	1,49	0,075	0,210	Gobp
REACTOME_RNA_POL_I_RNA_POL_III_AND_MITOCHONDRIAL_TRANSCRIPTION	106	1,42	0,096	0,210	Reactome
ATGCACG,MIR-517B	18	1,46	0,048	0,211	MIR
FAELT_B_CLL_WITH_VH3_21_UP	43	1,53	0,040	0,211	CGP
TRANSLATIONAL_INITIATION	37	1,49	0,087	0,211	Gobp
DACOSTA_UV_RESPONSE_VIA_ERCC3_TTD_UP	63	1,53	0,029	0,211	CGP
BIOCARTA_NGF_PATHWAY	18	1,49	0,057	0,212	BIOCARTA
ESTABLISHMENT_OF_CELLULAR_LOCALIZATION	346	1,49	0,009	0,212	Gobp
XU_HGF_SIGNALING_NOT_VIA_AKT1_48HR_DN	20	1,53	0,058	0,212	CGP
DNA_METABOLIC_PROCESS	247	1,51	0,032	0,212	Gobp
PATTERN_SPECIFICATION_PROCESS	30	1,48	0,031	0,212	Gobp

SYNAPSE_ORGANIZATION_AND_BIOGENESIS	23	1,50	0,088	0,212	Gobp
RNA_SPLICINGVIA_TRANSESTERIFICATION_REACTIONS	32	1,48	0,073	0,212	Gobp
PROTEIN_TARGETING	106	1,50	0,010	0,213	Gobp
GTPASE_BINDING	34	1,46	0,040	0,214	Gomf
REGULATION_OF_CELL_CYCLE	182	1,48	0,022	0,214	Gobp
INTRACELLULAR_TRANSPORT	275	1,51	0,015	0,214	Gobp
BIOCARTA_ARAP_PATHWAY	17	1,71	0,012	0,214	BIOCARTA
CCTGAGT,MIR-510	41	1,40	0,046	0,214	MIR
CCTGCTG,MIR-214	231	1,51	0,005	0,215	MIR
BOYAULT_LIVER_CANCER_SUBCLASS_G123_UP	44	1,88	0,009	0,215	CGP
BIOCARTA_CCR3_PATHWAY	23	1,48	0,055	0,215	BIOCARTA
CREIGHTON_AKT1_SIGNALING_VIA_MTOR_DN	22	1,53	0,061	0,216	CGP
GENTILE_UV_RESPONSE_CLUSTER_D5	39	1,52	0,036	0,216	CGP
NEGATIVE_REGULATION_OF_TRANSCRIPTION	183	1,48	0,013	0,217	Gobp
CROONQUIST_NRAS_SIGNALING_DN	71	1,81	0,022	0,217	CGP
PUJANA_BREAST_CANCER_WITH_BRCA1_MUTATED_UP	55	1,52	0,093	0,218	CGP
HATADA_METHYLATED_IN_LUNG_CANCER_DN	35	1,52	0,059	0,219	CGP
FRASOR_RESPONSE_TO_SERM_OR_FULVESTRANT_DN	50	1,89	0,009	0,220	CGP
CHROMATIN_ASSEMBLY_OR_DISASSEMBLY	26	1,79	0,007	0,220	Gobp
WEST_ADRENOCORTICAL_CARCINOMA_VS_ADENOMA_UP	21	1,52	0,056	0,220	CGP
CAFFAREL_RESPONSE_TO_THC_DN	31	1,52	0,051	0,221	CGP
YAMASHITA_LIVER_CANCER_WITH_EPCAM_UP	51	1,85	0,002	0,221	CGP
CAMP_UP.V1_UP	189	1,40	0,076	0,222	C6
REACTOME_APC_C_CDC20_MEDIATED_DEGRADATION_OF_MITOTIC_PROTEINS	64	1,41	0,125	0,222	Reactome
TOMIDA_METASTASIS_UP	24	1,51	0,045	0,222	CGP
NUCLEAR_EXPORT	32	1,88	0,000	0,223	Gobp
MALONEY_RESPONSE_TO_17AAG_DN	77	1,51	0,075	0,223	CGP
RICKMAN_TUMOR_DIFFERENTIATED_MODERATELY_VS_POORLY_DN	15	1,51	0,071	0,224	CGP

PUJANA_XPRSS_INT_NETWORK	163	1,51	0,085	0,224	CGP
BOYAULT_LIVER_CANCER_SUBCLASS_G23_UP	51	1,51	0,118	0,225	CGP
NOVAK_MET	16	1,36	0,149	0,225	HCCsignatures
ZHAN_VARIABLE_EARLY_DIFFERENTIATION_GENES_DN	30	1,51	0,052	0,225	CGP
REACTOME_CDT1_ASSOCIATION_WITH_THE_CDC6_ORC_ORIGIN_COMPLEX	54	1,40	0,156	0,225	Reactome
DACOSTA_UV_RESPONSE_VIA_ERCC3_COMMON_UP	72	1,51	0,011	0,225	CGP
COLLER_MYC_TARGETS_UP	25	1,51	0,057	0,225	CGP
PEART_HDAC_PROLIFERATION_CLUSTER_UP	55	1,51	0,050	0,225	CGP
REACTOME_TRANSPORT_OF_MATURE_TRANSCRIPT_TO_CYTOPLASM	53	1,40	0,126	0,226	Reactome
HEIDENBLAD_AMPLIFIED_IN_PANCREATIC_CANCER	30	1,86	0,004	0,226	CGP
PUIFFE_INVASION_INHIBITED_BY_ASCITES_UP	78	1,51	0,041	0,226	CGP
SINGLE_STRANDED_DNA_BINDING	33	1,44	0,073	0,226	Gomf
CELLULAR_LOCALIZATION	364	1,47	0,014	0,227	Gobp
REACTOME_PHOSPHORYLATION_OF_THE_APC_C	17	1,40	0,133	0,227	Reactome
NEGATIVE_REGULATION_OF_METABOLIC_PROCESS	256	1,46	0,012	0,228	Gobp
REACTOME_ASSOCIATION_OF_TRIC_CCT_WITH_TARGET_PROTEINS_DURING_BIOSYNTHESIS	26	1,40	0,081	0,228	Reactome
ATPASE_ACTIVITY_COUPLED_TO_TRANSMEMBRANE_MOVEMENT_OF_IONS	24	1,44	0,067	0,228	Gomf
REACTOME_HOMOLOGOUS_RECOMBINATION_REPAIR_OF_REPLICATION_INDEPENDENT_DOUBLE_STRAND_BREAKS	16	1,40	0,108	0,229	Reactome
SU_TESTIS	74	1,50	0,083	0,230	CGP
WU_HBX_TARGETS_1_DN	23	1,50	0,045	0,230	CGP
MELLMAN_TUT1_TARGETS_UP	19	1,50	0,057	0,230	CGP
BREUHAHN_GROWTH_FACTOR_SIGNALING_IN_LIVER_CANCER	21	1,50	0,054	0,231	CGP
WHITFIELD_CELL_CYCLE_LITERATURE	44	1,50	0,139	0,231	CGP
PECE_MAMMARY_STEM_CELL_DN	134	1,50	0,074	0,231	CGP
AAGCACA,MIR-218	394	1,33	0,030	0,232	MIR
GRADE_METASTASIS_DN	44	1,49	0,079	0,232	CGP
AGGAGTG,MIR-483	65	1,35	0,076	0,233	MIR
SIG_CHEMOTAXIS	45	1,30	0,099	0,234	SignalGateway

REACTOME_PI_3K_CASCADE	54	1,38	0,067	0,234	Reactome
REACTOME_CLEAVAGE_OF_GROWING_TRANSCRIPT_IN_THE_TERMINATION_REGION_	43	1,39	0,135	0,235	Reactome
TACGGGT,MIR-99A,MIR-100,MIR-99B	23	1,35	0,091	0,235	MIR
REACTOME_DOWNSTREAM_SIGNAL_TRANSDUCTION	91	1,39	0,042	0,235	Reactome
REACTOME_BIOSYNTHESIS_OF_THE_N_GLYCAN_PRECURSOR_DOLICHOL_LIPID_LINKED_OLIGOSACCHARIDE_LLO_AND_TRANSFER_TO_A_NASCENT_PROTEIN	26	1,38	0,120	0,235	Reactome
GGGATGC,MIR-324-5P	49	1,51	0,034	0,236	MIR
GENERAL_RNA_POLYMERASE_II_TRANSCRIPTION_FACTOR_ACTIVITY	32	1,42	0,064	0,236	Gomf
REACTOME_PERK_REGULATED_GENE_EXPRESSION	27	1,38	0,114	0,237	Reactome
REACTOME_REGULATION_OF_MRNA_STABILITY_BY_PROTEINS_THAT_BIND_AU_RICH_ELEMENTS	80	1,39	0,123	0,237	Reactome
BIOCARTA_MPR_PATHWAY	33	1,45	0,076	0,237	BIOCARTA
ODONNELL_TARGETS_OF_MYC_AND_TFRC_DN	45	1,49	0,134	0,237	CGP
REACTOME_MRNA_CAPPING	27	1,38	0,116	0,237	Reactome
CACTGTG,MIR-128A,MIR-128B	333	1,33	0,041	0,238	MIR
REACTOME_TRANSCRIPTIONAL_REGULATION_OF_WHITE_ADIPOCYTE_DIFFERENTIATION	72	1,38	0,064	0,238	Reactome
NAKAYAMA_SOFT_TISSUE_TUMORS_PCA2_UP	85	1,89	0,005	0,238	CGP
ATGCTGC,MIR-103,MIR-107	214	1,37	0,034	0,238	MIR
NUCLEAR_ENVELOPE_ENDOPLASMIC_RETICULUM_NETWORK	94	1,32	0,126	0,239	GOcc
GGGACCA,MIR-133A,MIR-133B	196	1,32	0,083	0,239	MIR
WOO_LIVER_CANCER_CHOLANGIOCA_LIKE_UP	233	1,32	0,197	0,239	HCCsignatures
CONRAD_STEM_CELL	39	1,49	0,041	0,240	CGP
PROTEIN_AMINO_ACID_O_LINKED_GLYCOSYLATION	18	1,45	0,054	0,240	Gobp
NEGATIVE_REGULATION_OF_CELLULAR_METABOLIC_PROCESS	254	1,45	0,020	0,240	Gobp
ACAGGGT,MIR-10A,MIR-10B	123	1,33	0,081	0,240	MIR
CAGCAGG,MIR-370	150	1,35	0,072	0,240	MIR
GEORGES_CELL_CYCLE_MIR192_TARGETS	61	1,48	0,066	0,241	CGP
BILD_MYC_ONCOGENIC_SIGNATURE	195	1,48	0,042	0,242	CGP
GARGALOVIC_RESPONSE_TO_OXIDIZED_PHOSPHOLIPIDS_TURQUOISE_DN	52	1,48	0,113	0,242	CGP
CCACACA,MIR-147	62	1,34	0,075	0,242	MIR

BIOCARTA_EIF_PATHWAY	16	1,44	0,104	0,243	BIOCARTA
VANHARANTA_UTERINE_FIBROID_WITH_7Q_DELETION_UP	66	1,48	0,057	0,243	CGP
ST_INTEGRIN_SIGNALING_PATHWAY	81	1,29	0,095	0,243	SignalTransductionKE
REGULATION_OF_DNA_METABOLIC_PROCESS	43	1,44	0,059	0,243	Gobp
POMEROY_MEDULLOBLASTOMA_PROGNOSIS_UP	45	1,48	0,048	0,243	CGP
BLUM_RESPONSE_TO_SALIRASIB_UP	243	1,48	0,023	0,243	CGP
RUIZ_TNC_TARGETS_DN	141	1,48	0,106	0,243	CGP
LE_NEURONAL_DIFFERENTIATION_DN	19	1,47	0,103	0,244	CGP
GRADE_COLON_VS_RECTAL_CANCER_DN	54	1,47	0,055	0,244	CGP
CTCAGGG,MIR-125B,MIR-125A	324	1,34	0,065	0,245	MIR
AGUIRRE_PANCREATIC_CANCER_COPY_NUMBER_UP	286	1,48	0,040	0,245	CGP
ACCAATC,MIR-509	46	1,37	0,064	0,245	MIR
WANG_RESPONSE_TO_GSK3_INHIBITOR_SB216763_DN	352	1,48	0,064	0,245	CGP
TTGGGAG,MIR-150	89	1,36	0,070	0,247	MIR
REACTOME_TRANSPORT_OF_MATURE_MRNA_DERIVED_FROM_AN_INTRONLESS_TRANSCRIPT	33	1,37	0,131	0,248	Reactome
PIGMENT_METABOLIC_PROCESS	18	1,44	0,081	0,248	Gobp
REACTOME_HOST_INTERACTIONS_OF_HIV_FACTORS	120	1,36	0,144	0,248	Reactome
BIOCARTA_BARRESTIN_SRC_PATHWAY	15	1,74	0,005	0,248	BIOCARTA
GTGCCAA,MIR-96	302	1,37	0,032	0,249	MIR
LIU_SOX4_TARGETS_DN	300	1,47	0,037	0,249	CGP
CELL_CORTEX	39	1,31	0,114	0,249	GOcc
NIKOLSKY_BREAST_CANCER_20Q12_Q13_AMPLICON	141	1,47	0,081	0,249	CGP
CCATCCA,MIR-432	55	1,37	0,065	0,249	MIR
REACTOME_TRNA_AMINOACYLATION	42	1,36	0,142	0,250	Reactome

Gene sets enriched (FDR<0.25) in patients with mortality index < 230

Gene Set (ordered based on FDR value)	#genes	Normalized Enrichment Score	p-value	FDR(<0.25)	Database (http://www.broadinstitute.org/gsea/msigdb/)
KEGG_DRUG_METABOLISM_OTHER_ENZYMES	42	-1,80	0,003	0,033	KEGG
KEGG_STEROID_HORMONE_BIOSYNTHESIS	46	-1,82	0,005	0,033	KEGG
KEGG_PRIMARY_IMMUNODEFICIENCY	35	-1,78	0,002	0,035	KEGG
KEGG_TRYPTOPHAN_METABOLISM	40	-1,77	0,009	0,035	KEGG
KEGG_TYPE_I_DIABETES_MELLITUS	40	-1,80	0,007	0,036	KEGG
KEGG_HEMATOPOIETIC_CELL_LINEAGE	85	-1,78	0,007	0,038	KEGG
KEGG_ALLOGRAFT_REJECTION	35	-1,82	0,007	0,038	KEGG
KEGG_ABC_TRANSPORTERS	43	-1,75	0,007	0,040	KEGG
KEGG_ALPHA_LINOLENIC_ACID_METABOLISM	17	-1,74	0,011	0,040	KEGG
KEGG_GRAFT_VERSUS_HOST_DISEASE	36	-1,74	0,009	0,040	KEGG
KEGG_PENTOSE_AND_GLUCURONATE_INTERCONVERSIONS	20	-1,83	0,004	0,044	KEGG
KEGG_AUTOIMMUNE_THYROID_DISEASE	48	-1,86	0,007	0,047	KEGG
KEGG_VIRAL_MYOCARDITIS	68	-1,71	0,009	0,049	KEGG
KEGG_RETINOL_METABOLISM	55	-1,83	0,009	0,052	KEGG
KEGG_CELL_ADHESION_MOLECULES_CAMS	130	-1,88	0,000	0,053	KEGG
KEGG_DRUG_METABOLISM_CYTOCHROME_P450	61	-1,70	0,018	0,054	KEGG
KEGG_LINOLEIC_ACID_METABOLISM	27	-1,69	0,013	0,061	KEGG
KEGG_PROPANOATE_METABOLISM	32	-1,66	0,028	0,068	KEGG
KEGG_ASCORBATE_AND_ALDARATE_METABOLISM	17	-1,63	0,027	0,069	KEGG
KEGG_ANTIGEN_PROCESSING_AND_PRESENTATION	77	-1,63	0,042	0,069	KEGG
KEGG_TOLL_LIKE_RECEPTOR_SIGNALING_PATHWAY	98	-1,66	0,006	0,071	KEGG
KEGG_COMPLEMENT_AND_COAGULATION_CASCADES	67	-1,65	0,059	0,071	KEGG
KEGG_ASTHMA	28	-1,63	0,043	0,072	KEGG
KEGG_ARACHIDONIC_ACID_METABOLISM	55	-1,63	0,007	0,073	KEGG
KEGG_GLYCINE_SERINE_AND_THREONINE_METABOLISM	31	-1,64	0,027	0,074	KEGG

KEGG_NATURAL_KILLER_CELL_MEDIATED_CYTOTOXICITY	127	-1,61	0,032	0,075	KEGG
KEGG_METABOLISM_OF_XENOBIOTICS_BY_CYTOCHROME_P450	60	-1,64	0,033	0,077	KEGG
KEGG_STARCH_AND_SUCROSE_METABOLISM	40	-1,90	0,002	0,078	KEGG
KEGG_BETA_ALANINE_METABOLISM	22	-1,60	0,047	0,080	KEGG
HOSHIDA_S3	256	-1,74	0,033	0,093	HCCsignatures
KEGG_INTESTINAL_IMMUNE_NETWORK_FOR_IGA_PRODUCTION	45	-1,56	0,061	0,105	KEGG
YE_LIVER_CANCER_INTRAHEPATIC_METS	22	-1,56	0,021	0,106	HCCsignatures
CHIANG_LIVER_CANCER_SUBCLASS_POLYSOMY7	59	-1,60	0,046	0,128	HCCsignatures
FURUKAWA_DUSP6_TARGETS_PCI35_UP	73	-1,94	0,002	0,134	CGP
KEGG_CYTOKINE_CYTOKINE_RECEPTOR_INTERACTION	251	-1,52	0,054	0,136	KEGG
KEGG_PRIMARY_BILE_ACID_BIOSYNTHESIS	16	-1,51	0,087	0,136	KEGG
WINTER_HYPOXIA_DN	49	-1,91	0,000	0,140	CGP
ATM_DN.V1_DN	144	-1,64	0,002	0,140	c6
SANA_RESPONSE_TO_IFNG_UP	73	-1,89	0,002	0,145	CGP
CATION_HOMEOSTASIS	107	-1,69	0,007	0,149	Gobp
CHEMICAL_HOMEOSTASIS	153	-1,61	0,005	0,153	Gobp
ION_HOMEOSTASIS	127	-1,62	0,007	0,154	Gobp
IMMUNE_SYSTEM_PROCESS	322	-1,70	0,014	0,155	Gobp
KRAS.300_UP.V1_DN	134	-1,61	0,010	0,156	c6
CELLULAR_HOMEOSTASIS	145	-1,62	0,000	0,159	Gobp
DETECTION_OF_STIMULUS_INVOLVED_IN_SENSORY_PERCEPTION	21	-1,69	0,019	0,159	Gobp
BIOCARTA_IL17_PATHWAY	15	-1,81	0	0,159	BIOCARTA
POSITIVE_REGULATION_OF_TRANSLATION	34	-1,67	0,016	0,161	Gobp
REGULATION_OF_CYTOKINE_BIOSYNTHETIC_PROCESS	38	-1,64	0,016	0,162	Gobp
CYTOKINE_BIOSYNTHETIC_PROCESS	41	-1,62	0,020	0,163	Gobp
REGULATION_OF_MULTICELLULAR_ORGANISMAL_PROCESS	146	-1,71	0,003	0,163	Gobp
POSITIVE_REGULATION_OF_CYTOKINE_BIOSYNTHETIC_PROCESS	25	-1,73	0,010	0,164	Gobp
CYTOKINE_METABOLIC_PROCESS	42	-1,60	0,019	0,164	Gobp

CELL_ACTIVATION	73	-1,62	0,038	0,164	Gobp
LOCOMOTORY_BEHAVIOR	94	-1,59	0,021	0,165	Gobp
MULTI_ORGANISM_PROCESS	160	-1,59	0,008	0,167	Gobp
LEUKOCYTE_ACTIVATION	66	-1,67	0,026	0,167	Gobp
REGULATION_OF_LYMPHOCYTE_ACTIVATION	33	-1,65	0,030	0,167	Gobp
POSITIVE_REGULATION_OF_MULTICELLULAR_ORGANISMAL_PROCESS	64	-1,66	0,012	0,167	Gobp
PTEN_DN.V1_DN	174	-1,65	0,003	0,167	c6
POSITIVE_REGULATION_OF_T_CELL_ACTIVATION	21	-1,59	0,039	0,167	Gobp
POSITIVE_REGULATION_OF_IMMUNE_RESPONSE	28	-1,63	0,025	0,168	Gobp
RESPONSE_TO_OTHER_ORGANISM	81	-1,62	0,026	0,168	Gobp
KEGG_LEUKOCYTE_TRANSENDOTHELIAL_MIGRATION	113	-1,48	0,051	0,168	KEGG
T_CELL_PROLIFERATION	19	-1,67	0,014	0,169	Gobp
KEGG_B_CELL_RECEPTOR_SIGNALING_PATHWAY	75	-1,47	0,054	0,169	KEGG
GAURNIER_PSMD4_TARGETS	70	-1,87	0,002	0,170	CGP
CALCIUM_INDEPENDENT_CELL_CELL_ADHESION	22	-1,58	0,018	0,171	Gobp
LYMPHOCYTE_ACTIVATION	58	-1,63	0,032	0,171	Gobp
ADAPTIVE_IMMUNE_RESPONSE	24	-1,57	0,035	0,171	Gobp
CELLULAR_CATION_HOMEOSTASIS	104	-1,71	0,003	0,174	Gobp
SODIUM_ION_TRANSPORT	22	-1,65	0,013	0,175	Gobp
ADAPTIVE_IMMUNE_RESPONSE_GO_0002460	23	-1,57	0,041	0,175	Gobp
REGULATION_OF_T_CELL_PROLIFERATION	16	-1,63	0,021	0,176	Gobp
CALCIUM_MEDIATED_SIGNALING	15	-1,57	0,040	0,179	Gobp
DEFENSE_RESPONSE	257	-1,73	0,005	0,180	Gobp
T_CELL_ACTIVATION	42	-1,71	0,016	0,183	Gobp
REGULATION_OF_IMMUNE_RESPONSE	32	-1,56	0,038	0,183	Gobp
KEGG_JAK_STAT_SIGNALING_PATHWAY	150	-1,45	0,075	0,185	KEGG
RESPONSE_TO_DRUG	20	-1,74	0,007	0,186	Gobp
KEGG_BUTANOATE_METABOLISM	34	-1,44	0,122	0,187	KEGG

KEGG_ONE_CARBON_POOL_BY_FOLATE	17	-1,45	0,071	0,187	KEGG
IMMUNE_RESPONSE	228	-1,81	0,005	0,194	Gobp
CAIRO_HEPATOBLASTOMA_DN	263	-1,84	0,017	0,199	CGP
KEGG_LEISHMANIA_INFECTION	68	-1,42	0,119	0,202	KEGG
KEGG_FATTY_ACID_METABOLISM	39	-1,42	0,137	0,204	KEGG
KRAS.600.LUNG.BREAST_UP.V1_DN	275	-1,52	0,013	0,210	c6
RESPONSE_TO_VIRUS	49	-1,54	0,052	0,210	Gobp
CELLULAR_DEFENSE_RESPONSE	53	-1,74	0,005	0,213	Gobp
BIOCARTA_IL12_PATHWAY	21	-1,63	0,021	0,214	BIOCARTA
KEGG_HISTIDINE_METABOLISM	29	-1,40	0,110	0,215	KEGG
REACTOME_CYTOCHROME_P450_ARRANGED_BY_SUBSTRATE_TYPE	50	-1,77	0,007	0,215	Reactome
REGULATION_OF_DEFENSE_RESPONSE	19	-1,84	0,000	0,216	Gobp
KEGG_T_CELL_RECEPTOR_SIGNALING_PATHWAY	107	-1,39	0,088	0,218	KEGG
KEGG_CHEMOKINE_SIGNALING_PATHWAY	179	-1,39	0,095	0,219	KEGG
INFLAMMATORY_RESPONSE	124	-1,53	0,048	0,223	Gobp
JNK_DN.V1_UP	184	-1,50	0,008	0,225	c6
REACTOME_IMMUNOREGULATORY_INTERACTIONS_BETWEEN_A_LYMPHOID_AND_A_NON_LYMPHOID_CELL	60	-1,83	0,005	0,228	Reactome
KRAS.50_UP.V1_DN	45	-1,52	0,042	0,232	c6
KRAS.LUNG.BREAST_UP.V1_DN	135	-1,53	0,014	0,233	c6
ACTIVATION_OF_IMMUNE_RESPONSE	16	-1,50	0,060	0,233	Gobp
TURASHVILI_BREAST_DUCTAL_CARCINOMA_VS_LOBULAR_NORMAL_DN	66	-1,81	0,005	0,235	CGP
PEPTIDYL_TYROSINE_PHOSPHORYLATION	26	-1,50	0,038	0,236	Gobp
REACTOME_PHASE1_FUNCTIONALIZATION_OF_COMPOUNDS	69	-1,73	0,010	0,236	Reactome
KRAS.LUNG_UP.V1_DN	138	-1,72	0,005	0,238	c6
REGULATION_OF_PEPTIDYL_TYROSINE_PHOSPHORYLATION	17	-1,52	0,032	0,238	Gobp
POSITIVE_REGULATION_OF_IMMUNE_SYSTEM_PROCESS	49	-1,77	0,000	0,239	Gobp
POSITIVE_REGULATION_OF_LYMPHOCYTE_ACTIVATION	23	-1,50	0,073	0,240	Gobp
T_CELL_DIFFERENTIATION	15	-1,51	0,075	0,240	Gobp

NEGATIVE_REGULATION_OF_TRANSCRIPTION_FACTOR_ACTIVITY	15	-1,51	0,052	0,240	Gobp
CHIANG_LIVER_CANCER_SUBCLASS_INTERFERON	26	-1,37	0,163	0,242	HCCsignatures
REACTOME_BIOLOGICAL_OXIDATIONS	124	-1,79	0,009	0,243	Reactome
REGULATION_OF_RESPONSE_TO_STIMULUS	57	-1,49	0,041	0,243	Gobp
STEROID_BIOSYNTHETIC_PROCESS	23	-1,50	0,043	0,245	Gobp
RPS14_DN.V1_UP	188	-1,65	0,026	0,246	c6
REGULATION_OF_T_CELL_ACTIVATION	27	-1,75	0,010	0,249	Gobp
BIOCARTA_IL7_PATHWAY	17	-1,71	0,013	0,250	BIOCARTA

Supplementary Table 4: Methylation normals versus HCC markers

TargetID	F	UCSC_REFGENE_NAME
cg18247055	115,196274	SPAG6
cg15841063	107,659997	FOXD3
cg08441806	102,355967	NKX6-2
cg07055616	101,574579	NKX6-2
cg25537993	94,4485251	ZSCAN1
cg27392792	92,1900185	PTPRN2
cg06268694	84,3620216	CELSR1
cg05080154	83,1159092	SALL3
cg23016129	81,0480221	SPAG6
cg17536595	80,961124	RSPH9
cg16086620	80,9338937	CHGA
cg11068946	79,6668413	NKX6-2
cg11823511	79,2613027	BARHL2
cg05904135	75,5291113	NKX6-2
cg12377139	73,3130122	SPAG6
cg19761848	71,6162116	GBX2
cg06769546	71,0502262	NKX6-2
cg14231297	70,6580049	ZSCAN18
cg17996619	68,9151409	NKX6-2
cg25032595	68,8557568	CLDN10
cg16657538	68,593844	ZNF397OS
cg20129213	68,2029	RIMS2
cg24426072	67,2347139	TRIL
cg16949120	67,181187	NKX6-2
cg26923490	65,9478214	KCNA7
cg09053680	65,7291766	UTF1
cg16823083	65,1968796	WDR8
cg19792599	65,0538646	PUS3; DDX25
cg22557662	65,0285326	PPP1R14A
cg02571816	63,6671985	PPP1R14A
cg20232102	63,6459583	PPP1R14A
cg09515953	62,7233754	PPP1R14A
cg24659054	61,620433	NKX6-2
cg00884093	61,4700382	CELSR1
cg13902210	61,1612045	KCNC4
cg11377136	60,9956336	PKDREJ
cg16648062	60,2275723	RIMS2
cg23246885	59,4021644	FZD7
cg14823851	59,1013917	TBX4
cg15611336	59,0363678	RPP25
cg09894698	58,7904188	ASCL2
cg13879483	58,0081957	USP44
cg22158769	57,7483782	LOC375196
cg05495949	57,5494509	RADIL
cg01566592	56,9526169	RIMS2

cg12296772	56,8808456	MTMR7
cg10171448	56,6985154	NKX6-2
cg22796507	56,3730728	FOXE3
cg20449685	55,7916996	ZSCAN1
cg17003293	55,7436675	INSM2
cg03323696	55,3095034	PDE4D
cg13564825	55,0564946	PPP1R14A
cg24154839	54,5704099	GABRA4
cg15466862	54,3128061	SOX1
cg01281911	54,1375638	FOXE3
cg20106459	54,1074349	COX6B2
cg19499748	53,9433272	TRIL
cg06572160	53,3622836	KCNC3
cg15912800	53,1664243	MIR196B
cg01227537	52,7686596	ZIC1
cg11173146	51,8117269	EFNB2
cg01923218	50,8068481	CCDC67
cg14473102	50,503657	HOXD8
cg14709460	50,3418651	TRIL
cg04823311	50,337962	TRIL
cg01384488	49,871573	NKX6-2
cg20809087	49,6784281	BRUNOL6
cg26844246	49,3630032	TLX3
cg23842255	49,2134877	NEFH
cg16582779	49,144746	FOXG1
cg05095158	48,8953094	RASSF10
cg12744820	48,8747092	OLIG3
cg12188986	48,874371	CCDC67
cg09260089	48,7739829	NKX6-2
cg18862481	48,7339431	TRH
cg06648277	48,6404743	NKX6-2
cg00699945	48,5832305	NKX6-2
cg16087093	48,3924322	FOXI1
cg19852958	48,1218342	NKX3-2
cg25720804	48,0131804	TLX3
cg15304699	47,9957787	NKX6-2
cg10700424	47,9808215	GLB1L2
cg04786857	47,8727968	SPDYA
cg14251622	47,5340801	INSM2
cg26476852	47,1514509	HOXA9
cg02578368	47,1487038	HIST1H3F; HIST1H2BH
cg27362525	46,9043468	ZNF232
cg05057720	46,897471	CLEC14A
cg08288811	46,8741491	PCDHA3
cg26460092	46,7067947	TM6SF1
cg10655046	46,6314305	FOXD4L1
cg12206199	46,6014801	LOC375196
cg11935147	46,5867978	PDE4DIP

cg18233405	46,5605228	TSPYL5
cg03468349	46,4721334	SH3YL1; ACP1
cg18815943	46,4616068	FOXE3
cg03840594	46,1628793	POU3F2
cg23923856	46,0823209	WNT2B
cg10526374	45,5512381	ASCL2
cg18932798	45,5109799	INA

Supplementary Table 5: Methylation normals versus HCC markers (common in Heptromic and Song cohorts)

TargetID	F	UCSC_REFGENE_NAME
cg18247055	115,196274	SPAG6
cg15841063	107,659997	FOXD3
cg05080154	83,1159092	SALL3
cg23016129	81,0480221	SPAG6
cg05904135	75,5291113	NKX6-2
cg12377139	73,3130122	SPAG6
cg14231297	70,6580049	ZSCAN18
cg25032595	68,8557568	CLDN10
cg16657538	68,593844	ZNF397OS
cg20129213	68,2029	RIMS2
cg24426072	67,2347139	TRIL
cg16949120	67,181187	NKX6-2
cg16823083	65,1968796	WDR8
cg19792599	65,0538646	PUS3; DDX25
cg24659054	61,620433	NKX6-2
cg00884093	61,4700382	CELSR1
cg16648062	60,2275723	RIMS2
cg23246885	59,4021644	FZD7
cg09894698	58,7904188	ASCL2
cg13879483	58,0081957	USP44
cg05495949	57,5494509	RADIL
cg01566592	56,9526169	RIMS2
cg12296772	56,8808456	MTMR7
cg10171448	56,6985154	NKX6-2
cg22796507	56,3730728	FOXE3
cg24154839	54,5704099	GABRA4
cg01281911	54,1375638	FOXE3
cg19499748	53,9433272	TRIL
cg11173146	51,8117269	EFNB2
cg01923218	50,8068481	CCDC67
cg04823311	50,337962	TRIL
cg01384488	49,871573	NKX6-2
cg20809087	49,6784281	BRUNOL6
cg05095158	48,8953094	RASSF10
cg09260089	48,7739829	NKX6-2
cg15304699	47,9957787	NKX6-2
cg27362525	46,9043468	ZNF232
cg26460092	46,7067947	TM6SF1
cg10655046	46,6314305	FOXD4L1
cg11935147	46,5867978	PDE4DIP
cg18233405	46,5605228	TSPYL5
cg03468349	46,4721334	SH3YL1; ACP1
cg10526374	45,5512381	ASCL2

Supplementary Table 6: Candidate novel epidrivers during hepatocarcinogensis.
Top 500 F-scored between HCC and normal liver

TargetID	F score	UCSC_REFGENE_NAME	UCSC_REFGENE_GROUP
cg18247055	115,196274	SPAG6	TSS200
cg15841063	107,659997	FOXD3	1stExon
cg08441806	102,355967	NKX6-2	1stExon
cg07055616	101,574579	NKX6-2	TSS1500
cg25537993	94,4485251	ZSCAN1	TSS1500
cg27392792	92,1900185	PTPRN2	TSS1500
cg06268694	84,3620215	CELSR1	1stExon
cg05080154	83,1159092	SALL3	TSS1500
cg23016129	81,0480221	SPAG6	TSS200
cg17536595	80,961124	RSPH9	1stExon
cg16086620	80,9338937	CHGA	1stExon; 5'UTR
cg11068946	79,6668413	NKX6-2	1stExon
cg11823511	79,2613027	BARHL2	TSS1500
cg05904135	75,5291113	NKX6-2	1stExon
cg12377139	73,3130122	SPAG6	TSS200
cg19761848	71,6162116	GBX2	TSS200
cg06769546	71,0502262	NKX6-2	TSS1500
cg14231297	70,6580049	ZSCAN18	TSS200
cg17996619	68,9151409	NKX6-2	TSS1500
cg25032595	68,8557568	CLDN10	5'UTR; 1stExon
cg16657538	68,593844	ZNF397OS	5'UTR
cg20129213	68,2029	RIMS2	TSS1500
cg24426072	67,2347139	TRIL	1stExon
cg16949120	67,181187	NKX6-2	TSS1500
cg26923490	65,9478214	KCNA7	1stExon
cg09053680	65,7291766	UTF1	1stExon
cg16823083	65,1968796	WDR8	TSS1500
cg19792599	65,0538646	PUS3; DDX25	TSS1500; 5'UTR; 1stExon
cg22557662	65,0285326	PPP1R14A	TSS1500
cg02571816	63,6671985	PPP1R14A	TSS1500
cg20232102	63,6459583	PPP1R14A	TSS200
cg09515953	62,7233754	PPP1R14A	TSS200
cg24659054	61,620433	NKX6-2	TSS1500
cg00884093	61,4700382	CELSR1	1stExon
cg13902210	61,1612045	KCNC4	1stExon
cg11377136	60,9956336	PKDREJ	1stExon
cg16648062	60,2275723	RIMS2	TSS1500
cg23246885	59,4021644	FZD7	1stExon
cg14823851	59,1013917	TBX4	TSS1500
cg15611336	59,0363678	RPP25	1stExon
cg09894698	58,7904188	ASCL2	1stExon
cg13879483	58,0081957	USP44	TSS1500; 5'UTR

cg22158769	57,7483782	LOC375196	TSS200
cg05495949	57,5494509	RADIL	5'UTR
cg01566592	56,9526169	RIMS2	TSS200
cg12296772	56,8808456	MTMR7	TSS200
cg10171448	56,6985154	NKX6-2	TSS1500
cg22796507	56,3730728	FOXE3	1stExon
cg20449685	55,7916996	ZSCAN1	5'UTR
cg17003293	55,7436675	INSM2	1stExon
cg03323696	55,3095034	PDE4D	1stExon
cg13564825	55,0564946	PPP1R14A	TSS200
cg24154839	54,5704099	GABRA4	TSS200
cg15466862	54,3128061	SOX1	1stExon
cg01281911	54,1375638	FOXE3	1stExon
cg20106459	54,1074349	COX6B2	5'UTR; 1stExon
cg19499748	53,9433272	TRIL	1stExon; 5'UTR
cg06572160	53,3622836	KCNC3	1stExon
cg15912800	53,1664243	MIR196B	TSS200
cg01227537	52,7686596	ZIC1	TSS200
cg11173146	51,8117269	EFNB2	TSS200
cg01923218	50,806848	CCDC67	1stExon; 5'UTR
cg14473102	50,503657	HOXD8	TSS200
cg14709460	50,3418651	TRIL	TSS200
cg04823311	50,337962	TRIL	1stExon
cg01384488	49,871573	NKX6-2	TSS1500
cg20809087	49,6784281	BRUNOL6	1stExon; 5'UTR
cg26844246	49,3630032	TLX3	TSS200
cg23842255	49,2134877	NEFH	1stExon
cg16582779	49,144746	FOXG1	1stExon
cg05095158	48,8953094	RASSF10	1stExon
cg12744820	48,8747092	OLIG3	1stExon
cg12188986	48,874371	CCDC67	5'UTR; 1stExon
cg09260089	48,7739829	NKX6-2	TSS1500
cg18862481	48,7339431	TRH	5'UTR; 1stExon
cg06648277	48,6404743	NKX6-2	TSS1500
cg00699945	48,5832305	NKX6-2	TSS1500
cg16087093	48,3924322	FOXI1	1stExon
cg19852958	48,1218342	NKX3-2	1stExon
cg25720804	48,0131804	TLX3	1stExon
cg15304699	47,9957787	NKX6-2	TSS1500
cg10700424	47,9808215	GLB1L2	1stExon; 5'UTR
cg04786857	47,8727968	SPDYA	5'UTR
cg14251622	47,5340801	INSM2	1stExon
cg26476852	47,1514509	HOXA9	1stExon
cg02578368	47,1487038	HIST1H3F; HIST1H2BH	1stExon; TSS1500
cg27362525	46,9043468	ZNF232	5'UTR
cg05057720	46,897471	CLEC14A	1stExon

cg08288811	46,8741491	PCDHA3	1stExon
cg26460092	46,7067947	TM6SF1	5'UTR; 1stExon
cg10655046	46,6314305	FOXD4L1	1stExon
cg12206199	46,6014801	LOC375196	TSS200
cg11935147	46,5867978	PDE4DIP	1stExon
cg18233405	46,5605228	TSPYL5	5'UTR; 1stExon
cg03468349	46,4721334	SH3YL1; ACP1	TSS200; TSS1500
cg18815943	46,4616068	FOXE3	1stExon
cg03840594	46,1628793	POU3F2	1stExon
cg23923856	46,0823209	WNT2B	5'UTR; 1stExon
cg10526374	45,5512381	ASCL2	TSS1500
cg18932798	45,5109799	INA	1stExon
cg12781700	45,5046189	C17orf104	TSS200
cg13717446	45,4394088	LOC146880	TSS200
cg22538054	45,3671719	USP44	5'UTR
cg24604013	45,1581521	SOX1	TSS1500
cg18724565	45,1001369	FSCN1	1stExon
cg22740547	45,0859848	RASSF10	1stExon
cg14688104	45,0574393	KCNS2	1stExon;5'UTR
cg20049415	44,8848702	NKX2-4	1stExon
cg18854169	44,8736462	RBP3	1stExon
cg23806621	44,7717707	BHLHE23	TSS200
cg21790626	44,6564055	ZNF154	1stExon; 5'UTR
cg08558397	44,6058753	PRKAR1B	5'UTR; 1stExon
cg07759394	44,5744915	GLB1L2	1stExon; 5'UTR
cg19464917	44,4608216	ISL2	TSS1500
cg14715697	44,422618	HRNBP3	5'UTR
cg24368848	44,3727806	ZSCAN1	TSS1500
cg07382554	44,2958466	SALL3	TSS200
cg11498870	44,2463711	DCAF4L2	5'UTR; 1stExon
cg22789900	44,2458408	MIXL1	1stExon
cg15834072	43,9776574	DCHS2	1stExon
cg19078576	43,7897175	BASP1; LOC285696	1stExon; 5'UTR; TSS1500
cg11176990	43,7264955	LOC375196	TSS200
cg17630392	43,5558758	NPR3	1stExon
cg13794530	43,3355475	VIPR2	5'UTR; 1stExon
cg20270188	43,2837182	BCAN	5'UTR; 1stExon
cg05546863	43,2492895	CMTM2	TSS200
cg13204512	43,1078348	RNF135	1stExon
cg03063639	43,0486994	TM6SF1	5'UTR; 1stExon
cg10715223	42,9894128	SNX31	1stExon; 5'UTR
cg12783819	42,9754246	SEPT9	5'UTR
cg27049766	42,888811	ZNF154	1stExon; 5'UTR
cg14625175	42,793574	HOXA10	TSS200
cg19809499	42,75008	FOXE3	1stExon
cg06707978	42,6364026	ZIK1	TSS1500

cg18016181	42,5122885	FOXD4	1stExon
cg17264670	42,3343436	RGS17	TSS1500
cg20275528	42,3201694	SEPT9	1stExon; 5'UTR
cg08833577	42,2253901	VAX1	TSS1500
cg12127472	42,1053422	C17orf104	TSS200
cg18758796	42,0092163	PDLIM4	5'UTR; 1stExon
cg20146541	41,9828195	TRIM58	1stExon
cg16924337	41,836897	RGS17	TSS1500
cg01303723	41,8185941	NKX6-2	TSS1500
cg01532168	41,7557301	KCNK9	TSS1500
cg16579555	41,7554184	RNF135	1stExon
cg09639151	41,6465827	PCDHGA12	1stExon
cg06158650	41,6201084	TBX15	5'UTR
cg08304190	41,5324301	MIR663	TSS200
cg15157455	41,522442	HIST2H2BF	TSS1500
cg10791343	41,5178219	POM121L12	TSS200
cg21187554	41,4787871	ANKRD18A; C9orf122	1stExon; 5'UTR; TSS1500
cg03757145	41,3406134	CDKL2	TSS200
cg06469345	41,2834865	DRD5	TSS200
cg25485875	41,1008931	NKX6-2	TSS1500
cg21426003	41,05736	GBX2	TSS200
cg08876434	40,7882405	RASSF10	TSS200
cg06525651	40,6568541	FAM196A	5'UTR; 1stExon
cg19867649	40,625043	DKK3	1stExon; TSS1500; 5'UTR
cg13703049	40,6172304	HOXA10	1stExon
cg27252696	40,5648939	SIM1	TSS1500
cg11595545	40,5157775	KCNA3	5'UTR; 1stExon
cg26124318	40,46454	ADAM32	1stExon; 5'UTR
cg04034767	40,3083063	GRASP	1stExon
cg10703826	40,2684444	TBX15	1stExon; 5'UTR
cg26609631	40,1972767	GSX1	1stExon; 5'UTR
cg22399133	40,1945349	CRYGD	1stExon; 5'UTR
cg00661485	40,1484098	FOXI1	1stExon
cg21264189	40,0026204	POU4F1	TSS200
cg02339682	39,9972653	BEND6; DST	TSS1500; TSS200
cg02011074	39,9555663	DNM3	TSS200
cg04021697	39,8994563	WDR8	TSS1500
cg23543123	39,8609345	SLC10A4	5'UTR; 1stExon
cg14565725	39,7379085	TBX15	5'UTR; 1stExon
cg11667020	39,6495773	NKX2-4	1stExon; 5'UTR
cg00399175	39,6420409	FAM59B	TSS1500
cg00701692	39,5943346	NKX6-2	TSS1500
cg18371475	39,3967774	IRX2; C5orf38	1stExon; 5'UTR; TSS1500
cg21000072	39,3893728	WDR8	TSS1500
cg02604524	39,2661935	CCDC48	1stExon
cg13080379	39,2560691	TBX15	5'UTR

cg15728256	39,1752644	BMP8B	5'UTR; 1stExon
cg02892660	39,1736852	ZNF761	5'UTR
cg21647227	39,1592818	TBX15	5'UTR
cg26818735	39,0463684	TWIST1	1stExon
cg23095743	38,9758458	PITX3	5'UTR
cg02823783	38,8450727	DNAH10	TSS200
cg08171351	38,7572269	CECR6	1stExon
cg12973941	38,7529118	NKX3-2	1stExon
cg25951981	38,7360319	GABRA4	TSS200
cg07609862	38,7001079	MTNR1B	1stExon
cg05022673	38,6924289	DST; BEND6	TSS200; TSS1500
cg03905847	38,6436872	NKX6-2	TSS1500
cg07703401	38,5681797	HBQ1	1stExon; 5'UTR
cg04137594	38,5064927	NPBWR2	1stExon
cg13604246	38,4202505	ANKMY1	TSS200
cg00140112	38,4071003	DLGAP1	1stExon
cg12056138	38,3214803	C15orf60	TSS200
cg05789704	38,2524205	ADAM32	TSS200
cg22447539	38,215801	FSCN1	1stExon
cg23054189	38,0037125	TRIM58	1stExon
cg21884231	37,9504388	SLC7A14	1stExon; 5'UTR
cg02237540	37,9482498	PDE6B	1stExon
cg02288825	37,8770086	MYT1L	5'UTR
cg26822097	37,8618968	psiTPTE22	TSS1500
cg04600618	37,8530014	RSPH9	1stExon
cg07347092	37,7931989	DNAH10	TSS200
cg17295225	37,7898292	OLIG3	1stExon
cg00554413	37,6660571	TACSTD2	1stExon
cg08726248	37,6264538	DRD4	TSS1500
cg09972405	37,6223445	MYT1L	5'UTR
cg12315713	37,5826528	CCDC67	1stExon; 5'UTR
cg03731268	37,5286648	L1TD1	5'UTR
cg22010052	37,4735119	LVRN	1stExon
cg02109484	37,4542843	C2orf65	TSS200
cg24452347	37,4346899	CNR2	5'UTR
cg02401454	37,4342908	HBQ1	1stExon; 5'UTR
cg26440289	37,4222512	SNX31	TSS200
cg12989128	37,4187562	GDAP1L1	5'UTR; 1stExon
cg25920406	37,3825546	FZD8	1stExon
cg21588562	37,3760631	FTMT	TSS200
cg25948690	37,3758334	FGF6	1stExon
cg00824018	37,3255229	INA	1stExon
cg27583690	37,3179528	NKX6-2	TSS1500
cg00352417	37,2766738	FAM43A	1stExon
cg26173997	37,2388209	CDKL2	TSS200
cg07382920	37,1913054	WDR8; TP73	TSS1500; TSS1500

cg07963234	37,1537155	CRMP1	TSS200
cg11413039	37,1130676	DDX25; PUS3	1stExon; TSS1500
cg24274117	37,1052065	C20orf195	5'UTR
cg00926400	37,1014836	BOLL	TSS1500
cg07783282	37,09456	USP44	5'UTR; TSS1500
cg09652652	37,0773363	FAM43A	1stExon
cg24613080	37,0274007	ACCN1	TSS1500
cg19740859	36,8766554	MYT1L	5'UTR
cg21908638	36,8759641	FAM55C	TSS200; TSS1500
cg21684012	36,7124894	SIM1	TSS1500
cg18564989	36,7086189	MIXL1	TSS1500
cg22702772	36,5953081	CELSR3	1stExon
cg25189564	36,5774284	VIPR2	TSS1500
cg14159026	36,5292389	BVES	TSS1500; TSS200
cg15225844	36,4856463	MYT1L	5'UTR
cg02884176	36,4762027	FOXI3	TSS200
cg01995480	36,4142281	PHF21B	TSS200; TSS1500
cg19544662	36,4119767	FOXI3	TSS200
cg00939495	36,2748899	DRD5	5'UTR; 1stExon
cg13404054	36,2556229	NOTCH3	1stExon
cg03129384	36,2473663	FAM196A	TSS1500
cg04415176	36,2284952	HOXD13	1stExon
cg17301902	36,2127857	GNA14	1stExon; 5'UTR
cg23208513	36,1569796	RGS22	TSS200
cg06848185	36,1435859	SEPT9	5'UTR; TSS1500
cg15457058	36,0992319	FOXE3	1stExon
cg23881278	36,0922433	DRD2	TSS1500
cg22802813	36,0634232	USP44	5'UTR; TSS200
cg20616414	35,9473662	WNK2	1stExon
cg21825027	35,9383786	ACP1; SH3YL1	TSS1500; TSS200
cg07274618	35,8164451	GALR2	TSS200
cg07605211	35,727594	SUSD4	TSS1500
cg19947104	35,7096892	KCNC1	TSS200
cg23501406	35,5266837	DRD4	TSS1500
cg24416513	35,3940175	HOXD8	1stExon; 5'UTR
cg26595643	35,3827586	VAX1	TSS1500
cg21595709	35,3740323	EPHX3	TSS1500
cg19355087	35,349024	NKX6-2	TSS1500
cg19270505	35,3484099	RUNX3	1stExon; 5'UTR
cg02096396	35,3463867	FAM59B	TSS1500
cg03817667	35,3127158	VSTM2A	TSS200
cg23920953	35,3042222	C14orf162	TSS1500
cg18485193	35,2751304	MYO10	5'UTR; 1stExon
cg10602757	35,2308637	FOXD4L1	1stExon; 5'UTR
cg24437737	35,1458785	HIST2H2BF	TSS1500
cg05184938	35,1125033	SEPT9	5'UTR

cg13096208	35,0718827	ST8SIA3	1stExon; 5'UTR
cg16494597	35,0350621	OR10H1	1stExon
cg17366808	34,950746	C15orf60	TSS200
cg04138502	34,9358058	ADCY5	TSS200
cg13868604	34,9289977	GDAP1L1	1stExon; 5'UTR
cg24136205	34,9158489	ZIC5	TSS200
cg14443301	34,908965	FTMT	TSS200
cg21610164	34,8671963	HIST1H2BI	1stExon
cg06825142	34,8318276	DRD4	TSS200
cg02177231	34,8246065	TBX15	5'UTR
cg17259183	34,8144426	NKX6-2	TSS1500
cg16896847	34,8007859	MAFA	1stExon
cg05603791	34,7664493	FOXI1	1stExon
cg24085946	34,6880133	NFASC	5'UTR; 1stExon
cg00413617	34,6454826	KCNC1	TSS200
cg01354473	34,5947633	HOXA9	1stExon
cg20953187	34,4942043	SLC6A20	1stExon
cg00613752	34,3990455	GPR6	5'UTR; 1stExon
cg03070297	34,3840001	FAM196A	TSS200
cg27331241	34,3501274	PRKAR1B	5'UTR
cg11223367	34,2268517	FAM55C	TSS1500; TSS200
cg23337116	34,1877298	RASL11B	1stExon; 5'UTR
cg13794993	34,1772917	SALL3	1stExon
cg14263942	34,1371306	CDKL2	TSS200
cg22441312	34,1259982	POM121L12	TSS200
cg02567119	34,115651	TLX1NB; TLX1	TSS200; TSS200
cg24563094	34,1046342	FAM59B	TSS1500
cg26477573	34,0921824	EPHX3	1stExon
cg14422922	34,0547815	OR2B11	1stExon
cg10097295	34,0173797	FOXD3	1stExon
cg17512738	33,9921974	POM121L12	TSS200
cg00094518	33,9047588	KLF14	1stExon
cg20486569	33,8499253	CLDN5	1stExon; 5'UTR
cg22681279	33,8497431	NPBWR2	1stExon
cg02970297	33,8177341	DPY19L2P2	TSS1500; TSS200
cg25984344	33,7710138	FAM196A	TSS200
cg24680586	33,7546672	INA	TSS200
cg04321866	33,7359039	EFNB2	TSS1500
cg02623400	33,7237525	ELAVL4	5'UTR; 1stExon
cg09382601	33,6745044	PDE6B	1stExon
cg06425919	33,6640393	MYOD1	1stExon
cg04692403	33,619674	TCF21	1stExon
cg03929741	33,5910927	EFNB2	TSS1500
cg13974632	33,5519342	BDNF	5'UTR
cg02485642	33,4033536	MSLNL	TSS200
cg16561266	33,3600396	LOC146880	TSS200

cg20986370	33,3204207	IGFBP7	1stExon
cg25331703	33,2944318	LRRK1	TSS200
cg06190616	33,2826368	OR2B11	1stExon
cg18416576	33,2513758	HOXA10	TSS200
cg11594420	33,2205299	TEX101	TSS200
cg26560222	33,1720924	DMRTA2	5'UTR; 1stExon
cg15790820	33,0963811	ASCL2	TSS1500
cg22131234	33,0657047	VSTM2A	TSS200
cg04084088	33,0605033	RGS9BP	1stExon
cg12414557	33,0577761	RNF212	1stExon; 5'UTR
cg13562542	33,0536454	GPR27; EIF4E3	1stExon; 5'UTR
cg12997720	32,995797	HOXA11	TSS1500
cg01878345	32,8945221	POU3F3	TSS200
cg09433135	32,8589374	FLJ40125	1stExon
cg08097882	32,8354779	POU4F1	1stExon; 5'UTR
cg11964564	32,8068615	KCNS2	5'UTR
cg08100565	32,7696345	SLC25A36	1stExon; 5'UTR
cg20585869	32,7684148	NEFM	TSS200; 1stExon
cg05777962	32,7641047	OR2B11	1stExon
cg05374654	32,7478949	GPR83	TSS200
cg01428589	32,7301073	RGS9BP	1stExon
cg02553663	32,6449358	SECTM1	5'UTR; 1stExon
cg05201970	32,5713141	HCN1	1stExon; 5'UTR
cg07558472	32,5240581	CXXC5	5'UTR
cg09054633	32,5188616	SPOCK1	5'UTR
cg18729357	32,4757751	ZNF702P	TSS200
cg26949694	32,3545346	BDNF	5'UTR; TSS1500; 1stExon
cg24425021	32,3422964	POU4F1	5'UTR; 1stExon
cg12215340	32,3195517	ADRA1D	1stExon; 5'UTR
cg05506365	32,3146099	POU3F3	1stExon
cg14212850	32,2211273	HRNBP3	5'UTR
cg02119134	32,1716367	FOXD4L1	1stExon
cg07251711	32,1706235	NKX6-2	TSS1500
cg21425842	32,1680433	HIST1H4F	1stExon
cg13801416	32,0475889	AKR1B1	TSS200
cg17703554	31,9401408	DCAF4L2	TSS200
cg06763054	31,8938211	MTMR7	1stExon; 5'UTR
cg04380519	31,8903012	LIMD2	TSS1500
cg12204732	31,8825008	FAM196A	TSS200
cg07153665	31,8701382	CMTM2	TSS200
cg25945732	31,8539666	SH3YL1; ACP1	TSS200; TSS1500
cg17300544	31,8532545	SEPT9	TSS200; 5'UTR
cg20931042	31,7847764	DRD4	TSS200
cg08931647	31,7272939	MSLNL	TSS200
cg25644556	31,7163966	MIR196B	TSS1500
cg02849695	31,7023234	CCDC19	TSS200

cg06135139	31,6727204	BHLHE23	1stExon
cg13428480	31,6283745	VANGL2	TSS200
cg25307665	31,6174718	HOXA5	TSS1500
cg13878010	31,6080815	ADCY5	1stExon
cg19300568	31,5801025	NAT8L	TSS1500
cg24903183	31,5766073	SNX31	TSS200
cg10188823	31,567078	NEFH	1stExon; 5'UTR
cg02547394	31,5667747	SOX1	TSS200
cg01972751	31,382522	OLIG3	1stExon
cg00172597	31,3785144	SUSD4	TSS1500
cg02531437	31,2642945	PRLHR	TSS200
cg12640000	31,2505043	L1TD1	5'UTR
cg03289872	31,1740029	ZNF667	TSS1500
cg06784108	31,1567296	EFNB2	1stExon
cg03242819	31,15478	FAM196A	TSS200
cg06401019	31,0982367	MIR2277	TSS1500
cg27504802	31,0706095	TRIM67	TSS200
cg08101407	31,0371384	TSPYL3	TSS200
cg24393316	31,0366755	FOXE1	1stExon
cg02932314	30,9490219	C17orf104	TSS200
cg00384539	30,9453095	PRDM14	TSS200
cg26117023	30,9154964	LOXL3	TSS1500
cg21872764	30,8961752	CLDN5	1stExon
cg25209842	30,87233	FGF8	TSS1500
cg24239148	30,8182388	C10orf107	5'UTR; 1stExon
cg05652533	30,7596399	DPYSL4	TSS200
cg04686953	30,7560675	RNF212	1stExon; 5'UTR
cg06377278	30,6585357	RUNX3	1stExon; 5'UTR
cg13222752	30,6371636	TMEM90A	5'UTR
cg08382774	30,5962545	NKX6-2	TSS1500
cg11469098	30,5674649	EFCAB1	5'UTR; 1stExon
cg15140703	30,5648703	GPC2; STAG3	TSS1500; TSS200
cg14347199	30,55972	NXNL2	1stExon
cg14988503	30,5453381	CDKL2	1stExon; 5'UTR
cg14719865	30,5448499	SLCO6A1	1stExon
cg02306630	30,53482	NKX6-2	TSS1500
cg10084644	30,5278909	GPC2; STAG3	TSS1500; TSS200
cg14414971	30,5184792	SDK1	TSS200
cg07543830	30,5017686	PMEPA1	5'UTR
cg24745495	30,4990237	EPHX3	TSS1500
cg03172947	30,4850604	DBNDD2	5'UTR; TSS1500
cg23353952	30,4797833	NEFH	1stExon
cg18342279	30,4682333	ZAR1	1stExon
cg16024318	30,4604923	SLC6A7	5'UTR; 1stExon
cg15642758	30,3845709	HDGFRP3	TSS1500
cg08315202	30,3622628	NPTX2	TSS1500

cg17098147	30,3621014	SPAG6	TSS1500
cg20787173	30,3339274	EYA4	TSS200
cg24432073	30,3172372	CDKL2	5'UTR; 1stExon
cg13997645	30,3009728	INSC	TSS200
cg02310286	30,2946901	DCAF4L2	TSS200
cg08369368	30,2908896	NSD1	TSS1500; TSS200
cg06829830	30,2904046	RASGRF2	TSS1500
cg18560204	30,2638598	BNC1	TSS1500
cg15014975	30,2632012	RUNX3	TSS1500
cg06922635	30,2599799	ARL9	5'UTR; 1stExon
cg19505136	30,2272765	CHL1	5'UTR
cg13930892	30,1861893	ASCL2	1stExon; 5'UTR
cg17800654	30,1849553	DMRTA2	5'UTR
cg12872693	30,1438977	GNB4	5'UTR
cg24884142	30,1331278	TBX15	5'UTR; 1stExon
cg00529958	30,1266223	ZIC5	TSS200
cg15251385	30,1229043	SLC2A14	TSS200
cg20810478	30,1027768	TRIM58	1stExon
cg10064339	30,0740518	UCP2	5'UTR; 1stExon
cg05488632	30,0663204	EPHX3	5'UTR; 1stExon
cg26240185	30,0104386	FAR1	TSS200
cg15766075	29,9624715	ANKMY1	TSS200
cg17241776	29,925124	DLEU7	1stExon
cg10171347	29,8041201	NKX6-2	TSS1500
cg10661615	29,8016044	PRLHR	TSS200
cg06122660	29,7821895	SLC2A14	TSS200
cg04150495	29,7159632	MIR663	TSS1500
cg15100599	29,6789583	SUSD4	TSS1500
cg16043357	29,6515349	VAX1	TSS200
cg00556112	29,6181478	DRD4	TSS200
cg02885007	29,6147025	HOXD9	1stExon
cg10344081	29,6018833	CDKL2	TSS200
cg08074851	29,6002859	KCNK12	TSS200
cg23625660	29,5881099	FBXL21	5'UTR
cg04510874	29,5812879	FES	TSS1500; 5'UTR
cg22815110	29,5761915	FOXD3	1stExon
cg12338417	29,522526	TRIM71	1stExon
cg12058947	29,5220447	HDGFRP3	1stExon
cg14013195	29,504343	C2orf39	TSS200
cg02583525	29,5009797	C2orf39	TSS200
cg07068756	29,4299301	UCHL1	1stExon; 5'UTR
cg08109815	29,4131602	NMBR	1stExon; 5'UTR
cg04158367	29,4046798	GFI1	TSS1500; TSS200
cg10603275	29,3661951	CHL1	5'UTR
cg03740978	29,3616401	KCTD1	5'UTR; 1stExon
cg20447655	29,3264215	CTHRC1	TSS200

cg27147819	29,319036	NKX2-4	TSS200
cg13530938	29,3172311	LOC643387	TSS200
cg21384402	29,31128	INA	TSS1500
cg11293190	29,3084176	PLK5P	TSS1500
cg21270860	29,2263987	POU3F1	TSS1500
cg22900415	29,2183155	GJA3	TSS1500
cg17988546	29,1968651	MS4A13	1stExon; 5'UTR
cg17411190	29,1366777	CLDN5	1stExon
cg26563200	29,118973	TEX101	5'UTR; 1stExon
cg23290344	29,1111924	NEFM	1stExon; TSS1500
cg15600488	29,0374377	MTMR7	TSS200
cg16263367	29,0288103	LOC147804; ZNF761	TSS200; TS200
cg19779211	28,9991063	KCNQ1	TSS1500
cg21200656	28,9937331	NKX2-4	TSS200
cg26931862	28,9632596	HOXC12	1stExon
cg05386493	28,8878913	C3orf72; FOXL2	TSS1500; 5'UTR; 1stExon
cg10888031	28,8788996	ACTRT2	1stExon
cg15092343	28,8619453	MSX1	TSS1500
cg20800509	28,8415171	RIMS2	5'UTR; 1stExon
cg21800232	28,8205092	ANKRD34B	TSS200
cg16038120	28,7998183	FOXG1	TSS1500
cg12175729	28,7970089	KCNK9	TSS1500
cg02831587	28,7943174	FAR1	TSS200
cg22881914	28,785003	NID2	TSS1500
cg03326059	28,7634941	FAR1	TSS200
cg23244790	28,7476845	PCDHGA12	1stExon
cg16281276	28,7022797	CYB5R2	TSS1500
cg21290042	28,666871	CNIH3	TSS200
cg16980360	28,6530519	RNF135	1stExon
cg11429969	28,6400024	PCDHA3	1stExon
cg25335544	28,6390494	CAMKV	5'UTR; 1stExon
cg03811478	28,5533904	SOX14	1stExon
cg23034757	28,5517061	PCDHGB6	1stExon
cg06410537	28,5498721	TLX3	1stExon
cg27262412	28,5102817	TBX15	5'UTR
cg10776919	28,4391052	DMRTA2	TSS1500
cg16132520	28,4286214	AKR1B1	TSS200
cg02466113	28,3598176	CDKL2	TSS200
cg05040544	28,3575298	EFNB2	TSS1500
cg27043726	28,3554963	SNX31	1stExon; 5'UTR
cg21643403	28,3039024	CTHRC1	5'UTR; 1stExon
cg02694427	28,3033741	HOXD12	TSS200
cg09656389	28,2927779	PAX6	TSS1500
cg20443254	28,2663048	ASCL4	1stExon